MECHANOREGULATION OF ENDOCARDIAL TO MESENCHYMAL TRANSFORMATION AND SUBSEQUENT REMODELING DURING HEART VALVE DEVELOPMENT

By

Mary Kathryn Sewell-Loftin

Dissertation

Submitted to the Faculty of the

Graduate School of Vanderbilt University

in partial fulfillment of the requirements

for the degree of

DOCTOR OF PHILOSOPHY

in

Biomedical Engineering

May, 2014

Nashville, Tennessee

Approved:

W. David Merryman, PhD

Joey V. Barnett, PhD

Christopher B. Brown, PhD

Craig L. Duvall, PhD

Hak-Joon Sung, PhD

ACKNOWLEDGEMENTS

I would like to start by thanking my advisor, Dr. Dave Merryman, for all of his inspiration and support over the years. I never for a moment questioned my placement in his lab; I always knew I was where I was meant to be. His enthusiasm was infectious, motivating me to persevere throughout the challenging times. I also am indebted Dr. Christopher Brown for all of his work with me, including countless conversations that helped me to understand the "biological side" of my project and how to improve experimental designs. Additionally, I want to thank Dr. Joey Barnett who invested a significant amount of time in helping me appreciate how my work as a biomedical engineer could be applied to developmental biology. To Dr. Craig Duvall, I owe gratitude for help with polymer synthesis and analysis questions. I need to thank Dr. Hak-Joon Sung for additional help with polymer synthesis and assistance with gel topographical analysis via scanning electron microscopy. Finally, I wish to acknowledge the Department of Biomedical Engineering at Vanderbilt University for providing such a wonderful opportunity for me in their program and generous support in my Provost Graduate Fellowship.

I also wish to recognize my financial support from the American Heart Association in the form of a Pre-Doctoral Fellowship and all of the people who helped me craft the proposal that allowed me to work on this project. For my hydrogel and EMT experiments, I wish to acknowledge Tyson, Inc. for the

generous donation of chicken eggs. The digital image correlation software utilized in this project was developed by Christopher Eberl, Daniel Gianola, and Sven Bundschuh and downloaded from the MATLAB File Exchange program. Scanning electron microscopy was completed in the Vanderbilt Institute of Nanoscale Science and Engineering (supported by NSF ARI-R2 DMR-0963361) with the assistance of Angela Zachman of Dr. Sung's lab group.

I also need to thank the many students and post-docs who helped me in the journey of this dissertation, with both scientific contributions and moral support. This includes my lab family: Josh Hutcheson, Steve Boronyak, Joe Chen, Alison Schroer, Meghan Bowler, Nathan Bloodworth, and our "lab mom" Larisa Ryzhova. There are likewise several undergraduate students I had the pleasure working with who helped me grow as a mentor: Katrina Adlerz, Stephanie Preston, Chelsea Stowell, and J.R. Peacock. Additionally, I'd like to thank Dr. Scott Baldwin and his lab, including Dr. Paige DeBenedittis, LeShana Saint-Jean, Dan DeLaughter, and Kate Violette for their assistance in learning new techniques, assays, and general support. I also would like to thank Christopher Nelson, Angela Zachman, Spencer Crowder, and Hali Egnatchik for helping me with various other aspects of my project, including being practice audiences for several important presentations. I also owe gratitude to Dr. Christopher Brazel of the University of Alabama Department of Chemical and Biological Engineering for starting me on my scientific journey while I was still an undergraduate student.

While I have been extremely lucky in the highly supportive academic environment I've worked in for the past five years, I also have been incredibly blessed with an abundance of family and friends who have cheered me on in my scientific pursuits. To my husband, Christopher Loftin, I will never be able to thank you enough for all your love and dedication. To my mother, Priscilla Collums, and my father, Kerry Sewell, thank you for always believing in me, even when I could not believe in myself. To Jack and Mary Jo, thank you for always knowing how to make me smile. For my family members who are no longer here with us, thank you for instilling in me the belief that I could be anything I wanted to be, as long as I was willing to work for it.

TABLE OF CONTENTS

LIST OF TABLES

LIST OF FIGURES

Chapter 1

Introduction and Motivation

Heart valve (HV) replacement surgeries are one of the most common procedures for treating both severe cases of age-associated valve disease and congenital heart defects (CHDs) of newborns and infants. Worldwide, the incidence of CHD is approximately 1% of live births, and nearly 25% of these patients require valve replacement surgery [1-3]. Currently, the mechanical and porcine or bovine bioprostetic valves commercially available present significant disadvantages, especially in treating children with CHDs who require multiple operations to implant larger replacement valves as they undergo somatic growth. Thus, a viable HV replacement, one based on natural biomaterials, capable of growing and adapting with the patient would advance current treatment methodologies and greatly improve quality of patient life.

HV prostheses were developed as early as the mid-1940s, with animal experiments occurring in the 1950s and the first clinically successful human implants occurring by 1960 [4-7]. Early mechanical prosthetics were ball and cage models, made of silicone-based polymers, nylon, plexiglass, and stainless steel, all of which introduced increased risk of thrombosis due to *in vivo* responses to non-native materials [8]. Since then, significant strides have been

made in redesigning the prosthetic valve structure to include multiple leaflets, to mimic the native structure of HVs, and in material selection to reduce risk of thrombosis and embolization, resulting in life spans of nearly 20 years for such prosthetics [9]. Despite these advances, life-long anticoagulant therapy is required for any patient with a mechanical HV replacement, which represents an especially significant risk to active patient groups such as children who receive the prosthetics to correct CHDs. To address the risk of thrombosis and need for anticoagulants, bioprosthetic valves were developed in the 1970s by using porcine HVs treated with chemical crosslinkers such as gluteraldehyde [10-11]. However, there is an increased risk of calcification in bioprosthetic HVs, with some exhibiting life spans only between 10-15 years. Advances in bioprostheses utilize bovine pericardial tissues as well as alternate crosslinking methods in attempt to reduce the risk of calcific nodule formation on these valves. Recent developments have led to the capability to implant HV prostheses via transcatheter techniques, eliminating the need for open heart surgery in this vulnerable patient population, including children with HV defects or elderly patients suffering from valve disease. This is especially beneficial for patients requiring reoperations, such as pediatric patients who undergo somatic growth and need larger prostheses over time. Complicating the HV replacement process is the decision of when the procedure is absolutely necessary; that is, when do the benefits of a HV prosthetic outweigh the risks associated with the surgery and subsequent prosthetic function (e.g. thrombosis risk with mechanical valves and calcification risks with bioprosthetic valves) [9]. Many of the disadvantages

discussed above could be addressed with the creation of a viable TEHV replacement, capable of growing and remodeling appropriately once implanted inside a patient and that would not require anticoagulant therapy or introduce risk of calicific valve disease.

The development of a viable tissue engineered heart valve (TEHV) is dependent on our understanding of the native valve environment, consisting of complex spatial and temporal organization of extracellular matrix (ECM) proteins and signaling molecules designed to promote valve development and function. Recent work suggests that TEHV research would benefit from studying the process of embryonic valve development, or valvulogenesis [12-13]. Understanding the processes that lead to the correct formation of the valve should instruct researchers in how to create an artificial valve with these same crucial characteristics. Specifically, we wish to focus on the process of endothelial-to-mesenchymal transition or transformation (EMT), a vital first step in the formation of HVs.

The developing heart tube, consisting of a common atrium, atrioventricular canal (AVC), ventricle, and outflow tract (OFT) is lined with specialized endothelial cells known as endocardial cells (ECs). During EMT, a small population of ECs migrate out of the lining layer and into endocardial cushions of the AVC and OFT; these cushions, composed of primarily glycosaminoglycans (GAGs), are the tissues that eventually become mature valve leaflets. This occurs through remodeling of the endocardial cushion ECM by the transformed cells. The remodeling process induced by EMT introduces structural proteins,

including collagen and elastin, into the cardiac jelly and is controlled by a myriad of temporally-regulated signaling molecules, including members of the TGFβ family, BMP2, and MEKK3. Over time, these changes result in a dynamic biomechanical environment that also provides mechanotransduction signals to control the remodeling process. Furthermore hyaluronic acid (HA), the primary component in cardiac jelly, is necessary for EMT to occur in endocardial cushions and acts in mechanoregulatory fashion, supporting the concept that the mechanical environment associated with EMT will be important to consider in the development of viable TEHV.

The development of an *in vitro* model for endocardial EMT dates back to the 1980s, when a collagen gel assay was created to study cell transformation and migration [14]. In this assay, endocardial cushions of the developing AVC are explanted on the surface of a collagen gel and incubated for ~2 days. During this time, endocardial cells migrate out of the explant and onto the surface of the gel; some of these cells undergo EMT, elongating and migrating into the collagen substrate. This assay has been utilized for both avian and murine endocardial cushions, demonstrating remarkable levels of signaling conservation important in regulating EMT. Moreover, the collagen gel assay has been indispensible in defining the important biochemical signals that induce and inhibit EMT. However, little is known regarding the relationship between the mechanical environment and EMT; as endocardial cushions remodel into mature HV leaflets, biomechanical changes occur that could influence the progression of EMT and thus influence further valve remodeling. As an example, recent work has

demonstrated that higher levels of mechanical stress in endothelial cell layers induce increased EMT [15-16]. Since the biomechanical structure of the cushions and valve tissue control their function, it is necessary to study the mechanical context of EMT regulation and subsequent tissue remodeling.

Heart valves are in a mechanically active environment, both signaling based on mechanical inputs and altering structure as needed to respond to changes in the hemodynamic environment. This occurs due to interactions between valvular endothelial cells (VECs) and valvular interstitial cells (VICs). VICs, the cellular progeny of the endocardial cells that underwent EMT, are responsible for maintaining the valve structure throughout a person's lifetime. During normal physiological condition, VICs maintain a quiescent fibroblast phenotype; however, under pathological conditions VICs are activated into myofibroblast-like phenotypes that increase production of markers such as alpha-smooth muscle actin (αSMA) and type I collagen. Increases in these proteins lead to increased stiffness of the valve, which further impairs function and leads to a feed-forward loop of valve remodeling. Ultimately, the only viable treatment for severe valve disease is a total valve replacement. For the development of viable TEHV replacements, understanding the mechanical processes *in utero* that lead to the formation of HV leaflets is crucial.

We hypothesize that the understanding of the mechanical environment of developing leaflets, as measured by atomic force microscopy (AFM), can be used to inform biomimetic substrates composed of ECM proteins to create a

novel EMT model that permits interrogation of mechanical factors on heart valve development. To achieve this, we will address the following specific aims:

1. Develop and validate an AFM technique for mechanical analysis of HV tissues samples that permits concomitant study of ECM components via traditional histological techniques, and then utilize this technique to examine biomechanical changes that occur in developing heart valves.
2. Develop a combination crosslinked collagen-hyauronic acid hydrogel platform as an *in vitro* model for EMT that allows studies of mechanical regulation of EMT.

To begin, a discussion on the need for viable TEHV replacements will be presented, including a thorough review of biomaterials currently being investigated as TEHV platforms as well as an introduction to EMT and valvulogenesis as it relates to TEHV research. In subsequent chapters, each of the individual specific aims will be addressed with a focused introduction and complete description of methods employed. Finally, a discussion of the complete dissertation is included with the purpose of highlighting the overall impact of this work and future direction of this project. A graphical overview of the dissertation is presented in Fig. 1.1. To assist readers, a table including abbreviations for common terms, techniques, and proteins has been included below (Table 1.1).

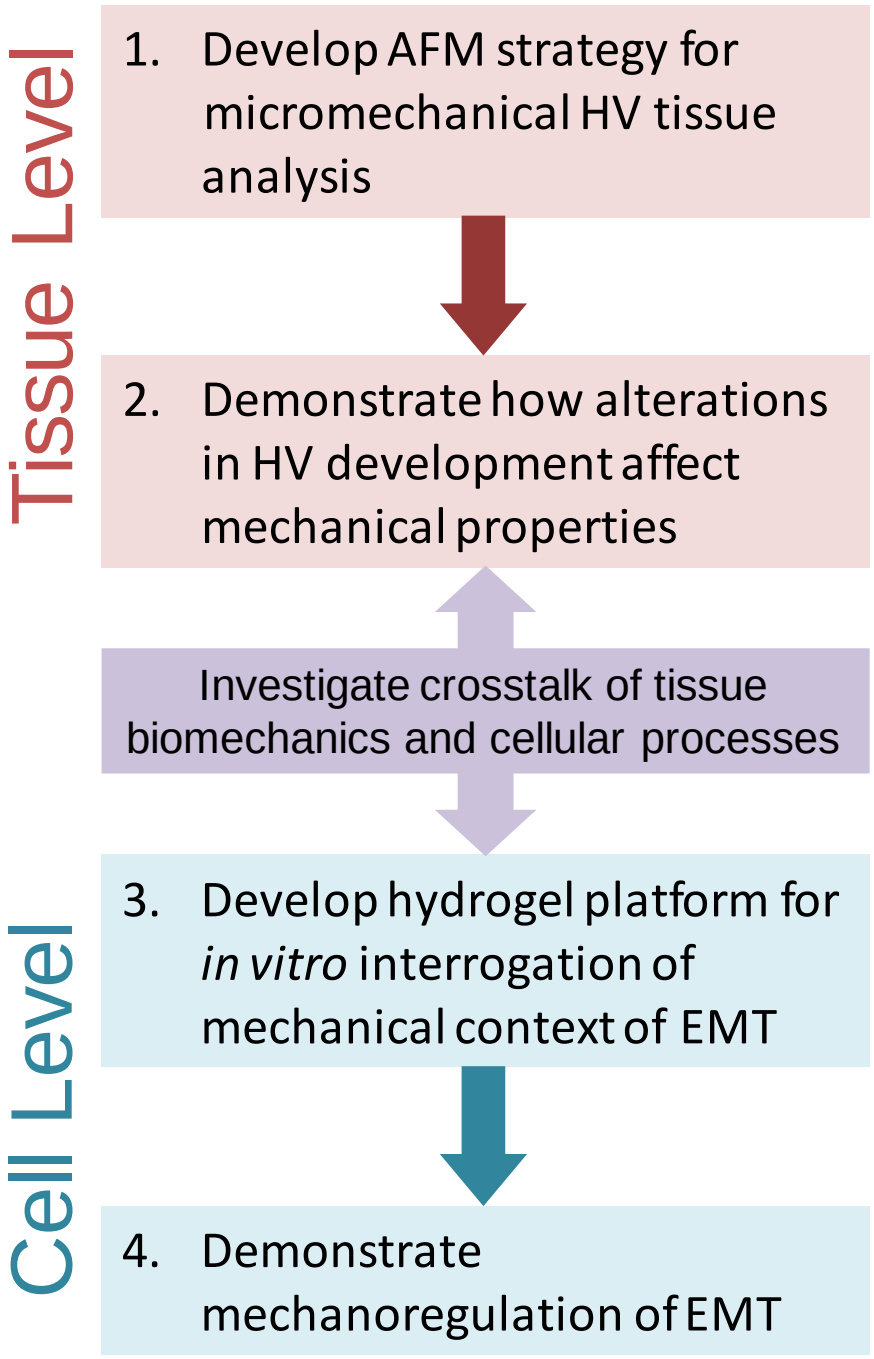

Fig 1.1 Overview of dissertation. The overall goal of this project is to study the interactions between tissue level mechanics and cellular mechanotransduction in the context of HV development.

Table 1.1. Abbreviations and Acronyms

AFM	Atomic force micrscopy
AVC	Atrioventricular canal
CHD	Congenital heart defect
Coll-MeHA	Collagen and methcrylated hyaluronic acid hydrogel
EC	Endocardial cell
ECM	Extracellular matrix
EMT	Epithelial to mesenchymal transition or transformation
EPC	Endothelial progenitor cells
ES	Electrospun
GAG	Glycosamingoglycan
HA	Hyaluronic acid
HV	Heart valve
MeHA	Methacrylated hyaluronic acid
MEKK	Mitogen-activated protein kinase
MMP	Matrix metalloproteinase
MSCs	Mesenchymal stem cells
OFT	Outflow tract
TEHV	Tissue engineered heart valve
TGFβ	Transforming growth factor β
VEC	Valvular endothelial cell
VIC	Valvular interstitial cell
αSMA	α Smooth muscle actin

Chapter 2

Background – Biomaterials and Heart Valve Replacements

Text for Chapter 2 taken from:

> Sewell-Loftin, M.K., Chun, Y.W, Khademhosseini A., and W.D. Merryman. EMT-Inducing Biomaterials for Heart Valve Engineering: Taking Cues from Developmental Biology. J Cardiovasc Transl Res, 2011. 4(5): 658-671.

2.1 Disease and Prevalence

Heart valve disease represents a leading cause of mortality and morbidity in today's world and many of these cases ultimately require valve replacement surgery. Nearly 300,000 valve replacement surgeries are performed each year, and this number is expected to triple as the aging population increases over the next 30 years [17]. While there are several valve replacement options available commercially, the currently available prostheses are not appropriate for pediatric patients due to size limitations and the need for reoperations as the patients grow [12]. Tissue engineering has been proposed as a way to address the lack of viable valve replacements, where complex scaffolds with biomimetic mechanical properties undergo growth, cellular invasion, and subsequent remodeling after being implanted in a patient. A particularly promising development is the rise of

cell-directive biomaterials which have tunable mechanical properties and are bioactive in their ability to control cell growth, protein synthesis, and ECM formation. In addition, the merging of developmental biology principles with tissue engineering strategies offers a chance to create an instructive biomaterial that will mimic the native environment of the developing heart valve and perhaps lead to the first viable TEHV replacements.

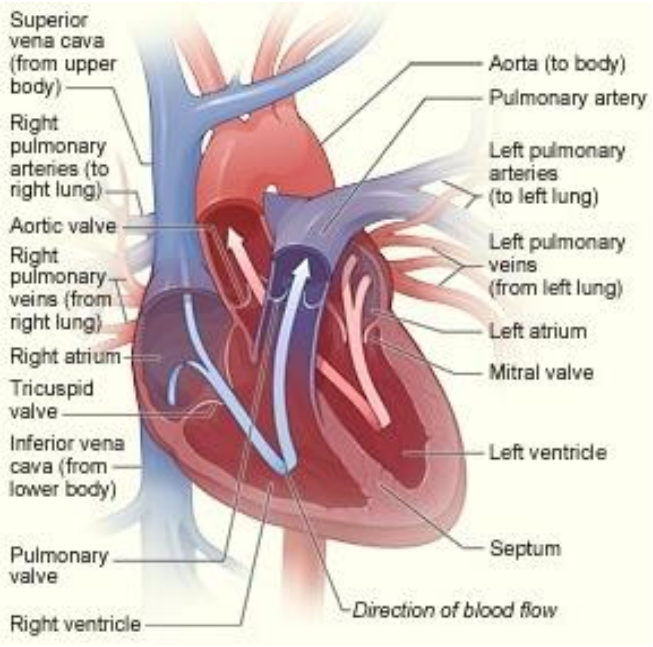

Fig 2.1. Anatomy of the heart. Major components of heart anatomy are presented, including position of valves and direction of blood flow (reprinted with permissions from the National Heart, Lung, and Blood Institute; National Institutes of Health; U.S. Department of Health and Human Services).

2.2 HV Anatomy and Biomechanics

The heart is a four-chambered pump, responsible for moving blood throughout the body to deliver oxygen to cells (Fig 2.1). The function of heart valves is to ensure the unidirectional blood flow within the heart as abnormal flow

profiles, including regurgitation or limited flow, cause environmental stresses to cells within the valves thus promoting fibrotic remodeling. The tricuspid and mitral valve are collectively known as atrioventicular valves, as they sit between the atria and ventricles of the right and left sides of the heart, respectively, and are open during diastole to permit blood flow into the ventricles. During systole as the ventricles contract, the hemodynamic pressure forces these valves closed while simultaneously forcing open the pulmonary and aortic valves, collectively termed the semilunar valves based on the half-moon shape of their leaflets. The cyclic contraction and relaxation of the heart provides the necessary forces to open the semilunar valves. Upon diastole, when these valves snap shut, the pressure of blood pushing down on the leaflets introduces significant stress in the tissues that can prompt a mechano-signaling response from VECs and VICs. Higher pressures present on the left side of the heart, responsible for pumping blood throughout the body, are evident in the increased mechanical properties of interstitial cells from the mitral and aortic valves (Fig 2.2) [18]. In infants with valvular CHDs, frequently the pulmonary valve will be moved into the aortic valve position in a surgery known as the Ross procedure. The immature pulmonary valve will undergo some remodeling to adapt to the increased pressure on the left side of the heart; a prosthetic valve is then implanted into the pulmonary position, which exhibits a less stressful environment for the prosthesis.

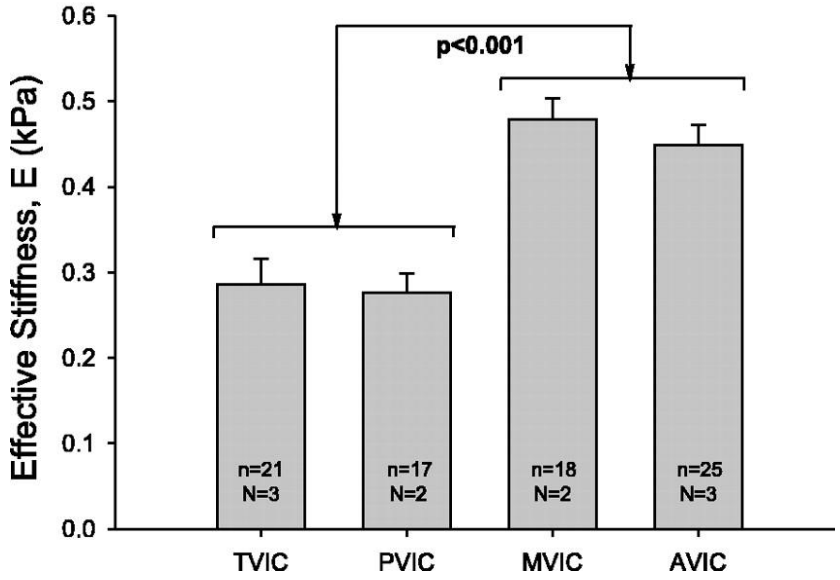

Fig 2.2. Valve interstitial cell stiffness. A comparison of valvular interstitial cell stiffness between left (MVIC and AVIC) and right (TVIC and PVIC) sides of the heart demonstrate significantly stiffer cells present in mitral and aortic valves where higher transvalvular pressures are present (reprinted with permissions [18]).

2.3 Drawbacks of Currently Used HV Replacements

The two types of clinically utilized prostheses are mechanical and bioprosthetic heart valve replacements. Of the roughly 90,000 annual aortic valve replacements in the U.S., approximately 50% receive either porcine or bovine derived bioprosthetic vales, 43% receive mechanical valves, and 7% receive human valves, either cadaveric allografts or autografts via the Ross procedure [19]. Mechanical valves are usually composed of metals, pyrolytic carbon, and expanded poly(tetraflouoroethylene) (ePTFE) and have a product life-span of greater than 20 years [20]. Various models, each with its own advantages and drawbacks, have been developed over the years including ball and cage valves, tilted disk valves, and bileaflet valves [21-26]. Unfortunately, thrombosis is a

significant risk after implantation of these devices, as a body's response to foreign materials can stimulate the formation of blood clots. Therefore a patient must remain on anticoagulants for the remainder of his or her life. This is an especially significant disadvantage for young or extremely active patients. These prosthetic valves also can experience hemodynamic failures, where the valve mechanism becomes 'stuck' in either the opened or closed position, a severe and potentially fatal complication.

Most clinically used bioprosthetic valves are porcine valves or bovine pericardial tissues, which have been decellularized to reduce antigenicity [21, 23-36]. Porcine heart valves and bovine pericardium are decellularized through a variety of techniques and chemically crosslinked before sterilization and implantation. Usually the valve or valve construct is washed in enzyme solutions (DNAse, RNAse, etc.) to remove cells and cellular debris, followed by chemical crosslinking with glutaraldehyde or similar agents. Although this crosslinking process has been used since the 1960s, it leads to *in vivo* calcification and altered mechanical properties [22, 37-39]. Modifications of the washing and crosslinking process are currently being investigated. Several promising animal studies using such valves have been performed, although there are some reviews that report a lack of data and significant failure in preclinical trials [23, 25, 29-30, 40]. While patients who receive these bioprosthetic valves do not require anticoagulant treatment, the valves also exhibit shorter life spans, due to mechanical failures and extensive calcification, which can lead to the need for further reoperations when compared to patients receiving mechanical valves.

Nearly 65% of patients under age 60 who receive a xenograft or allograft valve require at least one reoperation after 15 years [20]. Other studies report even shorter life spans for these valves, with patients needing a new replacement in less than 10 years [30]. Younger patients who receive bioprosthetic valves tend to live more active lifestyles than older recipients; thus, those who receive such implants have increased hemodynamic and metabolic demands on valve replacements that can hasten mechanical failure. The major disadvantage of both mechanical and bioprosthetic valves clinically available is that they are nonviable. In other words, these valves are incapable of growing or remodeling after being implanted and essentially begin to 'wear out' from the moment they are implanted. This is a significant drawback, especially in pediatric patients who will require future operations to implant new, larger valves as the patients grow. The field of tissue engineering has been promoted as a way to create a viable prosthetic heart valve, with improved biocompatibility, reduced antigenicity, and the ability to grow and remodel *in vivo*.

2.4 How Tissue Engineering Can Improve HV Replacements

Heart valve tissue engineering follows one of a few methods of development (Fig. 2.3). In one approach, synthetic or natural polymer scaffolds are created in a mold or platform. Other groups use xenografts as their scaffold starting material, chemically or physically altering the structure prior to additional work [41]. The primary function of heart valves is to ensure unidirectional blood

flow, which places significant mechanical forces on the leaflets during a cardiac cycle. During diastole, the aortic and pulmonary valves are closed and under significant transvalvular pressure to resist retrograde blood flow [18, 42-43]. Because of these loading demands *in vivo*, any TEHVs must be pre-conditioned *in vitro* to withstand mechanical loads. Numerous groups have designed protocols and bioreactors that improve hemodynamic and mechanical properties of polymer scaffolds both with and without pre-seeded cells from a variety of sources [44-54]. Some studies pre-seed scaffold constructs with cells, while others relied on circulating cells to repopulate the scaffold *in vitro*. These circulating cells may be responsible for replenishing cells within native heart valves [39]. Ideally, autologous cells should be used, which improve patient response to the prosthetic valve as well as provide remodeling of the ECM in the valve leaflets, improving biocompatibility.

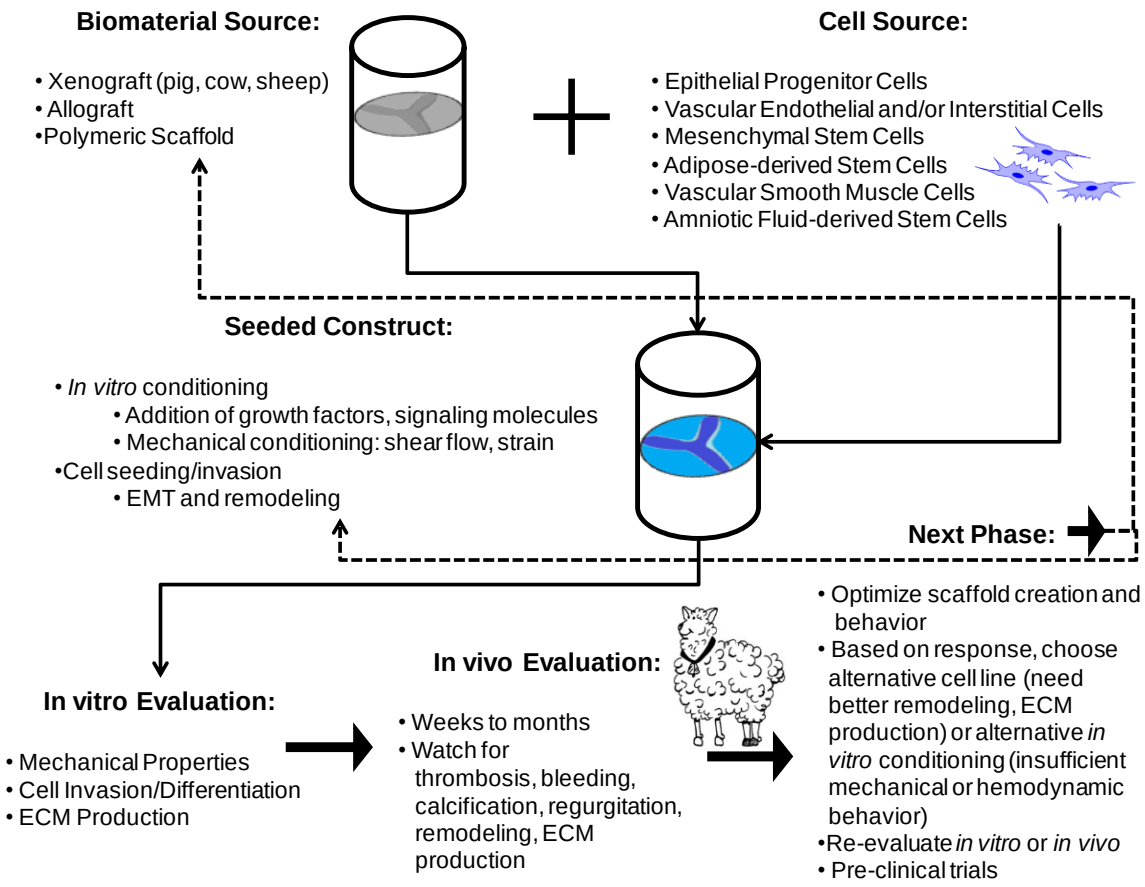

Fig 2.3. Overview of common TEHV tissue scheme. Other factors considered in evaluation of valve construct are as follows: *in vitro/in vivo* loading environment and forces, material properties (degradation, geometry, and fiber architecture), cellular invasion, protein synthesis/ECM production. Dashed lines represent the feedback of results into selection of new valve and/or cell sources or alterations to in *vitro/in vivo* conditioning, thus illustrating the reiterative nature of creating TEHV. Adapted from [13, 55].

After the replacement valve is implanted, it may undergo further remodeling. This response can be a positive factor in that the valve becomes integrated into the patient's heart and can be remodeled to resemble a naturally occurring valve. However, it is also possible that an implanted replacement valve may cause thrombosis or develop fibrotic tissue. Currently available xenografts from porcine and bovine tissue can develop significant calcification, as non-human cell remnants promote formation of calcific nodules and chemical crosslinking can alter calcium regulation [23]. Another drawback of porcine and bovine xenografts is the possibility that non-human pathogens can be transmitted to the patient, including porcine endogenous retrovirus and bovine spongiform encephalopathy [56-57]. It is worth noting that the use of xenografts may not be considered tissue engineered valves, as they are already 'formed' and only require processing before implantation. However, several tissue engineering research groups are using these approved valve replacements in combination with biomaterials or pre-seeded cells to create a TEHV platform. Several scaffolds have been designed to promote endothelialization *in vivo*, so that acellular grafts encourage host cells to populate and remodel the valve scaffold once it has been implanted. The next generation of TEHVs should have improved biocompatibility, hemodynamic/mechanical properties, as well as promote re-cellularization and remodeling, all while reducing immunogenic responses, limiting calcification and thrombosis, and reducing stress-related failures associated with current clinical heart valve replacements.

2.5 Importance of Valvulogenesis in TEHVs

An emerging area of biomaterials research for TEHV seeks to fuse the techniques and approaches of tissue engineering with the essentials of developing heart valve biology. To better imitate the natural environment that leads to heart valves *in utero*, understanding the mechanical and biological signals that control valve development is necessary [13, 58-61]. A crucial first phase in the embryonic development of the heart valves is EMT. In the developing heart valve, this process occurs when cells from the endocardium differentiate into mesenchymal cells and migrate into the cardiac jelly that forms the developing pre-valve cardiac cushions of the AVC, which eventually become the mitral and tricuspid valves, and OFT, which eventually remodel into the aortic and pulmonary valves. These activated cells are responsible for synthesizing the ECM proteins that form the leaflets and organizing these proteins into the fully mature valve structure (Fig. 2.4) [62-70]. The cardiac cushions are primarily composed of GAGs, such as chondroitin sulfate and HA, and filled with signaling molecules that regulate further valve development [63, 65]. Although the exact composition is unknown, some of the molecules that elicit or control EMT behavior include cytokines such as transforming growth factor-β1, -β2, and -β3 (TGF-β1, 2,3), vascular endothelial growth factor (VEGF), bone morphogenetic protein 2 (BMP2), MEKK3, and Notch1 [61-63, 68-77]. Pathways incorporating these EMT driving signals may be important to include and manipulate in developing *in vitro* TEHVs.

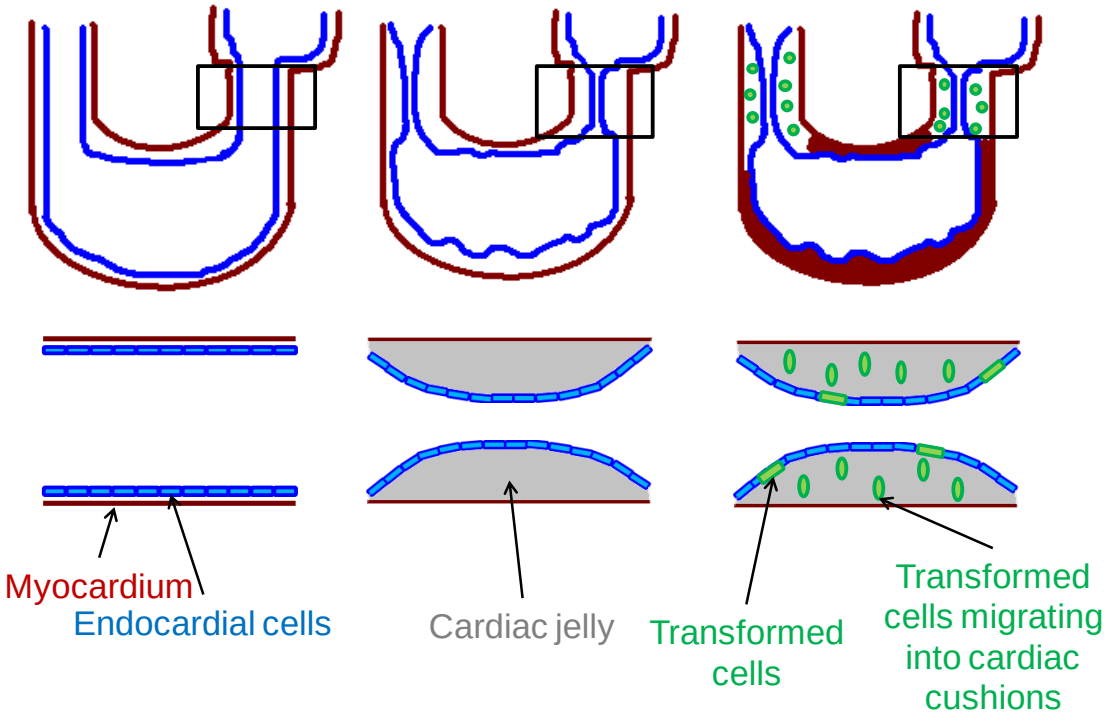

Fig 2.4. Illustration of EMT in the developing heart. Inserts are enlargement of atrioventricular canal. *Left:* Developing heart tube prior to cardiac cushion formation. Endocardial cells (shown in blue) line inside of u-shaped tubular heart separated from the myocardium (red) by a layer of cardiac jelly. *Middle:* The expansion of cardiac jelly, caused by secreted GAGs such as chondroitin sulfate and HA, leads to the development of cardiac cushion which contain signaling molecules (including, but not exclusive to TGF-β1 and β2, VEGF, BMP2, Notch1). *Right:* Endocardial cells undergoing EMT (shown in green) break down cell–cell junctions, elongate, and begin migrating into the cardiac cushions. Adapted from [71].

The expression of signaling molecules to initiate EMT is not sufficient to control the process. Chiu et al. demonstrated that there is specific temporal-dependent localization of TGF-β3, BMP2, and VEGFA in different areas of endocardial cushions during the overall process of EMT and valve remodeling (Fig. 2.5) [73]. The cardiac cushions regulate a complex synthesis of ECM molecules, leading to the elegant architecture that is heart valve leaflets and a fully functional valve. The properties of this ECM dictate short- and long-term function and durability of the valve; any defect present in the ECM architecture

can lead to valve dysfunction or failure. Understanding how such a complex system naturally arises in the developing valve presents an opportunity to create a superior TEHV built on the same fundamental developmental cues that occur *in utero*. We believe that biomaterials designed to promote and control EMT will provide the next generation of TEHVs, synthesized including native signaling molecules and mechanical properties.

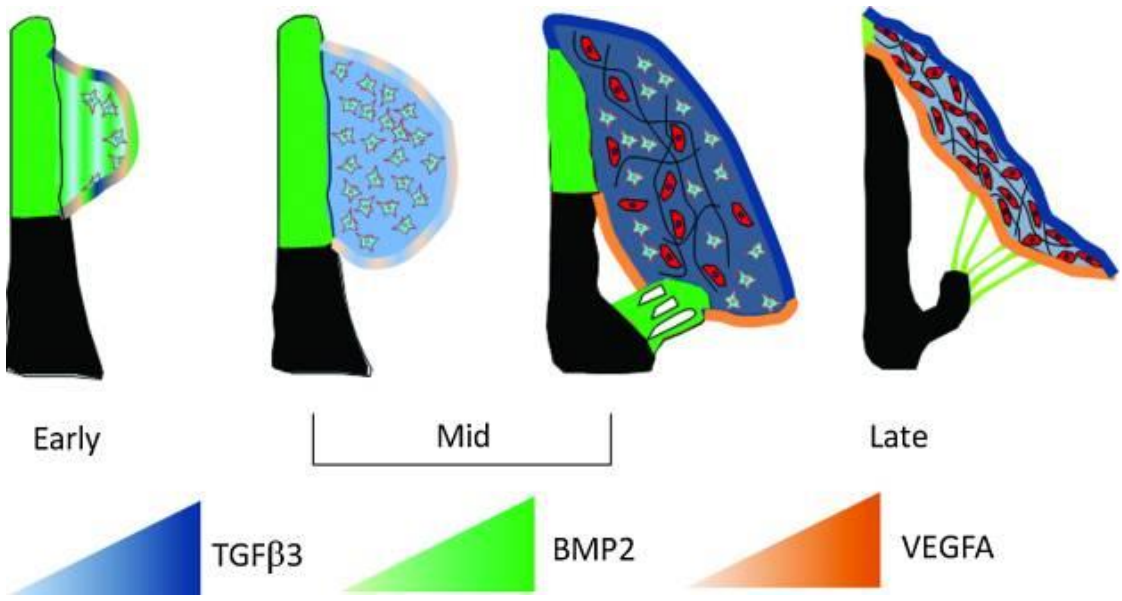

Fig 2.5. Spatiotemporal distribution of EMT regulators. In atrioventicular valves, early EMT is regulated by tight control over TGFB3 and BMP2. Over time, the intensity of signaling molecules varies and is restricted to certain regions of the valve, implicating mechanical signaling via hemodynamic forces may play a role in EMT (reprinted with permission from [73]).

2.6 In Vitro Models for EMT

Currently there are limited *in vitro* models available for studying EMT. These include an avian model collagen assay first described by Bernanke and Markwald over 30 years ago, in which AVC explants at stage HH16-17 are plated on a type I collagen gel (Fig. 2.6) [78]. Once explanted onto the gels, endocardial

cells migrate from the explants and form a monolayer called an endocardial sheet on the surface of the gel. After 24h, the endocardial cells on the surface of the collagen gel begin to migrate and some of these cells transform from cobblestone-shaped into elongated morphologies. These cells then begin to migrate into the collagen gel. Functional EMT is said to have occurred when cells exhibit the traditional elongated morphology of mesenchymal cells and migratory ability. Additionally, the collagen gel assay has been used to study similar explants from mouse hearts and demonstrated that many signaling pathways regulating EMT are conserved in both model systems [72, 79]. The primary difference between murine and avian explants is that the murine endocardial cells do not form a monolayer on the surface of the gel prior to invasion. Explants from the developing ventricle are used as controls in this system, as these explants do not normally undergo EMT; although EMT can be induced in these specimen with appropriate signals, for example TGF-β3 [80]. The other assay commonly used in studying EMT *in vitro* is based on the Boyden chamber assay [81-82]. For EMT studies, this assay involves isolating individual cells from pre-EMT tissues and plating them on a gel substrate, usually collagen or Matrigel on top of a semi-permeable membrane, and incorporating growth factors, chemotractants, or inhibitors in the lower chamber beneath the gel and membrane. Cells respond to the chemokine gradient and migrate through the gel and to the underside of the semi-permeable membrane where they are stained and quantified.

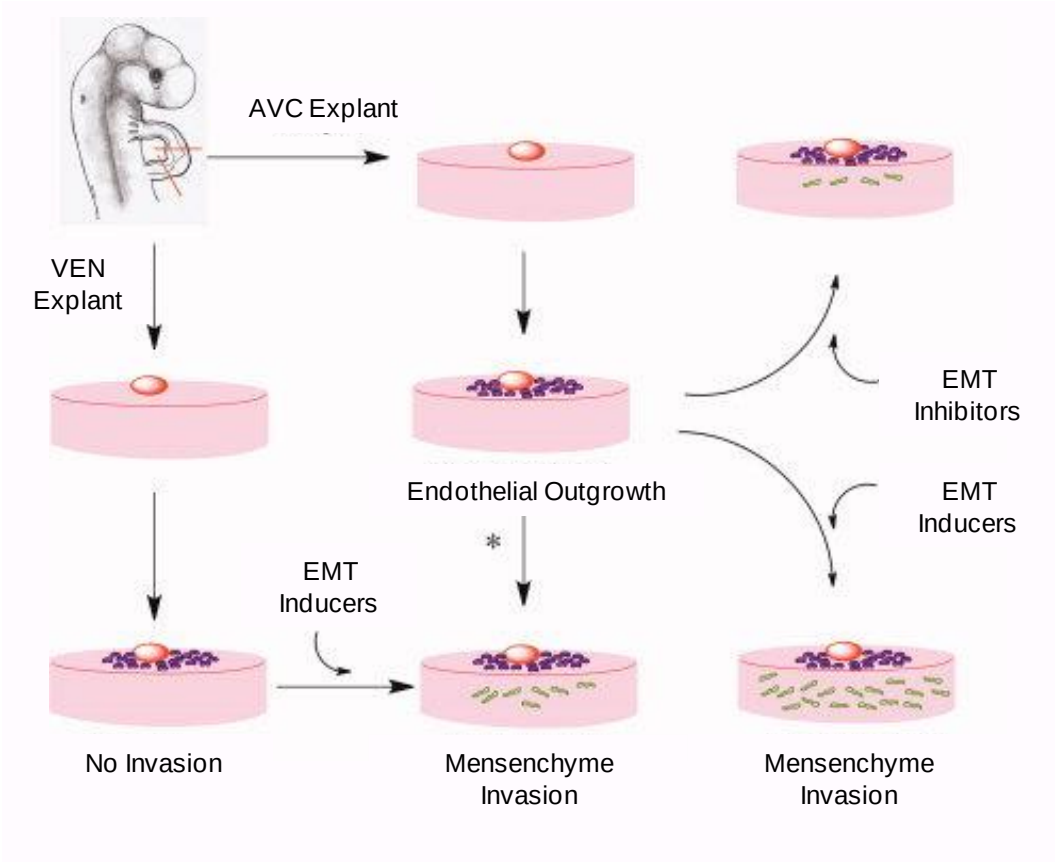

Fig 2.6. Illustration of traditional EMT assay. Endocardial cells migrate from the explant on the surface of the collagen gel and undergo EMT before invading into the substrate. Ventricular explants are used as a negative control, as these cells do not typically undergo EMT. However, EMT can be induced in these tissues by providing certain soluble factors (reprinted with permission from [83]).

While these assays have been useful in elucidating parts of the signaling pathways involved in EMT, there are several limitations in these systems [84-85]. Most notably, neither of these systems fully mimic the native environment of the developing valve, including complex 3D biomechanical environmental cues. In other words, results observed *in vitro* are not always recapitulated in *in vivo* models. For example, mice lacking TGF-β3 receptor do not undergo EMT *in vitro* however compensatory mechanisms *in vivo* exist that permit endocardial EMT. Furthermore, while both TGFβ-2 and -3 can induce EMT in murine and avian specimen in the collagen gel assay, *in vivo* only TGFβ-2 has shown to be necessary in regulating the initiation and cessation of EMT [86]. Currently the mechanical properties of these gel-based assays are not widely studied as they relate to EMT behavior, even though the biomechanical environment of heart valves is extremely important in determining proper function. After EMT, the transformed cells actively secrete ECM proteins, remodeling the cardiac cushions and altering the mechanical environment. These biomechanical changes can then affect cellular signaling through mechanotransduction pathways, thus creating a feedback loop where precise regulation is required to form HV leaflets correctly.

The development of HVs is a complicated process that is not fully understood. EMT represents the initial step of valve formation which must be completed correctly before the endocardial cushion can remodel and eventually develop into a mature valve leaflet. Numerous studies show that knockout of genes important in EMT, such as hyaluronan synthase 2 (HAS2) and MEKK3,

result in lethal mutations. Camenisch et al. showed that mice lacking HAS2 do not have HA present in cardiac jelly which prevents proper formation of cardiac cushions and ultimately EMT [79]. In an experiment using the collagen gel assay with AVC explants from these mice, EMT was rescued if soluble HA was included in the gel or as a factor in the media. In a study with MEKK3 knockout mice, authors observed reduced endocardial cell proliferation, such that EMT could not occur [72]. Such studies indicate that although post-EMT remodeling of cardiac cushions may be important for proper mature valve formation and function, the initial process of EMT is the critical first step that may need to be focused on for future TEHV studies. Biomaterials capable of promoting or controlling these initial stages of valve formation may be key in creating *de novo* TEHV.

An additional consideration in the development of TEHVs, is the changes in valve morphologies with increasing age. Several prominent research groups have discussed the role of valvular remodeling during disease, noting that a number of valvular defects may be caused by a genetic abnormality or functional defect related to the developmental process [87-88]. Fetal and post-natal valves demonstrate a high level of remodeling, due primarily to dramatic changes in system pressure immediately after birth and the activated myofibroblast-like phenotype of VICs which proliferate quickly in early stages of development but de-activate and become quiescent in adult valves [88-89]. These VICs are the cellular progeny of the mesenchymal cells derived from the endocardium during EMT and are implicated in degenerative aortic valve disease [43, 90-92]. A better

in vitro model for EMT studies may ultimately lead to revelations in degenerative valve disease research, especially considering the similarities in these diseases with developmental biology. In addition to VICs, a large amount of remodeling occurs post-natally due to shunts in the fetal cardiac system closing and an increase pressure in the left side of the heart (Fig. 2.7) [93-95]. The changes in the hemodynamic environment lead to altered cellular and biomechanical signaling, which promotes the further remodeling of HV leaflets.

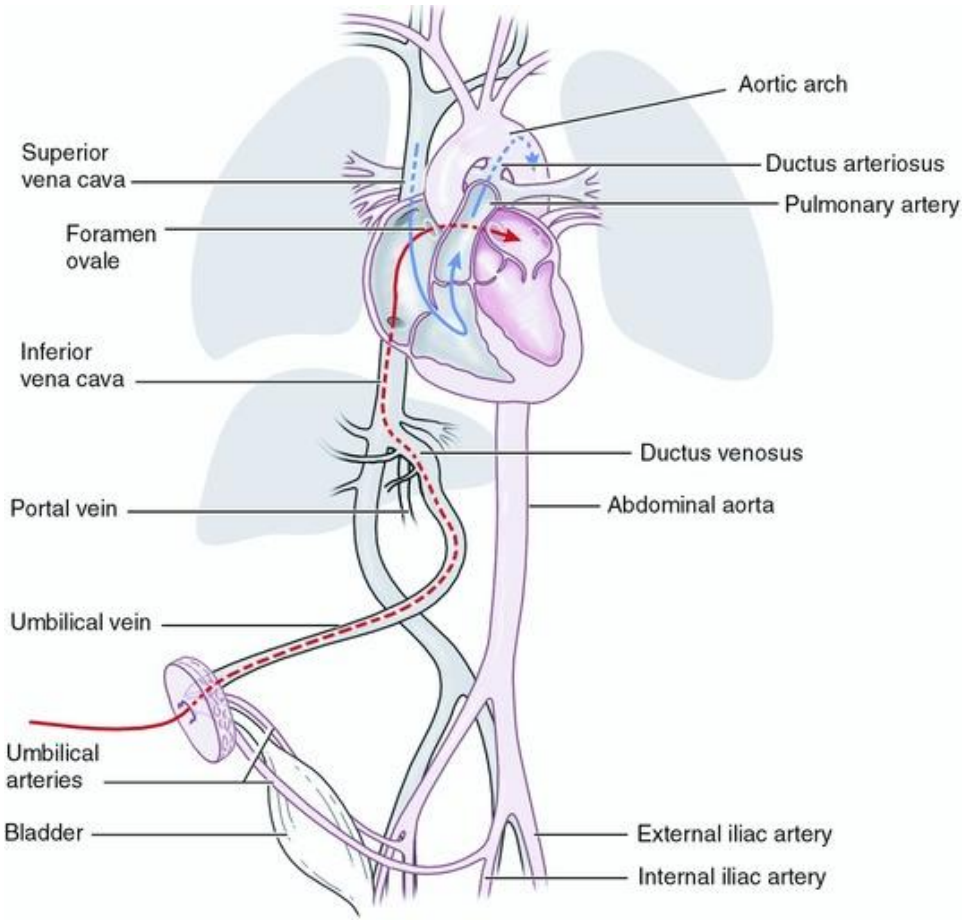

Fig 2.7. Fetal circulatory system. In developing embryos, the lungs are bypassed as blood is shunted directly between left and right sides of the heart by the foramen ovale. Additionally, the ductus arteriosus and ductucs venosus act as portals between oxygenated and deoxygenated blood. After birth, the first breath of air in the lungs causes a dramatic shift in pressures which initiates remodeling and closing of these features (reprinted with permission from [96]).

Changes in mature valve characteristics are due to the alteration of ECM production or organization during valve maturation. Stephens et al. studied changes in material behavior of porcine mitral and aortic valves in animals ranging from 6 weeks to 6 years, simulating child to adult characteristics (Fig 2. 8) [97]. They observed that as the animals aged, there were significant increases in fibrosa thickness, leaflet stiffness, and loss of extensibility. This group also reported that there was an increase in collagen content as the animals aged and a marbling effect in the fibrosa with collagen fibers interspersed with GAGs. Although not directly related to EMT or valvulogenesis, age of the patient will need to be considered when developing viable valve replacements. In this light, biomaterials which elicit EMT behavior may be more suitable for developing heart valves for neonates or other young patients who need heart valve replacements which exhibit characteristics of native neonatal or juvenile valves. Although understanding the natural mechanical formation of HVs may permit the development of a ‘fast-track’ conditioning system that would be useful in developing TEHVs for patients of all ages.

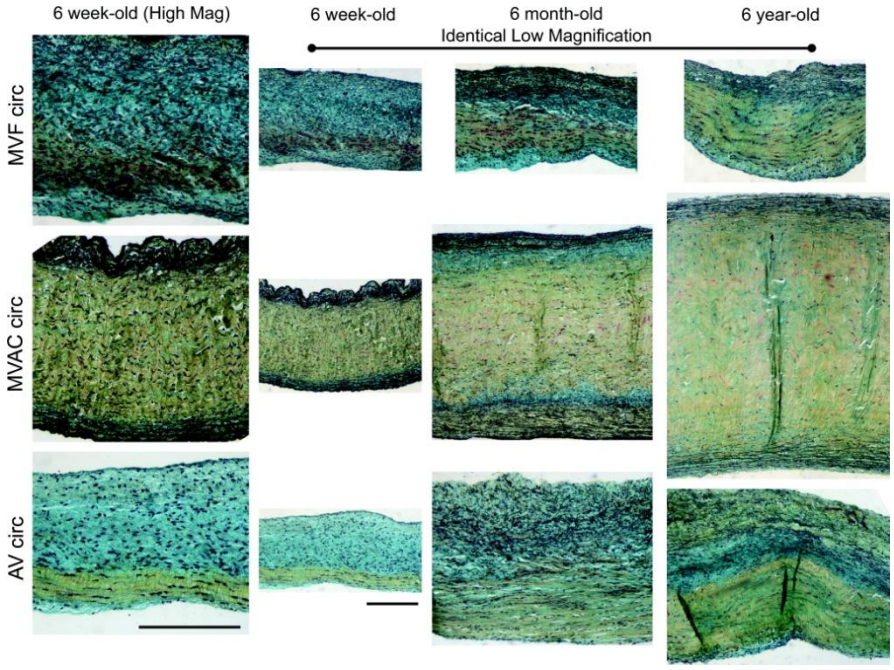

Fig 2.8. Remodeling of ECM in HVs. Movat's Pentachrome staining shows type I collagen (yellow), GAGs (blue), elastin (dark purple), and nuclei (black) as the mitral valve (MVAC—anterior leaflet, F—free edge) and aortic valve (AV) leaflet remodel over time in a porcine model. For orientation purposes, the lower edge of the leaflet is the fibrosa for both MV and AV specimen. Of interest, an increase in type I collagen is observed as age increases, even while marbling of GAGs becomes more apparent in the fibrosa layers (reprinted with permissions from [97]).

2.7 Biomechanical Properties of HVs

Considering the importance of the biomechanical environment of valve leaflets, surprisingly little data is available regarding these mechanical changes in valve stiffness during developmental stages. Mature HV leaflets exhibit an extremely complex and highly organized ECM that is synthesized and maintained by VICs via mechanical and hemodynamic environmental cues [39]. The mature semilunar valve has a distinct trilaminar structure, with each region populated with specific proteins for specific purposes (Fig. 2.9). The ventricularis, on the side facing the ventricles, contains elastin fibers that support changes in valve

leaflet shape during the cardiac cycle. The spongiosa is comprised of GAGs and acts as a shock-absorbing and lubricating layer in the valve. The fibrosa is rich in collagen fibers, aligned in such a way that they are responsible for the majority of the valve's mechanical strength. Understanding this environment is a critical step if we wish to develop improved TEHVs.

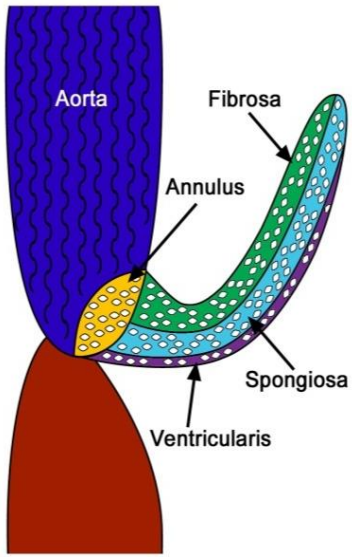

Fig 2.9. Structure of aortic valve leaflets. The trilaminar structure of mature aortic valve leaflets includes the collagen rich fibrosa, GAG-rich spongiosa, and elastin rich ventricularis. The unique structure permits rapid opening and closing of the valve under hemodynamic forces from blood flow (reprinted with permissions from [98]).

The most-used technique for measuring the stiffness of these valves is micropipette aspiration, which is difficult to execute and requires full leaflet tissues [99]. Recent work has shown small changes in valve stiffness of mouse leaflets from ages 1-12 months (mo), which was speculated to represent age-associated valve degeneration (Fig. 2.10) [99]. Additionally, some work has been done to show increasing stiffness of post-EMT cardiac cushions from developing chick embryos over time, although the study is limited in scope and does not

cover remodeling occurring directly after EMT [100-101]. More recently, Young and Engler utilized AFM to measure the changes in myocardium stiffness during the development of embryonic chicks, including time points occurring during EMT [102]. While these results show a dramatic increase in tissue stiffness over time, the myocardium mechanical environment differs from the cardiac cushions that eventually are remodeled into the valve leaflets. A comprehensive study to determine the timeline of biomechanical changes in cardiac cushions and embryonic HV leaflets, including structure and composition of the ECM before, during, and after EMT, will provide considerable insight into the necessary biological and mechanical cues needed to create a viable TEHV.

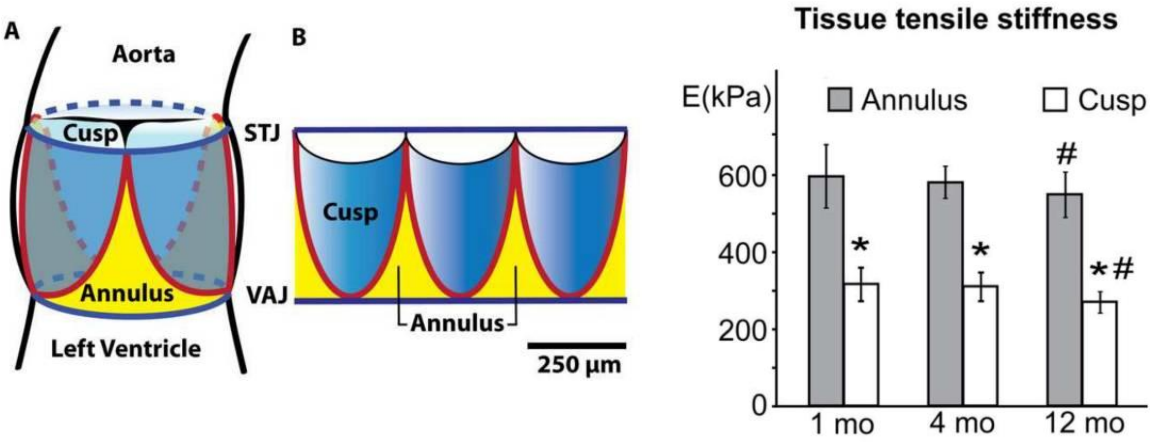

Fig 2.10. Biomechanical analysis of whole mouse HV leaflets. *Left:* This cartoon illustrates how authors bisected and managed leaflets during mechanical analyses. *Right:* Micropipette aspiration reveals that leaflet tissues are significantly softer than annulus samples (* $p < 0.0001$) and that there is a small but significant degradation in mechanical strength in 12mo mouse samples (# $p < 0.001$ (annulus), 0.05 (cusp)) (reprinted with permission from [99]).

2.8 HVs Engineered from Synthetic Biomaterials

Since the rise of tissue engineering nearly 20 years ago, biomaterials have been an obvious answer to the question of how to create scaffolds to

promote regeneration of natural tissues [103]. In this same time span, the rise of polymer science has created a plethora of materials with a wide range of mechanical and chemical properties. Several of these have received wide use in the clinic such as poly(lactic acid) (PLA), poly(glycolic acid) (PGA) and poly(lactic-co-glycolic acid) (PLGA), primarily as bioabsorbable sutures. Some of the advantages of synthetic biomaterials is the ability to vary the mechanical properties over a large range, alter the chemical properties to achieve numerous configurations, and tailor *in vivo* degradation times. In addition, since several of these materials have already been approved by the Food and Drug Administration for medical applications, numerous researchers have used them as a platform for new projects. Table 2.1 summarizes synthetic and natural polymer materials currently researched in tissue engineered heart valves and is located at the end of this chapter.

One of the most common polymers used in biomaterials research is poly(ethylene glycol) or PEG [104-108]. When implanted in the body, PEG chains become hydrated, presenting a hydrophilic surface rendering it bio-inert [104]. PEG also allows for numerous modifications: crosslinking, chemical modification via the addition of peptide chains or bioactive molecules, and co-polymerization to alter mechanical properties. Recently, dynamically tunable PEG-based systems have been developed that respond to either mechanical or optical cues. Benton et al. investigated a highly crosslinked PEG hydrogel loaded with an MMP-sensitive peptide for studying the behavior of porcine VICs [104-105]. Similar work on a photosensitive PEG-based gel has been done to create a

system with tunable mechanical properties. These gels show that encapsulated cells respond by differentiation due to gradients in substrate stiffness created using UV light [106-108]. More recently, these materials have been used to modulate between quiescent and activated phenotypes in VICs by exposing PEG-based substrates to UV light and altering the gel modulus [109]. Polyurethanes are another attractive option for heart valve tissue engineering, as several are incorporated into commercially available such as Elast-Eon medical products including plastic surgery implants or as insulation on pacemaker leads. These materials can withstand ~500 million cycles when tested in a flow system mimicking heart valve hemodynamics [110]. Composite scaffold leaflets made from polycarbonate soft segments (PCU, a soft polyurethane) and polyhedral oligomeric silsesquioxanes (POSS) nanoparticles showed improved mechanical properties compared to PCU control samples [110]. These same studies showed that the PCU-POSS leaflets had reduced platelet affinity, meaning these materials should be non-thrombogenic.

Biodegradation is another important property to consider for TEHVs. Scaffolds that can be enzymatically or hydrolytically degraded as cells invade and remodel present an attractive option for potentially viable HV replacements. This is especially interesting for exploiting the developmental pathways, such as inducing EMT, to promote cellularization and ECM synthesis in valve replacements. Several groups use such biodegradable polymers as a base for their scaffolding system, incorporating additional polymers to provide enhanced mechanical properties. Because PLA and PGA were already accepted as

biocompatible, biodegradable polymers, initial heart valve tissue engineering research focused on testing these materials. PLA and PGA composite scaffold leaflets were seeded with human fibroblasts and then had bovine aortic endothelial cells added to create a leaflet that mimicked native valve structure [111-112]. However, early non-woven versions of the scaffold system were too soft to be tested in animal models, and woven PLA:PGA scaffolds implanted in the pulmonary valve position in a lamb model had a failure rate of 75% due to infection and problems with implant shrinkage and deformation [111]. Because the traditional PGA-based scaffolds did not exhibit sufficient mechanical properties to promote further research, additives and other polymers have been added to PGA-systems to create tissue engineered valve replacements [12, 113]. One of the most common involves the addition of a polyhydroxyalkanoate called poly-4-hydroxybutyrate (P4HB), a bioabsorbable thermoplastic that can be molded into the complex shape of a heart valve and sealed together without the use of sutures [114]. In a seminal study that has not been replicated, ovine VICs and VECs were seeded on PGA valve scaffolds coated with P4HB before implantation into a lamb model [115]. Results indicated ECM protein synthesis and mechanical properties similar to native valves after 20 weeks of study, while the polymer implant itself degraded within 8 weeks. More recently, another study where these valves were implanted in sheep using a catheter showed that the valves functioned up to 8 weeks [116].

Despite what seems like initial success, this material has not been accepted for clinical use yet due to numerous uncertainties in how the valves

function *in vivo*. Another study showed that the enhanced mechanical properties due to P4HB coatings on these valves degraded within a few weeks of *in vitro* conditioning in a bioreactor [47]. More work has been done on this polymer system to explore if cellularization can improve scaffold function. In 2003, Dvorin et al. showed that ovine VECs and endothelial progenitor cells (EPCs) respond to VEGF and TGF-β1 signaling when seeded onto PGA/P4HB gels [117]. The gels seeded with EPCs also promote increased DNA content and ECM protein synthesis; however, they also have much higher modulus than unseeded control scaffolds (7x) and native valves (40x) [118]. While these materials exhibit improved mechanical properties and have shown good hemodynamic properties in conditioning bioreactors, they are often not physiologically relevant in respect to presenting a scaffold that can be invaded and remodeled by cells. For this reason, another class of materials, one more familiar to the body, is being investigated to provide the biological cues to promote and control cell growth.

2.9 Natural Biomaterials as TEHV Scaffolds

While they offer less flexibility in functionalization than their perhaps more well-known synthetic counterparts, biomaterials based on naturally occurring biomolecules do provide mechanical properties comparable to native tissues and the possibility of biological cues needed to direct and control cell growth. This, coupled with their inherent biocompatibility makes natural biomaterials prime candidates for TEHVs. These materials also promote natural developmental

processes, potentially including EMT, in order to achieve optimum scaffold function. Because they expose cells to proteins present in native developing valves, it may be possible to ‘trick’ cells into undergoing valvulogenesis thereby growing a replacement heart valve *in vitro* for patients of all ages, including newborns with CHDs. Gels made from collagen, fibronectin, HA, elastin, and other ECM components expose cells to signals that promote *in vitro* and *in vivo* remodeling. If the valve can remodel after implantation, its overall function may be improved, leading to a better quality of life for patients.

The two most examined natural biomaterials for TEHVs are HA and collagen [113, 119-126]. Both of these materials are present in native valves at various developmental stages in relatively large amounts. The cardiac cushions in the developing heart valve contain a significant amount of HA, which plays a role in regulating ECM production, initiation, and control of EMT in endocardial cells [63, 127]. HA gels undergo slow biodegradation through hyaluronidases, making them an excellent scaffold system for *in vitro* or *in vivo* remodeling. The spongiosa of native valves contains >90% HA and chondroitin sulfate, indicating these materials are non-thrombogenic and non-immunogenic. It is also hypothesized that utilizing HA in gel scaffolds may provide biological cues to cells and promote specific ECM production. For example in a study where neonatal rat smooth muscle cells were grown on HA gels, elastin production increased compared to cells grown on plastic after 4 weeks of culture [113]. Elastin is an important component of the mature valve, responsible for supporting the closed structure of the valve during diastole. Crosslinkable HA gels modified with

methacrylate groups and co-polymerized with PEG-diacrylate showed encapsulated porcine VICs alter production of ECM proteins based on molecular weight of HA degradation products [119]. Moreover, HA has recently been implicated in overriding traditional mechanotransduction signaling pathways via integrins, such that cells grown on soft HA gels demonstrate actin stress fibers and other hallmarks usually only observed on stiffer substrates [128].

Collagen is one of the main ECM proteins produced in developing valves and maintained in mature valves, inducing anisotropic mechanical properties that the valve utilizes for proper function for up to three billion cardiac cycles. Because it provides a significant amount of mechanical strength and its circumferential alignment results in anisotropic strain response, collagen is often included in composite scaffold systems [123, 129]. However, on its own, collagen lacks the necessary mechanical properties to create a physiologically relevant heart valve replacement. Crosslinkable, methacrylated HA used in combination with collagen is another attractive choice for TEHVs [130-132]. In this composite material, collagen provides the fibrous structure of native valve leaflets, and crosslinked HA promotes increased mechanical strength. This material has been shown to promote proliferation of fibroblasts [121-122]. The addition of HA alters the formation of collagen fiber network, meaning that cells cannot significantly contract the composite gels compared with the collagen only networks. Collagen has also been combined with another GAG, chondroitin sulfate, to create mitral valve leaflet replacements [120]. These scaffolds showed *in vitro* development into similar architecture as native valves when seeded with porcine VICs and

VECs, suggesting that a combination of collagen and GAG matrices may be a promising novel *in vitro* model for valve development.

While HA and collagen are the most widely studied biopolymers in the TEHV literature, other natural materials are being investigated as well. Fibrin gels present another potentially viable alternative for tissue engineered heart valves, since they can be derived from the patient thereby eliminating the worry of an adverse immunogenic response. Although studies of fibroblasts encapsulated in fibrin gels show increased collagen production and anisotropic mechanical properties, these materials do not have sufficient mechanical properties needed to be considered sustainable heart valve scaffold materials [129, 133-136]. Studies testing mechanical conditioning in the form of cyclic distension of fibrin scaffolds seeded with either porcine VICs or human dermal fibroblasts showed increased mechanical properties and collagen production compared to statically grown control samples [137]. This could indicate that fibrin-based scaffolds remodel and thus might eventually generate sufficient mechanical properties for implantation, if conditioned correctly. As an example of this, Sydeain et al. have demonstrated the ability to synthesize a fibrin tube and populate it with cells to remodel and align the fibers (Fig. 2.11); this structure can then be slid onto a frame that allows for the formation of a valve-like structure capable of further remodeling under flow [129, 138-139]. Another approach for TEHVs involves improving clinically used mechanical valves. Hydroxyapaptite, a naturally occurring biomaterial present in bones, has been investigated as a coating for mechanical valves. The thought is that by increasing biocompatibility of the

material presented *in vivo* of mechanical valves, hopefully the problems of thrombogenesis will be lessened and the need for anticoagulant therapy will be eliminated for these patients [140].

One technique to introduce enhanced mechanical strength, as well as mimic the native fiber alignment of heart valves, would be to include biopolymer-based electrospun (ES) fibers. Electrospinning represents a unique technique which allows for the creation of nanoscale fibers that form fibrous scaffolds which mimic the architecture of natural ECM. Both synthetic and natural polymers are used in electrospinning for the creation of a wide variety of mechanical properties, structures, fiber diameters, and other characteristics. Since ES fibers result in increased surface area and interconnected three dimensional porous environments, the scaffolds represent a biomimetic system. These fibers also play an important role in modulation of mechanical properties. In light of this, there have been reports using electrospinning techniques for heart valve tissue engineering [141-145].

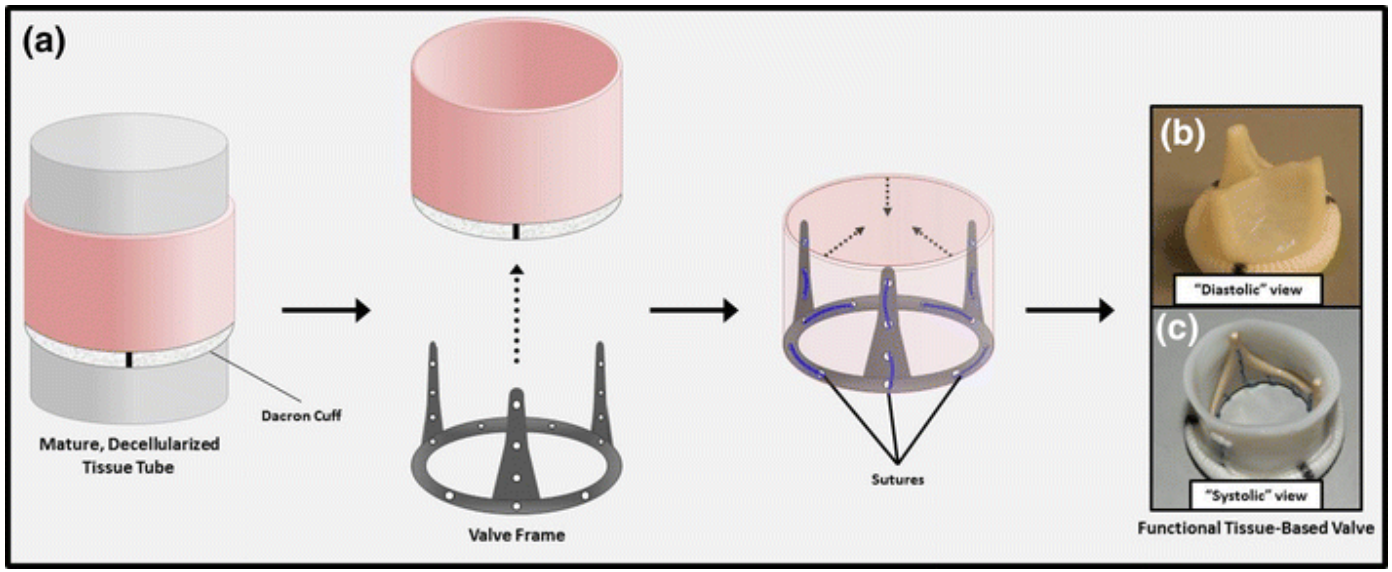

Fig 2.11. Tubular fibrin TEHV scaffold. A fibrin tube is first synthesized and 'matured' in a flow bioreactor with fibroblasts, which remodel the scaffold to include fiber alignment. The resulting tissue tube is fitted onto a frame and sutured into place in such a way that three coapting leaflets are formed, mimicking native semilunar valve structures (reprinted with permission from[139]).

The ability to alter the alignment of ES fibers also allows for the creation of anisotropic mechanical properties within a sample. It is precisely this anisotropy control that makes electrospinning attractive to tissue engineered heart valve biomaterials research. Unfortunately, the scale of ES scaffolds may be too small to promote cellular invasion, therefore researchers have begun to create complex, composite ES scaffolds pre-seeded with cells. For instance, while initial results in creating an ES poly(ester urea urethane) (PEUU) scaffold were successful in creating anisotropic mechanical properties similar to native pulmonary valves, little cellular invasion into these systems was observed [146]. Further work has been done to create an ES system capable of integrating smooth muscle cells into the PEUU fibers during the electrospinning process [147]. Such a composite system exhibits physiologically interesting mechanical properties as well as the ability to control cell alignment with external mechanical stimulation, as exhibited by Stella et al. (Fig. 2.12) [148]. Polycaprolactone fibers produced by electrospinning created a functional bioabsorbable scaffold that has leaflets which opened synchronously and exhibit correct coaptation in the diastolic phase although additional studies are needed [144]. Interestingly, a research group reported that mesenchymal stem cells seeded on polydioxaneone (PDO) electrospun bioabsorbable patches were implanted into the right ventricle outflow tract of 6 lambs for up to 8 months. They found that PDO scaffolds were completely degraded and replaced by endothelialized tissue with an ECM similar to native tissue [149].

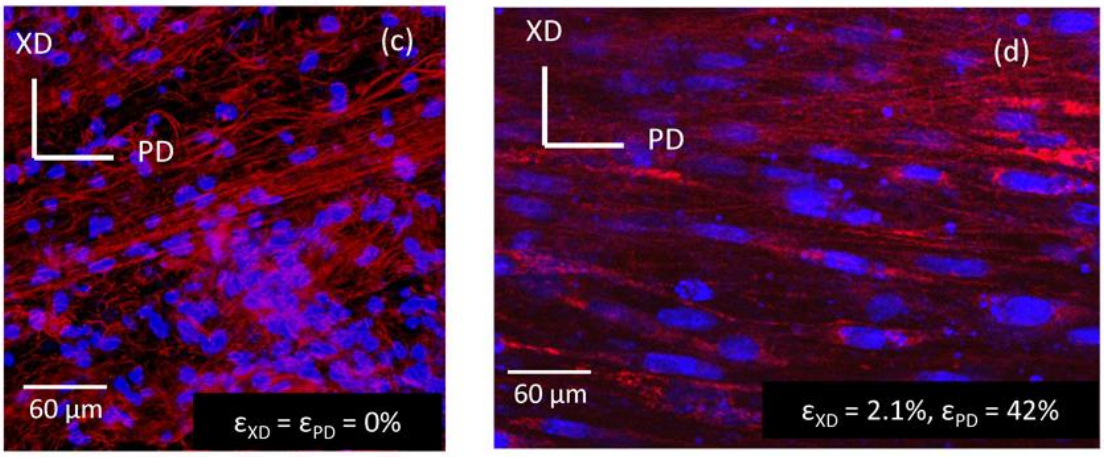

Fig 2.12. ES fibers and cell alignment. Fluorescent microscope images showing cell-scaffold constructs made via electrospinning PEUU and concurrently electrospraying rat vascular smooth muscle cells onto a rotating mandrel. (Left, c) Constructs in a static (non-strained) environment show rounded cell nuclei (blue) and random fiber orientation (red). (Right, d) Constructs under biaxial strain show elongated cell nuclei and PEUU fiber alignment, demonstrating enhanced mechanical properties of electrospun polymers compared with natural polymer systems (reprinted with permission [150]).

2.10 Cell Sources for TEHV

Another important consideration in future development of TEHV is the selection of a source of cells to seed onto scaffolds, since these cells would ultimately be responsible for remodeling the scaffold into a fully functional HV leaflet. Ideally a patient's own cells could be harvested for this purpose, however this may be impractical depending on the severity of the patient's condition [151]. In one study, Hoffman-Kim et al. looked at three different cell lines as potential seeding sources for tissue engineering scaffolds. Sheep cells from the tricuspid HV leaflet were compared to cells obtained from the jugular vein and carotid artery. Cells from the jugular veins showed higher initial production of collagen *in vitro* compared to the other lines. This study also demonstrated that synthesis of collagen, elastin, and GAGs significantly decreased as passage number

increased (up to passage 4, 28 days) in all cells lines. This trend may indicate a time and/or passage limit for seeded cells to perform necessary protein synthesis and organization in TEHV scaffolds. Other research groups are focusing on a wide variety of cell lines as potential sources for TEHVs. Numerous groups have previously reported the use of mesenchymal stem cells (MSCs), EPCs, or VICs and/or VECs to seed scaffolds in attempts to promote a specific type of cell behavior. A common behavior of all of these cells is that they exhibit remodeling potential that can be useful in controlling valve properties [152]. For example, Cebotari et al. demonstrated that allograft valves seeded with autologous EPCs in juveniles exhibited function and somatic growth, presumably due to cellular behavior within the valves [153]. However the feasibility and practicality of using autologous valve cells from a patient who needs a valve replacement is disputable. Also, it is uncertain that a sufficient number of valve cells could be grown in a suitable timeline for patients needing a valve replacement; although some initial work has been done to determine an appropriate seeding density of VICs [154]. Frank et al. report an *in vitro* conditioned human pulmonary valve seeded with autologous VICs showed significant cell proliferation and seeding within 4 days of culture, suggesting that it might be possible to generate valves seeded with autologous cells in a relatively short time frame. In another approach, researchers are attempting to use alternative cell types, and provide them with biological or mechanical signals necessary to generate valve-like cells. For example, Appleton et al. demonstrated that vascular smooth muscle cells harvested from rat aortas exhibit a myofibroblast-like phenotype when exposed

to TGF-β1, basic fibroblast growth factor (bFGF), and platelet derived growth factor (PDGF) [155]. Although this treatment showed increased collagen, fibronectin, and versican, there is some uncertainty in its potential use as a cell source in valve replacements, since a prolonged active phenotype is also the hallmark of numerous HV disease states. Ideally, a cell source for TEHVs will exhibit phenotype plasticity, or stem cell-like behavior by being able to modulate between active and quiescent phenotypes based on flow regimes, mechanical environment, and biochemical signaling factors.

It is important to note that VICs and their embryonic progenitors are obviously the first and best choice for creating viable TEHVs that most closely resemble natural valves. The exact characteristics of these cells are not well understood, although significant progress has been made in defining the genetic composition of VICs [156]. Equally important to understanding the genetic components, is to further our knowledge of the mechanical factors important in the development and maintenance of VICs and their progenitors. In particular, the dynamic mechanical environment of endocardial cushions and embryonic valve leaflets may regulate the maturation of VICs and ultimately define their expression profiles. Being able to mimic the appropriate signaling and mechanical environment of these cells would create a platform for utilizing these cells to develop and remodel natural biomaterial scaffolds into viable TEHVs.

Because initiating and controlling EMT is the proposed first key step in creating a TEHV, a cell type with behavior similar to cells formed during EMT represents a promising source for scaffolds. A study by Paruchuri et al.

demonstrated that human pulmonary valve progenitor cells show phenotypic plasticity that can be modulated between endothelial and mesenchymal states by introduction of VEGF or TGF-β2 treatment, respectively [90]. In these studies, clones of valve progenitor cells were shown to vary between endothelial markers and mesenchymal behavior (increased αSMA, migration, invasion, MMP-1 and 2). This control of behavior and phenotype is needed in an EMT-inducing platform for TEHVs. The mesenchymal cells that arise from endocardial EMT are the cellular progenitors of VICs in mature heart valves; as such, they possess all of the desired traits of cells for TEHV research purposes. These cells have been historically difficult to obtain as harvesting from embryonic timepoints has a low efficiency; thus a biomaterial platform, with controllable substrate mechanics, could provide a method of generating large enough populations of these cells for necessary studies to aide in synthesis of viable TEHV replacements.

2.11 Future Directions in TEHVs

The road to creating a usable TEHV replacement is a challenging one, filled with the need to improve chemical, biological, and mechanical properties of any proposed system. Advances in understanding the characteristics of the developing HV and the environment that creates it will allow researchers to pursue cell-directive materials for creation of a valve scaffold that can be invaded and remodeled after implantation in a patient. This prospective also provides a starting point for further biomaterial research, instead of the ‘ready, shoot, aim’

approach currently used by selecting a material used in other applications and then testing its functionality as a HV scaffold. Biomaterials that induce EMT and other developmental behaviors offer the ability to control and direct cellularization of potential HV replacements, but these materials alone lack the needed mechanical properties to be physiologically relevant. As we get closer to living valve replacements, we will also have to make decisions about how to best evaluate their structure and function. Current regulations for heart valve replacements are relevant only for the non-viable mechanical and bioprosthetic valves used clinically [157]. Such guidelines will be important for screening potential scaffold candidates for preclinical and clinical trials. The studies highlighted above represent interesting advances in biomaterials for tissue engineered hearts valves at different stages in their progress from bench to bedside. For the interested reader, additional reviews on heart valve tissue engineering are available [12, 29, 158-161].

2.12 Conclusions

To develop the next generation of TEHVs, focusing on viable systems that will permit cell invasion and ECM synthesis and remodeling, we must first understand the native biomechanical environment that gives rise to the complex architecture of fully mature HV leaflets. This includes improving our understanding of both the cellular and tissue level mechanics and mechanotransduction pathways important in regulating valve structure and

function. By studying the role of mechanics in EMT, we can better design scaffolds based on native materials that incorporate cell-directive cues. Despite advances in polymeric materials, no satisfactory unification of natural materials and native mechanical context exists for the study of mature or progenitor VICs. Understanding the mechanical environment of EMT, a critical first step in the formation of HVs, and how these biomechanical factors alter cell behavior is crucial in understanding the etiologies and pathologies of CHDs and degenerative valve disorders as well as developing viable TEHV platforms.

Table 2.1. Synthetic biomaterials used for heart valve tissue engineering

Biomaterial	Cell Line Used [a]	Implanted Into	References
PEG	hMSCs	na	[104-108, 162]
PGA/PLA	Ovine fibroblasts, ECs, Human fibroblasts, bovine aortic ECs	Lamb (2 weeks)	[111-112]
PGA/P4HB	Ovine myofibroblasts, ECs Ovine vascular and SCs, Ovine EPCs, VECs	Lamb (20wks) Sheep (8 weeks)	[114-118]
PCL	na	na	[143-144]
PEUU	Human myofibroblasts Rat SMCs	na	[146-148, 163]
PDO	Sheep MSCs	Sheep (1, 4, 8 months)	[149]
PCU-POSS	na	na	[110]

a: Cell Line Abbreviations. Human mesenchymal stem cells (hMSCs), endothelial cells (ECs), stem cells (SCs), smooth muscle cells (SMCs), human dermal fibroblasts (hDF), human umbilical vein endothelial cells (HUVECs), endothelial progenitor cells (EPCs), valvular endothelial cells (VECs), valvular interstitial cells (VICs). na = not applicable.

Table 2.2. Natural biomaterials used for heart valve tissue engineering

Biomaterial	Cell Line Used [a]	Implanted Into	References
Collagen	Porcine VICs	Rats	[123]
Hyaluronic Acid (HA)	Porcine VICs Rat SMCs	na	[113, 119, 121, 126]
Collagen/HA Composites	hDF	na	[121-122]
Collagen/Chondroitin Sulfate Composite	Porcine VICs,VECs	na	[120]
Fibrin/Fibronectin	hDF, Human aortic myofibroblasts, Porcine VICs Ovine arterial ECs	Sheep (3 months)	[129, 133-137]
Hydroxyapatite (HAp)	HUVECs	na	[140]

a: Cell Line Abbreviations. Human mesenchymal stem cells (hMSCs), endothelial cells (ECs), stem cells (SCs), smooth muscle cells (SMCs), human dermal fibroblasts (hDF), human umbilical vein endothelial cells (HUVECs), endothelial progenitor cells (EPCs), valvular endothelial cells (VECs), valvular interstitial cells (VICs). na = not applicable.

Chapter 3

Development of an AFM Technique for Micromechanical Analysis of HV Leaflets

Text for Chapter 3 taken from:

> Sewell-Loftin, M.K., Brown, C.B., Baldwin, H.S., and W.D. Merryman. *A Novel Technique for Quantifying Mouse Heart Valve Leaflet Stiffness with Atomic Force Microcscopy.* J Heart Valve Dis, 2012; 21:513-20.

3.1 Introduction

The creation of viable TEHVs, capable of growth and remodeling inside patients, depends on our understanding of the mechanobiology of the native tissues; HV leaflets are mechanically sensitive and active, using hemodynamic cues to VECs to instruct VICs in appropriate maintenance and/or remodeling of the leaflet ECM as necessary to ensure proper valve function. The stiffness of HV leaflets is critical in the proper opening and closing of the valve structure. If the leaflets are too stiff, they cannot fully coapt and thus permit retrograde blood flow. However, if the leaflets are overly soft then the valve will collapse under the weight of blood when in the closed position. Since mechanical stiffness is important in valve structure and function, we have developed a micromechanical analysis technique for HV leaflet tissues that permits concomitant interrogation of

valve stiffness and ECM composition via traditional histological techniques. Furthemore, we demonstrate that this technique is useful in profiling mechanical phenotypes of genetically-altered mouse models of HV disease.

Although in the past, acquired heart valve disease research has been limited due to a lack of appropriate animal models, during recent years the ApoE and Notch1 genetically altered animal models have been found to acquire aortic valve (AV) sclerosis, calcification, and stenosis at an age similar to humans [2, 164-167]. Specifically, AV sclerosis in ApoE homozygous mice is characterized by an increased AV flow velocity after 43 weeks of age compared to age-matched wild-type (WT) animals [165], with areas of ectopic calcification, cells positive for smooth muscle α-actin (αSMA) and osteoblast-related proteins, and frequent apoptosis, all of which are common markers of degenerative AV disease in humans [167]. Notch1 heterozygous mutations have been shown to cause bicuspid AVs and subsequently to increase the risk for calcific valve disease in humans [164, 166]. Similar to ApoE animals, 10-month-old Notch1 leaflets have been found to have significant calcification, over five-fold greater when compared to age-matched WT littermates. While ApoE and Notch1 mice have an apparent change in morphology and hemodynamics, the resulting functional biomechanical changes have not been quantified. The primary reason for this is that the biomechanical assessment of mouse AV leaflets is very difficult due to the small size of the leaflet tissue. Recently, micropipette aspiration was utilized to quantify the mechanical properties of mouse AV leaflets [99]; however, while the technique proved to be successful it was laborious and required the use of

entire leaflets. Consequently, an atomic force microscopy (AFM) strategy was developed to quantify the mechanical properties of mouse AV leaflets, with the aim of demonstrating this proof-of-principle technique using WT, ApoE, and Notch1 mice. The AFM technique described was also advantageous in that the leaflet tissue mechanical properties of genetically altered animals can be determined in conjunction with standard histological cryosectioning techniques.

The AFM technique was developed almost 30 years ago as an extension of scanning tunneling microscopy, where forces as small as 10^{-18} N were used to achieve Ångstrom-level resolution in the study of sample surfaces [168]. Although AFM was developed primarily for studying topography on hard surfaces, such as ordered graphite and silicate compounds, biopolymers soon became an interesting topic of examination using this method [169]. Several initial studies demonstrated the promise of AFM as a means of obtaining measurements of the mechanical and adhesive properties of tissues, cells, and even of biomolecules that, previously, had been impossible. Unfortunately, it has taken many years for AFM to be optimized to the point where mechanical measurements can be determined, due mainly to the limitations and complications associated with extremely soft and thin samples [170-171]. In AFM, a nanoscale tip is attached to a cantilever which has a reflective coating on the reverse side. The movement of the tip - and hence sample deformation - is measured by the degree to which a laser beam is deflected off the cantilever, as captured by a sensor. One problem here is that, as the extremely soft samples are often punctured by the AFM tip, this can result in a quantification of the

substrate beneath the sample. Consequently, tip and scan parameter selection is paramount to assure accurate measurements of biological samples.

In the present study, a novel AFM technique was developed for the mechanical analysis of mouse AV leaflets. Further, in order to ensure that the mechanical quantification of AV leaflet sections was accurate, the AFM tip and scanning parameters were validated on homogeneous and linear isotropic polymer standards over a range of leaflet stiffness values. The polymer standards were examined both with AFM and bulk mechanical testing methods, to establish the validity of the quantitative method described in this feasibility study. It should be noted that an extensive review of AFM techniques in the analysis of biological samples is available, if required [172].

3.2 Materials and Methods

Mice leaflets

The 2- and 17-month-old WT C57blk6 mice and 20-month-old ApoE homozygous mice on C57blk6 used in the studies were obtained from Jackson Laboratory (Bar Harbor, ME, USA). A Notch1 heterozygous male retired breeder on a mixed CD-1 background was a generous gift from Dr. Stacey Huppert (Vanderbilt University). All animals were maintained on a standard diet under approved IACUC protocols. The mice were euthanized by CO_2 asphyxiation and the hearts excised into cold phosphate-buffered saline (PBS). The AVs were then

removed into cold PBS, flash-frozen in optimal cutting temperature compound (OCT); sections (10 μm) were then cut and stored at -20°C until analyzed.

For analysis, the sections were stained for 30 min with 1:300 fluorescein isothiocyanate (FITC) CD31 (558738; BD Pharmingen, San Diego CA, USA) and Cy3 αSMA (C6198; Sigma, St. Louis, MO, USA) in Hank's buffered salt solution containing 0.2% fetal bovine serum (FBS) and 0.1μg/ml 4',6-diamidino-2-phenylindole (DAPI) nuclear stain. The slides were washed three times in PBS, rinsed in distilled water, and air-dried for 10 min prior to AFM scanning (Fig. 3.1). Adjacent tissue sections from the same animals used in the AFM study were also stained using Movat's Pentachrome (K042; Poly Scientific R&D Corporation, Bay Shore NY, USA). All histological images were recorded using a Nikon Eclipse E800 microscope (Nikon Inc., Melville, NY, USA) with a Spot RT3 camera (Spot Imaging Solutions, Sterling Heights, MI, NY).

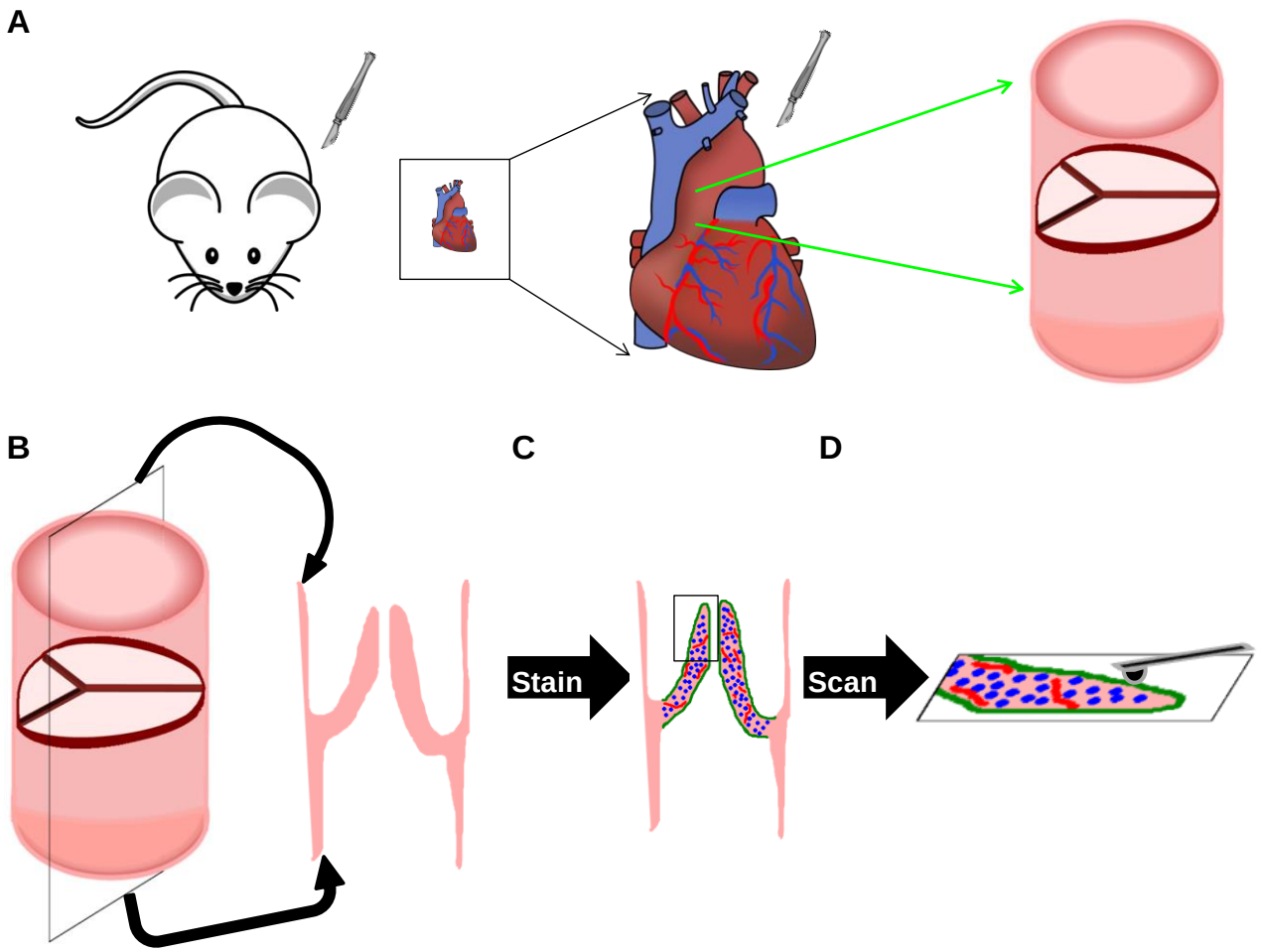

Fig 3.1. Scheme for HV processing for AFM analysis. (A) Schematic showing how mouse AV leaflets are harvested and sectioned. (B) Heart valve sections are positioned such that the cross-section of each leaflet is available for scanning, eliminating the concern of only observing surface phenomena with the AFM. (C) Slides are stained without fixation to ensure minimal disruption of the ECM. (D) Slides are subjected to scanning via PF-QNM mode of an AFM.

PDMS standards and bulk modulus measurements

Poly(dimethyl siloxane) (PDMS; Sylgard 184, Dow Corning, Midland, MI, USA) standards were prepared by mixing the base and curing agent in 10:1, 15:1, and 30:1 ratios before curing overnight under vacuum at 60°C. Bulk modulus measurements were made under uniaxial tension with standard masses (0.05-0.5 g for 10:1 and 15:1 gels, 0.01-0.2 g for 30:1 gels) used to deform the PDMS strips in a free-hanging set-up. The bulk modulus was calculated as the slope of the line generated by plotting a graph of stress versus strain (n = 4).

Atomic force microscopy

A Catalyst Bioscope atomic force microscope (Bruker AXS, Madison, WI, USA) was used for all measurements. The system was operated in Peak Force Quantitative Nanomechanical Mapping (PF-QNM) mode, which is a modified tapping-mode modality in a non-fluid environment. The sample modulus (E) is calculated by the software using the following equation after setting Poisson's ratio (υ) = 0.5:

$$\mathbf{F_{tip}} = \frac{\mathbf{4}}{\mathbf{3}}\mathbf{E}\sqrt{\mathbf{Rd^3}} + \mathbf{F_{adh}}$$

where F_{tip} is the force on the tip, R is the radius of the tip, d is the distance between the tip and sample, and F_{adh} is the adhesive force between the tip and sample. Borosilicate glass tips (Novascan Technologies, Inc., Ames, IA, USA) with a nominal diameter of 5 μm and nominal spring constant of 0.03 N/m were

used. Prior to sample measurements, the tip radii were calibrated using a PDMS calibration standard sample (E = 2.5MPa) provided by Bruker. Individual probe spring constants were calculated using the thermal tune method built into the AFM software; these values typically varied between ±25% from the nominal spring constant due to manufacturing variations. This parameter is crucial for the accurate calculation of F_{tip} and F_{adh} used in the above equation.

AFM scanning parameters

The AV leaflet sections were scanned at 20 × 20μm to 30 × 30μm areas, 0.1 Hz scan rate, and peak force set-points between 0.1 and 1nN, with peak force set-points being varied to ensure a correct calibration on the standard 2.5MPa PDMS sample. The scan areas were varied to ensure the correct alignment of features between AFM images and fluorescence microscopy images; changing this parameter had no effect on the stiffness values measured with AFM. For AV leaflet sections, at least two scans were taken on adjacent areas of each section of leaflet, and multiple sections and animals were used where possible. For PDMS standards, the scan parameters were 0.5 × 1μm scan areas, 0.25Hz scan rate, and peak force set-points between 10 and 100pN. On each PDMS sample, three adjacent areas were scanned to determine the PDMS modulus.

Porcine leaflet analysis

In order to compare the AFM micromechanical analysis technique to other methods, the stiffness of porcine AV leaflets that had been extensively mechanically characterized by other techniques [37, 173-176] was quantified. An AV leaflet from the heart of a mature pig was obtained from a local abattoir and treated in the same manner as the mouse leaflets, except that 3 μl of Hoechst 33342 (Invitrogen, Eugene, OR, USA) staining was substituted for DAPI, and no CD31 stain was utilized. For the AFM micromechanical analysis, a borosilicate particle tip with a nominal diameter of 5 μm and a nominal spring constant of 0.06 N/m was used. The tip was calibrated using the above-described method, using the same scan parameters. The extracellular matrix (ECM) composition of the sample was determined using Movat's Pentachrome stain.

Statistical analysis

Because the scan regions of the AV leaflets were not homogeneous, the AFM data were represented as modulus versus percentage of the scan area. The median of each scan distribution was taken as the representative modulus for that particular scan; variability within specimens was determined by averaging the median values (each representing a single scan) for a given sample of AV leaflets. The average median values of all groups were compared with ANOVA, while pair-wise multiple comparisons were made using the Holm-Sidak post-hoc testing method.

3.3 Results

PDMS standard bulk modulus and AFM modulus measurements

For PDMS, the AFM modulus was highly correlated (R^2 = 0.997) with the bulk modulus (Fig. 3.2), which indicated that the PF-QNM scanning and above-described calibration methods were appropriate for analyzing soft tissues such as AV leaflets, which have modulus values <2MPa. The use of PDMS as a standard (and as discussed here) is not specific to the types of sample to be analyzed by AFM; rather, it is used to verify that the AFM system has accurately reported nanomechanical properties that are highly correlated with the bulk modulus mechanical properties. Hence, this demonstrates that when a tip has been accurately calibrated, the software is capable of analyzing a wide variety of topographies, provided that the mechanical properties are similar to the calibration standard and that the force-displacement curves exhibit the same trend.

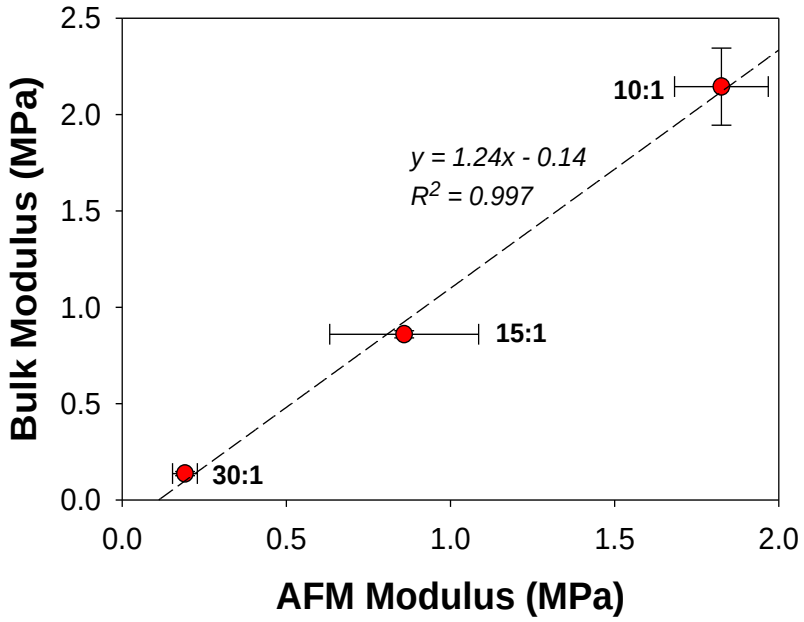

Fig 3.2. Validation of AFM calibration on soft substrates. Bulk modulus and AFM median modulus of PDMS gels show close agreement. Data shown as mean ± SE; n = 3(AFM) or 4(bulk).

Mouse AV leaflet modulus

Mouse AV leaflets have a heterogeneous ECM, with various proteins of different stiffness; thus, it was not surprising that the modulus of the leaflet tissues had a wide distribution (Fig. 3.3). As the shape and skew of the distributions varied between scans, median modulus values were chosen to compare differences between groups (Fig. 3.4). All leaflets were significantly stiffer compared to the 2- month-old WT leaflets (Fig. 3.4; $p < 0.05$), while the 10-month-old Notch1 leaflet modulus was significantly greater than that of all other groups (Fig. 3.4; $p < 0.01$). This particular AFM system has a unique feature that allows for three-channel fluorescence image guidance, as well as an ability to create topographical maps with color-coated modulus values overlaid to compare or correlate regional morphologies and stiffness values (Fig. 3.5).

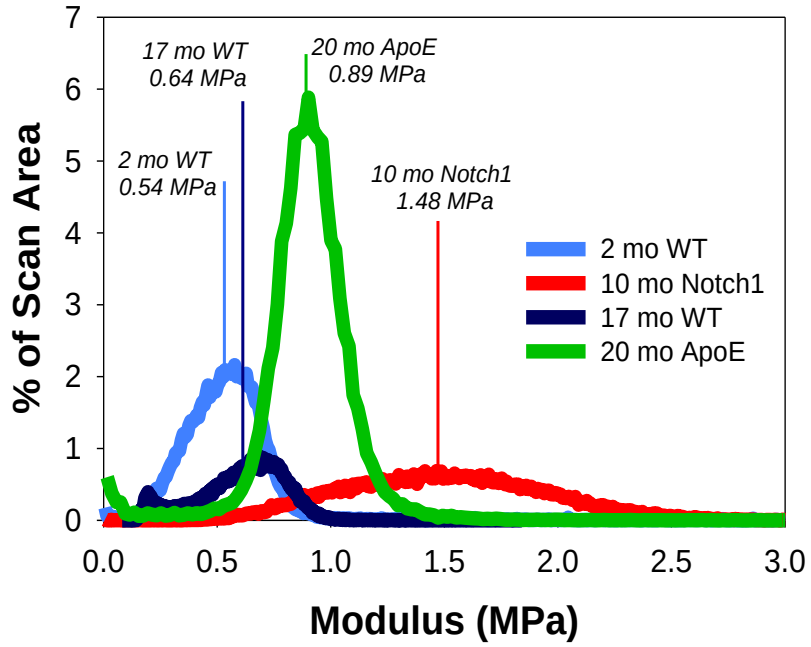

Fig 3.3. Representative modulus data from HV leaflet scans. Modulus data is extracted from AFM scans in histogram format, indicating frequency of a specific modulus value observed within that scan. Drawn vertical lines represent median modulus values, which are used to compare between sample groups.

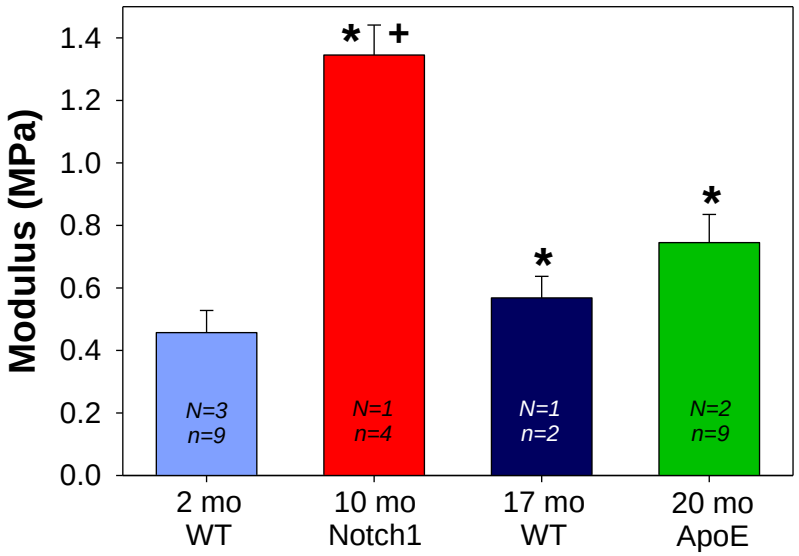

Fig 3.4. Average stiffness of HV leaflets. Median values from each scan were lumped together by age and genotype and aggregated into an average modulus to permit statistical analysis between samples. N = number of animals and n = number of scanned regions on sections of tissue used for analysis. AV leaflets from 10 month old Notch1, 17 month old WT, and 20 month old ApoE animals were significantly stiffer (* = $p<0.05$) versus 2 month old WT animals. The AV leaflets from the 10 month old Notch1 animal were significantly stiffer than all other groups (+ = $p<0.01$).

Mouse AV leaflet histology

As noted above, the AFM technique developed for these studies is particularly powerful as it allows for the mechanical quantification of leaflets, without requiring or destroying an entire leaflet. Specifically, this technique dovetails with standard histological processing, and consequently Movat's Pentachrome was used to analyze sections adjacent to those subjected to AFM scanning. The most common feature in all leaflets was an abundance of ground substance near the tip of the leaflet and surrounding the scan regions (Fig. 3.6, the circled regions approximate the scan region on an adjacent section). The older animals showed more structural ECM components, such as areas of collagen or elastin (as indicated by arrows), but this can be explained by the changes in valve structure that occur over the lifespan of the mouse [177]. It should be noted that there was no well-defined trilaminar matrix, as is seen in large mammals and human leaflets; this point was observed previously by Hinton et al. [89].

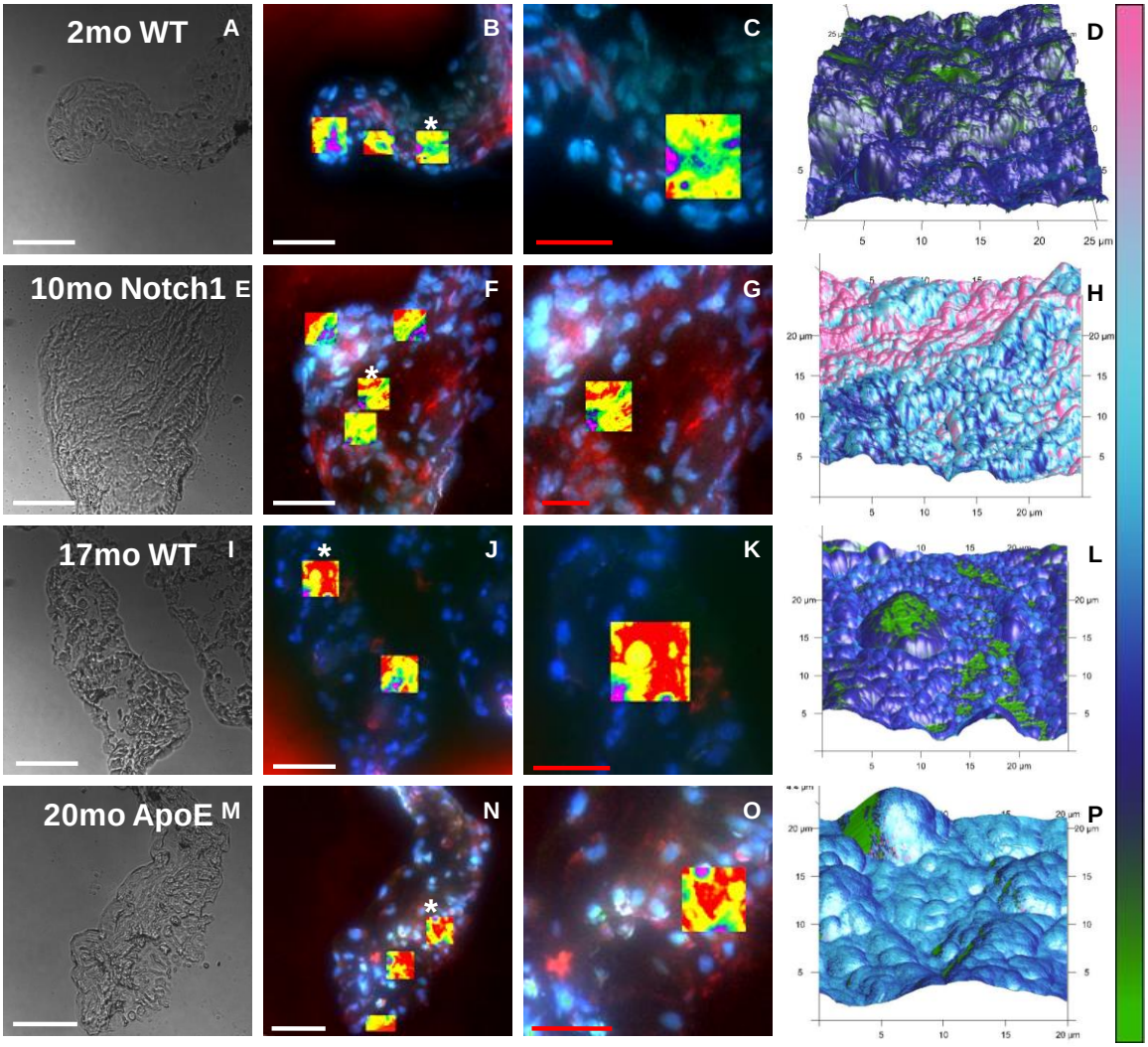

Fig 3.5. 3D topographical map of HV leaflet stiffness. Bright field and three channel fluorescent images (red = αSMA, green = CD31, and blue = nuclei) of leaflet sections analyzed by AFM. Rows correspond to sample group, in order of increasing age: 2mo WT, 10mo Notch1, 17mo WT, and 20mo ApoE. Bright field images at 40X: A,F,K,P. Fluorescent images showing all areas scanned by AFM, highlighted by overlay of height sensor data: B,F,J,N. Close-ups of areas marked by * in B,F,J,N, showing a scan region in more detail: C,G,K,O. Stiffness values overlaid on three-dimensional topographical maps corresponding to regions shown in third column: D,H,L,P. White scale bar = 50μm; red scale bar =25μm. Modulus scale bar = 0-2MPa.

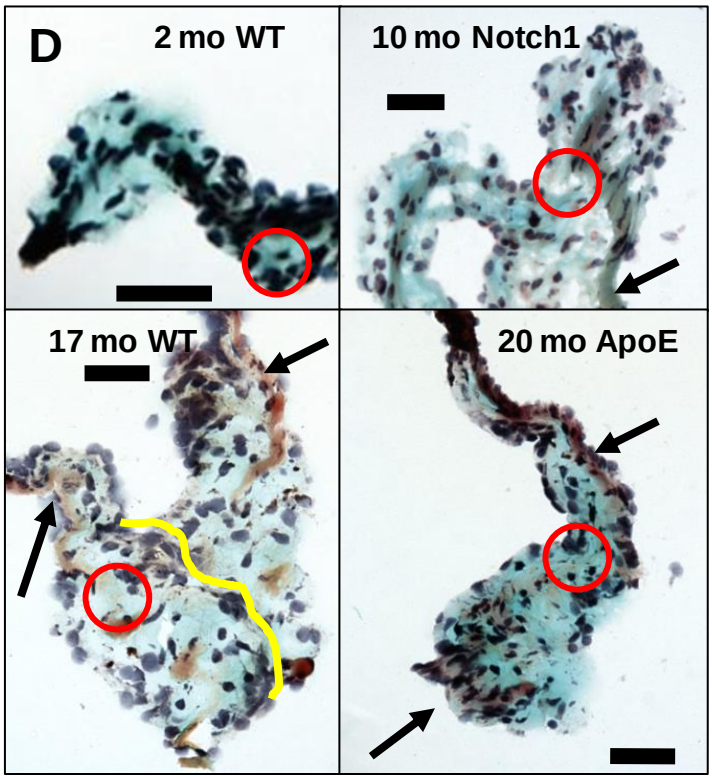

Fig 3.6. Histological images of HV leaflets in mechanical analyses. Staining with Movat's Pentachrome was used to ensure that comparable regions were selected for mechanical analyses on the valve samples. Arrowheads indicate regions of collagen (yellow); arrows indicate regions of elastin (purple/black) present in older animal sections. Line in 17mo WT added to show demarcation between the two leaflets. Black = nuclei; Purple = elastin; Blue = ground substance; Yellow = collagen; Red = Fibrous regions. Scale bar = 50 μm.

Porcine AV leaflet modulus and histology

The results showed that slight differences in stiffness occurred across the thickness of the leaflet, and that these corresponded to the spongiosa region being less stiff (though not significantly so) than both the fibrosa and ventricularis of the leaflet (Fig. 3.7A). The histological slides illustrated the definitive trilaminar structure of the porcine leaflets, which was similar to that of human valve leaflets (Fig. 3.7B). The stiffness values obtained in the present study were in the same range as values collected from mouse valves, thus reinforcing the benefit of using AFM to perform quantitative biomechanical analyses.

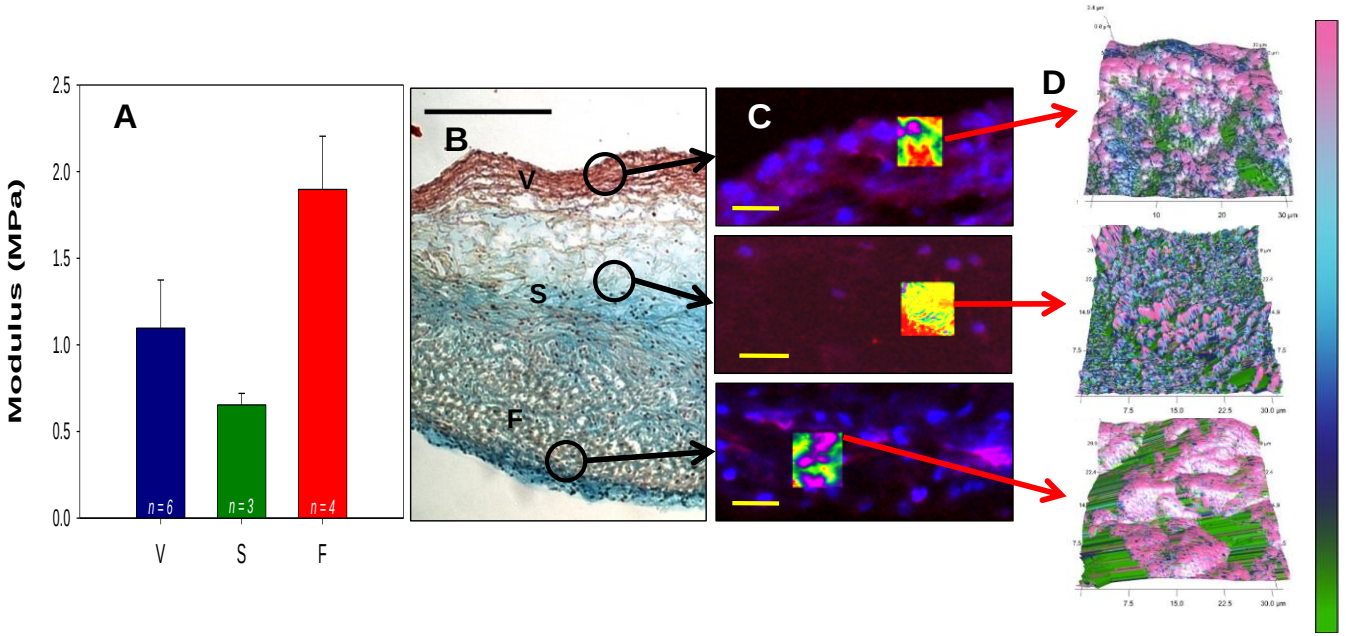

Fig 3.7. Micromechanical analysis of a porcine aortic valve leaflet. V = ventricularis, S = spongiosa, F = fibrosa. (A) Average median stiffness values of the three layers of the porcine AV leaflet, with the spongiosa the most compliant and the fibrosa the stiffest layer. (B) Histological image of porcine AV leaflet; circled areas indicated approximate regions scanned by AFM. Scale bar = 500□m. (C) Fluorescent images (red = □SMA, blue = Hoescht) of AV leaflet layer regions scanned by AFM. Areas highlighted are overlays of AFM height data, to indicate scan region. Scale bar = 30□m. (D) Call-outs show three-dimensional topographical map with stiffness values overlaid. Modulus scale bar: 0-2 MPa.

3.4 Discussion

AV leaflet stiffness increases with age and ApoE or Notch1 mutation

As expected, the AFM technique was able to detect slight variations in leaflet stiffness. Specifically, aged mice had stiffer AV leaflets than the young WT animals (Fig. 3.4), while the Notch1 animal had the stiffest AV leaflets, with a modulus more than two-fold higher than the aged WT animals ($p < 0.01$). The ApoE leaflets were slightly stiffer than the 'age-matched' WT leaflets, although not significantly so. The finding that ApoE leaflets were not significantly stiffer, even in this preliminary study with minimal samples, might indicate that the hemodynamic changes observed in these animals [165] may be caused by minor increases in AV leaflet stiffness. Finally, while the precise role of Notch1 in causing AV disease is unclear, the leaflets from the 10-month-old Notch1 animals in this study were significantly stiffer than the much older WT or ApoE leaflets, indicating that the Notch1 mutation may significantly alter AV leaflet ECM stiffness, perhaps at earlier time points than the ApoE mutation. Interestingly, the results of WT tissue analysis were in the range of results from micropipette aspiration measurements of mouse AV cusps, which were approximately 300 kPa for a wide age range of animals [99], and thus support the use of AFM as a technique to analyze the biomechanical properties of mouse heart valve leaflets.

Differences in AV stiffness is not revealed by histology

Histology results indicated heterogeneous profiles across all of the leaflets imaged (Fig. 3.6). Despite this variation, the thickest portions of the leaflets - those scanned by AFM - were composed primarily of ground substance with small amounts of structural proteins such as collagen or elastin. Although the leaflets from older animals showed more of these proteins than did those of young WT animals, the histological images indicated that similar areas had been scanned in all samples (Fig. 3.6). Whilst further studies are clearly required to determine the specific causes of stiffness differences between samples, these initial findings confirm the ability to characterize the biomechanical properties of tissues by using AFM.

Regional variations in stiffness of porcine AV leaflets

Porcine valve leaflets are more similar to human leaflets than those of mice, in that they exhibit a definitive trilaminar structure. The spongiosa, which is rich in glycosaminoglycans, is the softest portion of the valve leaflet, while the fibrosa and ventricularis, which are rich in collagen and elastin respectively, exhibit higher stiffness values than the spongiosa. The differences between the regions of the leaflet tissue highlight the importance of coupling histology with AFM when measuring leaflet stiffness since, without histological guidance, the differences between measured stiffness values could not be attributed to the physiological composition of the tissue. Moreover, by using Movat's Pentachrome to determine the boundaries between fibrosa, spongiosa, and

ventricularis, the selection of appropriate regions for AFM analysis becomes clear. In addition, the values measured in the present study were comparable to those determined using other methods, such as micropipette aspiration and three-point bending [99, 175].

Study limitations

The primary limitation of the micromechanical analysis of mouse AV leaflets using AFM was the need to identify appropriate and comparable scanning regions between leaflet samples, so as to ensure that any inter-sample differences were significant and not simply artifacts due to variations between scan locations. This limitation was a result of the complex, heterogeneous nature of the mouse heart valve leaflets, the free edges of which are composed of a poorly defined bilaminar structure of fibrosa and spongiosa [177], providing comparable regions for analysis. It is important to note that, in larger mammals such as pigs and sheep, the trilaminar structure of the AV leaflets is more similar to that of human AV leaflets. In the case of the porcine AV leaflet sample, differences in ECM composition revealed variations in stiffness; hence, multiple scans per section, as well as multiple sections per animal, would be required to ensure a correct characterization of the leaflets' mechanical properties. Likewise, an histologic analysis of adjacent tissue sections would be critical to determining the relevant ECM characteristics of the scanned regions.

Sample treatment prior to AFM scanning was also an important consideration. For example, after cryopreservation the heart valve leaflet tissues

retained their ECM composition, but the elastin and collagen fibers may have been deformed to some extent [178]. During freezing of the tissue, the formation of ice crystals can disrupt the complex ECM network [178-180], and this would lead to the disruption of a large portion of the valve leaflet section, such that the leaflet stiffness might be underestimated with AFM. Conversely, chemical fixatives permeate the cell membranes and crosslink the ECM proteins, increasing tissue stiffness. Alternative sectioning techniques (notably paraffin embedding) employ tissue dehydration and temperatures >50°C, which would cause protein denaturation and altered mechanical characteristics. Consequently, methods of sample collection and processing were selected that would have minimal effects on the biomechanical properties of valve leaflets. Finally, as the results obtained with the AFM technique corresponded to those acquired from mice valve leaflets analyzed using micropipette aspiration, it is highly likely that this processing strategy would cause minimal change in the leaflets' mechanical properties.

3.5 Conclusions

The strategy employed to determine the stiffness of mouse AV leaflets using AFM can provide a novel tool for research groups who utilize genetically altered animal models. Moreover, as the preparation involves standard cryosectioning techniques, the analysis can be applied without causing any significant loss of tissues that typically are required for biomechanical analyses.

In addition, because these AVs were obtained from animals that exhibited a diseased valve state similar to humans [164-167], the observed differences in stiffness values between sample types have, for the first time, described the biomechanical properties of these tissues as they relate to pathological states. Despite the present study being small in size, the quantification of valve leaflet stiffness via AFM was shown to be feasible for the biomechanical analysis of tissues in relation to heart valve disease. In the next chapter, this AFM technique will be employed to investigate alterations in biomechanical properties of HV leaflets due to genetic mutations that affect normal valvular development. Utilizing this protocol, which permits parallel mechanical and histological interrogation of HV tissues, to study how changes in developmental remodeling alter HV stiffness will help reveal important mechanobiological factors for consideration in the synthesis of TEHV scaffolds.

Chapter 4

Late Embryonic and Post-Natal Biomechanical Remodeling of Aortic Valves

Portions of Chapter IV taken from:

> Qu, X., Violette, K., Sewell-Loftin, M.K., Soslow, J., Saint-Jean, L., Brown, C.B, Hinton, R.B., Zhou, B., Merryman, W.D., and H.S. Baldwin. *A novel role for endothelial Tie1 in late gestational and post-natal semilunar valve remodeling.* Circulation; In Revision. Used with permission of H.S. Baldwin.

4.1 Introduction

Significance

The incidence of congenital heart defects is nearly 1 in 100 live births, with nearly 25% of these including some form of HV malformation [1-3]. These malformations and age-associated valve degeneration mean that nearly 300,000 HV replacement surgeries are performed each year [17]. Currently available heart valve replacements, including mechanical or bioprosthetic valves, demonstrate significant disadvantages ranging from the need for anticoagulant therapy for mechanical valve recipients to an increased risk of valve calcification with bioprosthetic replacements. Also, these prostheses lack the ability to grow and remodel once implanted, often leading to the need for reoperation to implant

larger valves in pediatric patients who are still growing. The development of viable TEHV replacements is limited by a number of factors, including a limited understanding of the biomechanical properties of developing heart valves. Studying the changes that occur during heart valve formation and maturation would provide novel insight in the development of therapeutic strategies, including biomechanical context of important signaling regulators and the synthesis of mechanically-suitable TEHV replacements.

Heart valve biomechanics

Mature aortic valve leaflets exhibit a well-defined trilaminar structure consisting of a fibrosa, spongiosa, and ventricularis [88]. Each layer is characterized by a unique extracellular matrix (ECM) composition as well as specific function within the leaflet. The fibrosa, adjacent to the aorta, is composed primarily of circumferentially aligned collagen fibrils that impart anisotropic strength that prevent retrograde flow under the high transvalvular pressures applied during diastole. The spongiosa is primarily composed of glycosaminoglycans (GAGs) and is responsible for acting as both shock-absorber and lubrication during normal valve function; although, this role is somewhat debated in the literature [181]. The ventricularis, adjacent to the left ventricle, consists mostly of elastin fibers that are capable of expanding and relaxing as necessary to maintain proper opening and full closure. The ECM of the leaflets is actively maintained by a resident population of valvular interstitial cells (VICs) that remain quiescent under normal physiological conditions but can

become activated into a myofibroblast-like phenotype by a myriad of signals. Prolonged VIC activation has been linked to fibrotic and calcific valve diseases [88-89, 182-183]. Activated VICs remodeling the valve leaflets increase alpha-smooth muscle actin (αSMA) and type I collagen present in the leaflet, limiting its flexibility and thus inhibiting proper function [42, 91, 184-185].

The signaling pathways indicted in the role of degenerative valve diseases are also relevant due to parallels with developmental processes; many of the same molecules involved in the degenerative remodeling of the valve leaflet structure are critical in the proper formation of the same structure during embryonic development [13]. In the embryonic heart tube, one directional blood flow is primarily achieved by endocardial cushions located in the atrioventricular canal (AVC) and outflow tract (OFT) which will eventually remodel into the mature valves [68, 83, 186]. These cushions are lined with endocardial cells and filled with a complex ECM, primarily composed of hyaluronic acid (HA), known as cardiac jelly [63, 65]. At approximately stage E9.5 in mice, a select population of endocardial cells will undergo epithelial to mesenchymal transition (EMT) and migrate into the cardiac jelly to begin remodeling the matrix into leaflet structures. The transformed cells, VIC progenitors, are of great interest in understanding the signaling regulators important in heart valve formation, maturation, and maintenance. Furthermore, significant valvular remodeling occurs during the post-natal period as the valve leaflets respond to the changes in transvalvular pressures imposed by shifting from fetal to mature circulation; in mice, this period of valvular remodeling lasts approximately 30 days before the leaflets are

considered mature [187]. The remodeling of immature endocardial cushions into the sophisticated laminar structures of mature valve leaflets is spatiotemporally regulated by a myriad of signaling factors [68]. However, very little is known about the biomechanical environment of the developing leaflets during this time. Since heart valve structure and function are inexorably linked to biomechanical properties, a more complete understanding of the dynamic mechanical properties of these tissues needs to be constructed. An understanding of valve biomechanical remodeling associated early valvular remodeling will illuminate this understudied mechanical context of embryonic heart valves and provide new insight for both degenerative valve disease research as well as the development of viable TEHVs.

Measuring biomechanical properties of leaflets

The traditional biomechanical assays for heart valves include micropipette aspiration, reserved for either cell-level analyses or small animals such as mice, and three-point bending typically utilized with larger tissue samples such as porcine valves. At the tissue level, these techniques require the utilization of the entire leaflet for mechanical tests, precluding any parallel analysis of ECM content via traditional histological techniques. Using micropipette aspiration, Krishnamurthy et al. showed some degradation of mechanical properties of heart valves during the aging process in mice [188]. While this study is useful in the context of age-associated remodeling of heart valves associated with pathological processes, the field of biomechanics of early heart valves is still

vastly underexplored. Using atomic force microscopy (AFM), we have developed a technique that allows for concomitant examination of biomechanical properties and extracellular matrix composition via histology of heart valve tissues [189]. Utilizing this technique, we wish to analyze biomechanical changes associated with the remodeling of valve tissues.

Endothelial Signaling and EMT

The receptor tyrosine kinase Tie1 is of critical importance in the proper formation of vascular systems in developing embryos. Studies indicate that this receptor is exclusively found in endothelial cells, including vasculature and lymphatic endothelial cells [190-192]. A Tie1 homozygous null mouse model showed that the mutation is embryonic lethal, with death occurring sometime after E13.5 due to vascular instability leading to severe edema and hemorrhaging [190-191]. The onset of death in these embryos occurs after EMT occurs, indicating that the while the receptor may not play a direct role in the onset of valvulogenesis, it could be important in crosstalk between endocardial cells and VIC progenitors derived during EMT [193]. Since the complete knockout of Tie1 is an embryonic lethal mutation, alternative methods have been developed to study late embryonic remodeling by utilizing a conditional knockout [191-192]. Such studies have been used to illustrate significant differences in Tie1 expression, and thus its role, in vasculature development and atherosclerotic processes [194]. Furthermore, siRNA knockdown studies have implicated that decreased Tie1 expression induces EMT in human microvasculature endothelial

cells, reinforcing the idea that Tie1 might be an important regulator of the crosstalk between endocardial cells and mesenchymal cells in the cardiac cushions post-EMT [195].

To further our understanding of endothelial regulation during EMT and subsequent remodeling, we took advantage of the identification of a unique population of endocardial cells which do not undergo EMT in the developing heart tube. These cells express a member of the nuclear factors of activated T-cell family (Nfat), namely Nfatc1 [196-197]. While these cells do not undergo EMT themselves, they support the remodeling of endocardium as the valve elongates into the thin, flexible mature leaflet structure. Signals from these cells also play a role in directing the different mesenchymal populations, endocardium-derived and neural crest-derived, present in the OFT endocardial cushions after EMT [196]. When proper Nfatc1 signaling is impaired, more endocardial cells undergo EMT leading to altered remodeling of the embryonic aortic and pulmonary valves. Because alterations in Nfatc1 and Tie1 signaling affect post-EMT valvular remodeling, the biomechanical development of the valves is most likely also impaired. Understanding the connection between flow-induced signaling in endocardial cells and how it affects the VIC progenitors that arise during EMT could elucidate novel data about the biomechanical development of heart valves. Such information could be important in developing platforms to better address the need for viable TEHV replacements. In this study, the role of Tie1 in the biomechanical context of valvulogenesis was examined; specifically,

AFM was utilized to determine if deletion of Tie1 in the endocardium negatively affected embryonic valve remodeling.

4.2 Materials and Methods

Mouse Studies

A conditional allele for Tie1 was generated as previously described and designated *Tie1*$^{fl/fl}$ [196]. *Tie1*$^{fl/fl}$ mice were crossed with *Tie1*$^{+/lz}$ mice, which are heterozygous for the Tie1 gene with the LacZ reporter replacing one allele. *Tie1*$^{+/lz}$ mice are phenotypically normal and serve as a reporter for Tie1 expression. The *Tie1*$^{fl/lz}$ mice were then crossed to the valvular endocardical-specific Cre transgenic mice designated *Nfatc1*^{en}*Cre*, such that some of the offspring exhibited targeted deletion of *Tie1* in only these cells. Both Cre negative *Tie1*$^{fl/fl}$ and *Tie1*$^{+/lz}$ mice were used as controls to compare to the mutant mice of *Tie1*$^{fl/lz}$;*Nfatc1*^{en}*Cre*. Mice were maintained on a standard diet under an approved IACUC protocol at Vanderbilt University. Animals were sacrificed via CO_2 asphyxiation. Hearts were excised into cold PBS, and the aortic and pulmonary valves were embedded in OCT without fixation. Aortic and pulmonary valves were stained using Movat's pentachrome. Collagen content was assayed for N = 3 animals per sample group using the Sircol Soluble Collagen Assay Kit (Biocolor Ltd.). GAG content was quantified using n = 12 leaflets (N = 4 animals per sample group per valve) with the Sulfonated Glycosaminoglycan Assay (Biocolor

Ltd.). Finally, AFM was utilized to determine mechanical differences between the specimen (N = 3 animals per group).

AFM Scanning

AFM scanning was completed using a Bioscope Catalyst AFM (Bruker) operating in Peak Force—Quantitative Nanomechanical Mapping mode in air. Sections for AFM mechanical analysis were prepared as previously described [189]. Briefly, sections were rinsed in PBS to remove OCT, blocked for 20min on ice in 10% FBS, and then stained for 30min on ice in 1% FBS with 1:300 FITC CD31 (558738 BD Pharmingen), Cy3-αSMA (C6198 Sigma), and 0.1 μg/ml DAPI nuclear stain. Slides were rinsed in PBS 3X for 5min each and finally rinsed in DI H2O before drying. For AFM scanning, borosilicate glass particle tips with nominal diameter 5um and spring constant 0.03N/m were used (Novascan); each tip radius and spring constant was calibrated prior to AFM scanning using a poly(dimethylsiloxane) standard provided by Bruker. Multiple scans from each section were taken for mechanical analysis with N = 3 animals per each sample group. Prior to AFM analysis, sections were selected for histological analysis using Movat's Pentachrome staining to ensure proper selections of tissue for AFM analysis.

Statistical Analysis

For comparison of heart leaflet valve stiffness, median modulus values were collected from multiple scan areas on multiple mouse samples and

aggregated into an average median modulus value [189]. Results are reported as the average median modulus ± SEM. All other results are reported as average ± SEM. Statistical comparisons were made using ANOVA with $p<0.05$; post-hoc testing was conducted via the Holm-Sidak method.

4.3 Results

Tie1 Deletion in Endocardial Cells Increases Valve Size

Mice lacking Tie1 expression in valvular endocardial cells demonstrate enlarged aortic valve leaflets starting at E18.5 and continuing until maturity at 2 months (mo) (Fig. 4.1). There is no detectable difference in valve sizes between sample groups at stage E14.5, indicating it is late embryonic and post-natal periods where differences in remodeling occur. There is no significant difference in pulmonary valve sizes between genotypes.

ECM Remodeling is Inhibited by the Loss of Tie1

Histological results from aortic and pulmonary valves demonstrate that valvular remodeling is suppressed in mutant mice compared to littermate controls in that there is lack of collagen synthesis and accumulation of GAGs (Fig. 4.2A-D). These differences were quantified for *Tie1*$^{fl/fl}$, *Tie1*$^{fl/lz}$, and the mutant *Tie1*$^{fl/lz}$*;Nfatc1*^{en}*Cre* animals (Fig. 4.2E-F).

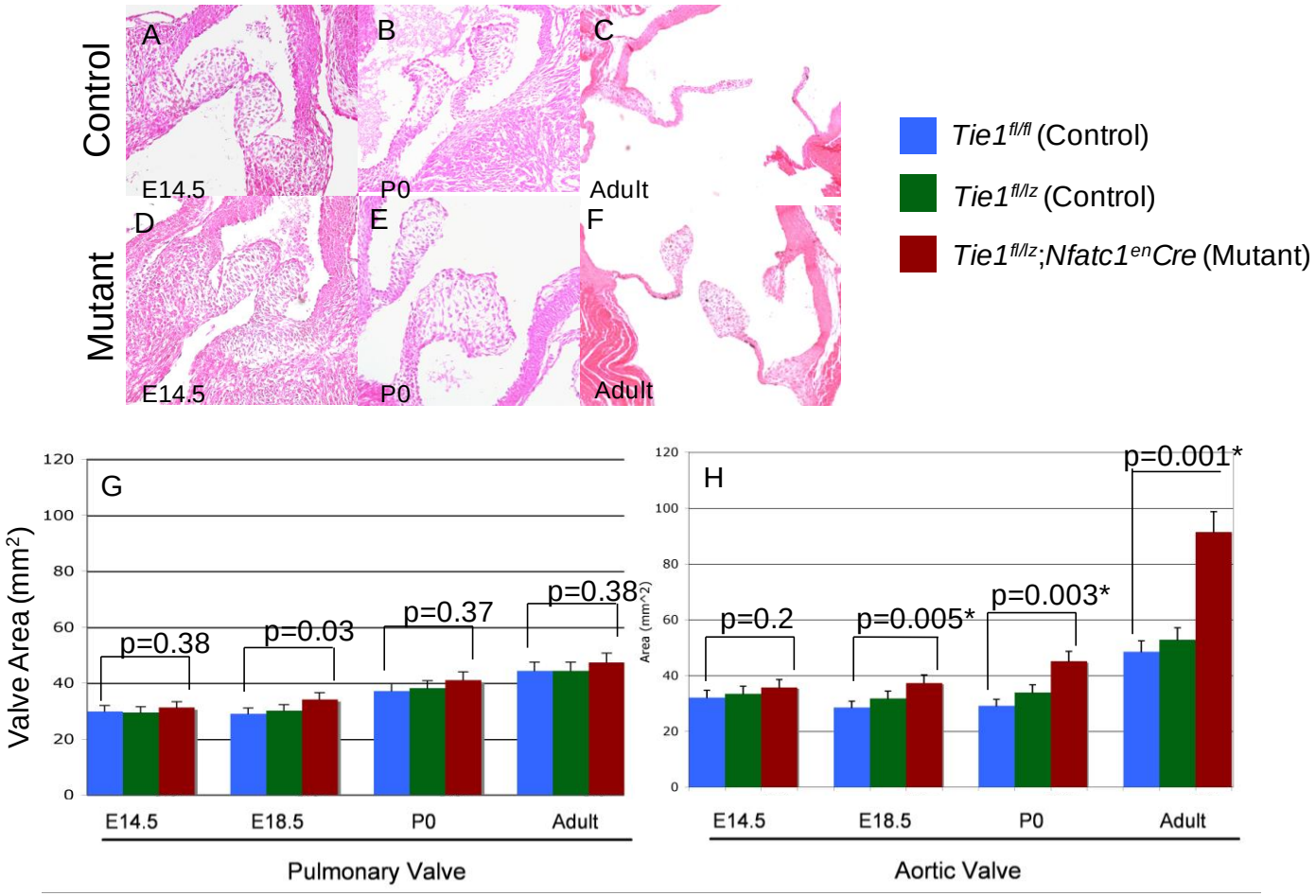

Fig 4.1. Influence of Tie1 on valve area. (A-F) H&E staining showing control and mutant aortic valves; loss of Tie1 in the valvular endocardium leads to enlarged leaflets, first notable at late embryonic stages and increasing over time. (G-H) Quantification of the differences in valve leaflet sizes. Used with permission of H.S. Baldwin.

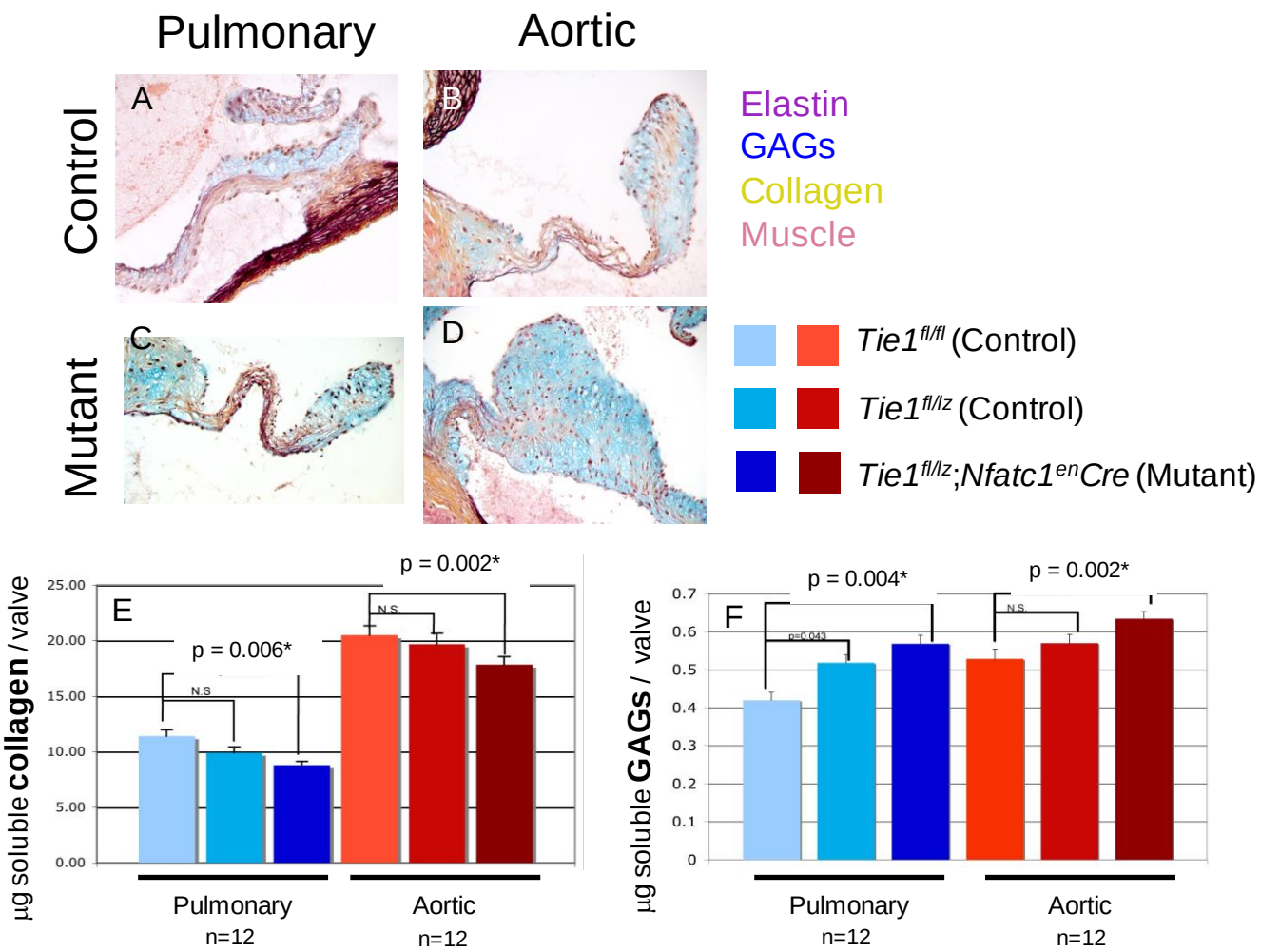

Fig 4.2. Inhibited ECM remodeling in Tie1 deficient mice. (A-D) Movat's pentachrome staining showing control and mutant aortic and pulmonary valves; loss of Tie1 in the valvular endocardium leads to enlarged leaflets, with an abundance of GAGs. (E) Small but significant decreases in collagen occur in animals lacking Tie1 expression in the valve endocardium ($p < 0.01$). (F) Small but significant increases in GAGs are exhibited by mutant valves compared to controls ($p < 0.01$). Used with permission of H.S.Baldwin.

Loss of Tie1 Leads to Decreased Aortic Valve Stiffness

Using AFM, we were able to quantify differences in aortic valve stiffness between mutants lacking Tie1 in the valvular endocardium and littermate controls (Fig. 4.3). Aortic valves lacking Tie1 in valve endocardial cells are significantly less stiff than controls. *Tie1*$^{fl/fl}$ valves measured demonstrated a modulus around 450kPa, which is similar to previous literature on wild type mouse valves [99].

4.4 Discussion

Results from this study indicate that late gestational and post-natal mechanical remodeling during embryonic heart valve development is dramatically impacted by the loss of Tie1 in endocardial cells lining the developing heart valves. This is highly evident in the structural and functional differences between mutant animals and their littermate controls. The presence of significantly more GAGs can be explained by a failure of proper remodeling to occur within these valves after the onset of EMT. Furthermore, as these valves fail to remodel the ECM they also do not generate the necessary collagen content and structure necessary for strengthened mechanical properties. The overall result is enlarged valves that lack the mechanical strength necessary for proper valve function.

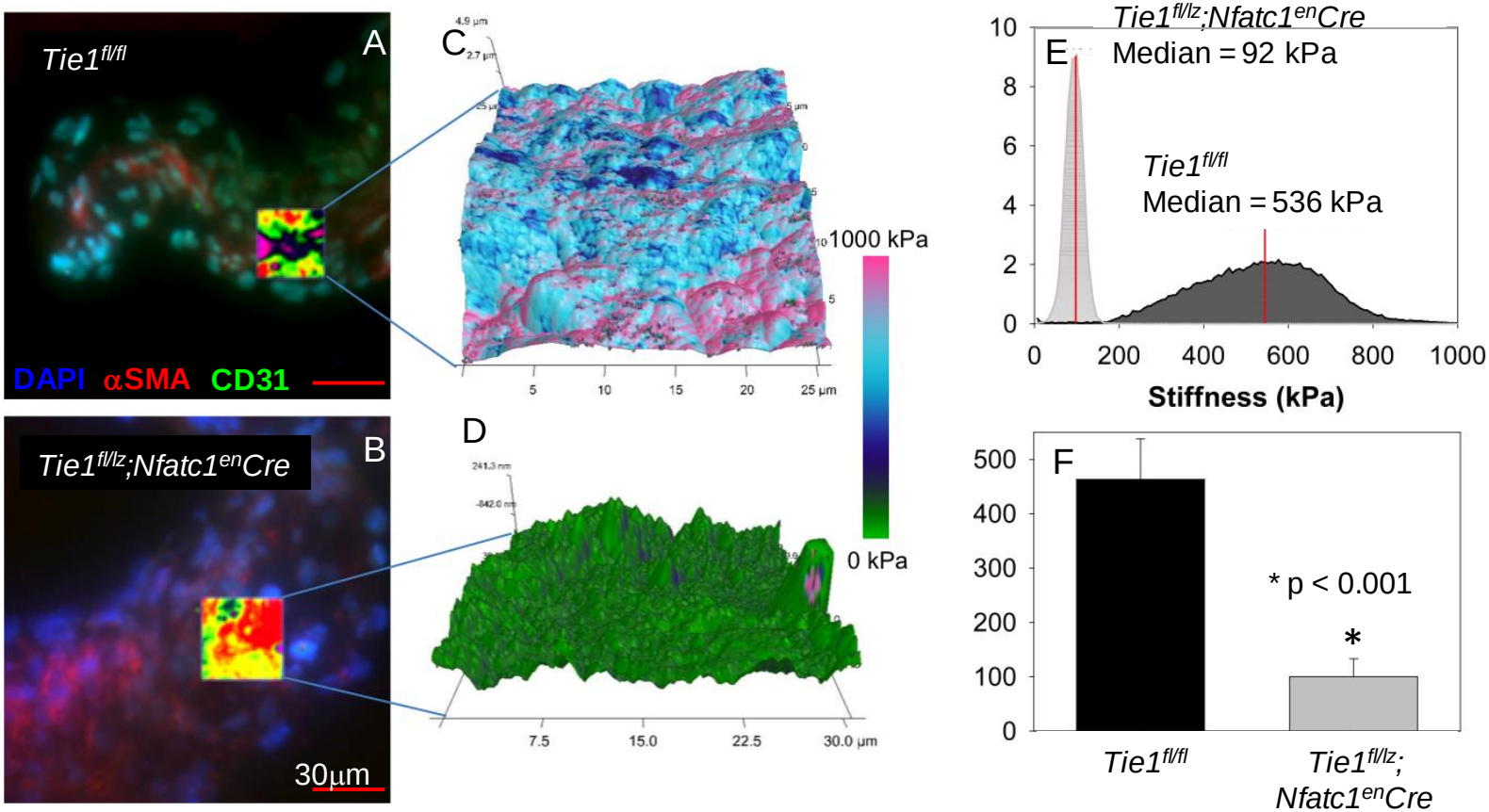

Fig 4.3. Biomechanical properties of HV leaflets in Tie1 deficient mice. *Tie1$^{fl/fl}$* is control; *Tie1$^{fl/lz}$;Nfatc1^{en}Cre* is mutant. (A-B) Fluorescent images showing murine aortic valves and areas scanned by AFM (highlighted callouts). Scale bar = 25μm. (Red = αSMA, Blue = Dapi, Green = CD31). (C-D) 3D topographical maps of stiffness values corresponding to callouts in A, B. (E) Representative scan data for scans shown in C,D. Vertical lines represent median modulus values. (F) Average moduli measurements for aortic valves show that Tie1 deletion in the valvular endocardium leads to significantly softer valves compared to controls ($p < 0.01$). Used with permission of H.S.Baldwin.

Since no differences between mutant and control valves were seen at E14.5, this indicates that the early remodeling initiated by EMT is not significantly affected by *Tie1* signaling from endocardial cells. This suggests that the later embryonic remodeling is sensitive to hemodynamic conditions, as the removal of *Tie1* from the endocardial cells lining the developing valve does not cause abnormalities until this period. These valvular deformities are further exacerbated during the post-natal remodeling period, as evidenced by the dramatic differences between aortic and pulmonary valves of mature mice. After birth, fetal shunts between the left and right side of the heart are closed as systemic pressure increases; the left side of the heart experiences the higher transvalvular pressures which results in the need for more mechanical strength of the aortic valve compared to the pulmonary valve. This increase in pressure may be partially responsible for the more dramatic deformities observed in aortic valves of *Tie1*$^{fl/lz}$*;Nfatc1*^{en}*Cre* mice in this study. Studies are currently planned to examine the pulmonary valves from these mice and determine if they exhibit similar differences in mechanical properties due to genetic alternation.

Tie1 is responsible for establishing stability in endothelial cells throughout the vascular system, and a decrease in Tie1 leads to increased EMT [195]. When cells lining the endocardial cushions have Tie1 removed, the resulting decrease in endocardial layer stability could lead to an increase in EMT where potentially more endocardial cells migrate away from the surface of the endocardial cushions and transform before migrating into the cardiac jelly. While more cells may be present that are capable remodeling the cushions, the

instability in the endocardial layer leads to decreased signaling between endocardial cells and transformed cells that subsequently inhibits remodeling. This study demonstrates a key link in cell-driven remodeling processes and HV tissue level biomechanical properties. Understanding how the mechanical environment of the developing valves changes over time, and how these changes depend on hemodynamic and biochemical signals, will ultimately allow us to better develop TEHV that are informed by native valve properties and environmental requirements.

4.5 Future Directions

To better understand the dynamic mechanical environment of embryonic heart valves, future studies currently include AFM analysis of AVCs and OFTs from murine embryos in stages E9.5 and E11.5, as these correspond to the onset of EMT and early valve remodeling, respectively. Histological analysis via Movat's pentachrome stain will be used to qualitatively determine differences in relative amounts of ECM proteins present at these time points. In addition, we are planning to examine EMT behaviors from murine endocardial cushions on combination collagen-hyaluronic acid hydrogels, with which we have recently demonstrated EMT regulation via mechanotransduction [198]. The inclusion of methacrylated hyaluronic acid allows for altering the mechanical properties of these gels, which will permit us to interrogate how different substrate moduli alter EMT-induced migration. Ultimately, the completion of these studies will provide a

more thorough understanding of the biomechanical changes initiated by EMT, which in turn will hopefully allow the development of viable TEHVs.

Chapter 5

Development of Coll-MeHA Substrate for EMT Studies and Mechanoregulation of EMT

Text for Chapter IV taken from:

> Sewell-Loftin, M.K., DeLaughter, D.M., Peacock, J.R., Brown, C.B., Barnett, J.V., and W.D. Merryman. *Myocardial contraction and hyaluronic acid mechanotransduction in epithelial to mesenchymal transformation of endocardial cells.* Biomaterials, 2014; 35(9): 2809-15.

5.1 Introduction

Understanding how heart valves develop *in utero*, including the complex spatiotemporal regulation of signaling mechanisms and dynamic biomechanical environment, will aid in the creation of viable TEHVs and novel treatment strategies for valve diseases. A crucial first step in the formation of heart valves is EMT of specialized endocardial cells, which gives rise to VICs which remodel the immature cardiac cushions into mature valve leaflets and maintain adult valves throughout life [61, 68-69, 182]. Additionally, VICs are implicated in disease mechanisms including calcific valve disease and have recently been shown to be responsive to hyaluronic acid (HA) signaling [126]. Previous chapters in this work have discussed tissue level biomechanical properties of HV leaflets as a function of genotype and thus valve degeneration or inhibited valve

remodeling. Because these mechanical properties are generated as a result of ECM deposition and/or remodeling, it is important to elucidate cellular behaviors associated with these properties. This includes how mechanics inform cell processes and how cell processes then feed back into tissue mechanics. As the influence of mechanical factors on EMT are not well understood, we decided to design an *in vitro* hydrogel model that allows for interrogation of mechanical factors on EMT. Investigating the role of mechanics at the onset of HV formation will provide novel insight into critical mechanical factors necessary for designing TEHV scaffolds [199] .

In humans, mice, and chicks, the developing heart tube consists of a common atrium, ventricle, and outflow tract. An initial step of heart valve formation occurs when regions in the atrioventricular canal (AVC) and outflow tract swell, forming endocardial cushions extracelluar matrix (ECM) termed cardiac jelly. EMT occurs when endocardial cells lining the developing heart tube receive a signal to detach from the endocardial cell layer and elongate, before migrating into the cardiac jelly [61, 63, 68]. The cardiac jelly is primarily composed of HA but also contains other ECM and signaling molecules [68-69, 72-75, 77, 200]. Over time, the transformed cells that migrate into the endocardial cushions respond to these signals by remodeling the cardiac jelly into the highly structured ECM architecture of mature HV leaflets. The spatial and temporal regulation of this process is important for the proper formation of HVs, and delays or alterations in this signaling can lead to significant impairment of the mature heart valve structure or function.

In vitro, endocardial EMT is studied via a collagen gel protocol developed nearly 30 years ago [14, 78]. Briefly, stage HH16 avian embryos are harvested, and the AVC endocardial cushions are removed before explanting endocardium-side down onto a collagen hydrogel. Over 2 days, endocardial cells migrate out of the explant and onto the surface of the collagen gel, forming an endocardial cell sheet; some of these cells undergo EMT and migrate into the collagen gel. This assay has been performed in both mouse and chicken and demonstrates the high degree of conservation between signaling mechanisms governing endocardial EMT between species, despite the fact that mouse explants do not form endocardial sheets [68, 71-72, 79, 83]. Also, as the ventricle of the developing heart tube does not undergo EMT, it is frequently used to test the ability for signaling molecules to induce EMT [80]. For a full review on endocardial EMT assays, see [83, 186]. After developing the original collagen gel assay, Bernanke et al. went on to show that soluble HA can affect the level of EMT that occurs *in vitro*, although this study was not pursued further [201]. Studies testing the effects of hyaluronate in embryonic rat hearts demonstrated that HA degradation prevented endocardial cushion formation [202]. Also, Camenish et al. showed that mice lacking HA-synthase 2 ($HAS2^{-/-}$) fail to form HVs, due to a lack of endocardial cushions, and die at approximately stage E11 with an absence of EMT [79]. However, *in vitro*, EMT can be rescued in $HAS2^{-/-}$ cells by the addition of soluble HA. Based on the role of HA as an important structural and signaling component in EMT, examination of its inclusion in the *in vitro* hydrogel assay to determine effects on EMT is warranted [119, 124, 130].

The primary limitation of the collagen gel assay is that it fails to mimic the *in vivo* environment of the developing heart valves in composition (chiefly, lacking HA) which has been recently identified as a key mechanotransduction protein [128]. Further, significant progress has been made in elucidating the signaling mechanisms important for driving EMT, but little work has been done in the biomechanical aspects of this process. Since the biomechanical properties of early and mature heart valve tissues directly relate to valve function, the current lack of knowledge about the relationship between EMT and mechanics needs to be addressed [88, 185]. The goal of our study was to create a hydrogel platform incorporating collagen and HA which can be used to study the mechanical context of EMT, in order to test our hypothesis that mechanical factors may play a previously unrecognized role in the regulation of endocardial EMT.

5.2 Materials and Methods

Gel synthesis

Coll-MeHA gels were synthesized following previously established protocols [130, 203-204]. Briefly, HA was modified to contain methacrylate crosslinking groups by reacting HA (#53747, Sigma Aldrich, St. Louis MO, ~1.6 MDa) with methacrylic anhydride in basic solution (pH~8) for 24 h at 4^{o}C. The methacrylated product was precipitated and washed in ethanol, before dialyzing against diH_2O for 48 h, and lyophilizing for 72 h. The resulting MeHA powder was dissolved in sterile PBS at a 1% w/v concentration and stored at 4^{o}C until further

use. Coll-MeHA gels were formed by mixing type I collagen (#354249, BD Biosciences, San Jose CA) with MeHA stock solution and neutralizing with 0.1 M NaOH. For crosslinking, 0.1wt% (to total gel weight) of Irgacure 2529 (#410896, Sigma Aldrich, St. Louis MO) was mixed into the solution. The pre-gel solution was cast into ether custom-made poly(dimethyl siloxane) (PDMS) molds for mechanical analysis or 4-well plates (#176740, Thermo Scientific Nunc, Pittsburgh PA) for explant studies. Gels were crosslinked for 5 min under a 365 nm UV wand before incubation at 37^{o}C and 5% CO_2 to complete collagen gelation. Prior to explant experiments, Coll-MeHA gels were equilibrated overnight in complete media.

Mechanical analysis of gels

AFM was utilized to measure the moduli of Coll-MeHA and collagen only gels. Samples were analyzed using a BioScope Catalyst AFM (Bruker AXS, Santa Barbara CA) operated in Peak Force – Quantitative Nanomechanical Mapping mode in fluid. Gels were fully hydrated in PBS prior to AFM measurements. Borosilicate glass particle tips (Novascan, Ames IA) with a nominal diameter of 5 μm and nominal spring constant of 0.03 N/m were used. Actual tip radii and spring constants were calibrated for each tip prior to scanning using a PDMS standard sample provided by Bruker. Median values from multiple scans on multiple gels were used to generate average moduli values ($n \geq 8$ per gel composition).

Gel topography analysis

The fiber structure and overall gel topography were visualized using a Hitachi S-4200 Scanning Electron Microscope (SEM) (Pleasanton, CA). Samples were prepared as described above, except pre-gel solutions were cast into small weigh boats for UV crosslinking and subsequent incubation. After full gelation, samples were moved to a -80^{o}C freezer and stored overnight; samples were then lyophilized for 24 h before being mounted on SEM posts using conductive tape. Before imaging, scaffolds were coated with gold for 20 seconds using a sputter coater Model-108 (Cressington Scientific, Watford, UK).

Chick AVC explant harvesting and culture

Stage HH16-17 were harvested as described elsewhere [14]. Briefly, AVCs were excised from embryos, cut open, and seeded endocardium-side down onto fully hydrated gel surfaces. As controls, 0.12wt% collagen only gels were utilized; this composition corresponds to the standard collagen gel assay [14, 78, 201]. Explants were given M199 media with 1% FBS, 1% antibiotic/antimycotic, and 1% insulin-selenium-transferrin solution, on the morning following seeding and fed every 2d after that until 7d total culture time was reached. Explants were imaged at 1d, 2d, 4d, and 7d using a Nikon-Ti300 inverted microscope (Nikon Inc., Melville NY) equipped with Hoffman Modulated Optics and a Spot RT3 camera (Spot Imaging Solutions, Sterling Heights MI). A minimum of 8 explants were seeded per condition and experiments were repeated with at least 3 different batches of eggs to ensure reproducibility. For

mechanical analysis, stage HH16-17 embryos were selected and fresh frozen in OCT according to established protocols [189].

EMT quantification

The surface of the gels was imaged to measure endocardial sheet size, which directly relates to the number of endocardial cells that have migrated out of the explant. To quantify cell transformation and invasion, images were taken every 50 μm throughout the depth of the gel where cell bodies were present. The series of images from an explant created a z-stack showing cell invasion. Both endocardial sheet size and number of transformed cells were quantified using ImageJ. A minimum of 10 explants per condition and time point, taken from at least 3 different batches of eggs, were analyzed for each output. Only viable explants were imaged for cell analysis; an explant was considered viable if the myocardium was still beating on the day of imaging.

Proliferation assay

Proliferation of cells from explants on gels was measured using BrdU. Briefly, gels were incubated with 1:1000 BrdU (RPN201V1, Amersham Biosciences, Pittsburgh PA) for 1hr at 37^{o}C before fixation with 4% paraformaldehyde. Systems were then subjected to a series of HCl incubations to permit DNA binding and subsequently washed with a borate buffer. Gels were blocked and permeabilized using 3% BSA + 0.05% Tween-20 for 2hr at room temperature. Gels were incubated with 1:200 anti-BrdU (#32323, Santa Cruz,

Dallas TX) overnight at 4^{o}C. Gels were next washed multiple times in PBS + 0.05% Triton-X + 0.2% BSA, before incubating with secondary antibody (goat-anti-mouse 568) at 1:500 overnight at 4^{o}C. Gels were then washed multiple times in PBS + 0.05% Triton-X + 0.2% BSA; one of these wash steps contained 1:1000 Hoechst 33342 (Invitrogen, Eugene, OR). Finally gels were mounted in ProLong Gold (#P36430, Life Technologies, Eugene OR) and allowed to dry overnight before imaging. Images were taken on a Nikon E800 (Nikon Inc., Melville NY) and processed using ImageJ.

Deformation measurements

Sequence images of viable explants were taken using the Spot Advanced software. Two images from each explant were selected from the sequence representing fully relaxed and fully contracted myocardium. These images were digitally subtracted using MATLAB and color coded to show deformation of cells and gels surrounding the explants. The area of this deformation was quantified and normalized to total endocardial sheet area of the relaxed myocardium at the time point of interest, resulting in regional gel deformation for each of the explants. Digital image correlation software was used to generate images of strain fields induced by myocardial beating; these images were overlaid with projections of total invaded cells counts to determine correlations between local strain magnitude and EMT.

Inhibition of contractile forces

To assess if active myocardial contraction was necessary for endocardial EMT, we devised a series of studies to prevent or slow explant beating without removing the signaling component provided by the explant. In the first series of experiments, explant contraction was reduced by administering 1.5 mM ethyl 3-aminobenzoate methanesulfonate salt (A5040, Sigma-Aldrich), otherwise known as the anesthetic tricaine [205]. Explants were allowed to adhere overnight to gels before administering the drug. Physical removal of the myocardium was tested by carefully removing the explant from the surface of the gel after the explant had adhered overnight. The explant remained in the well, unattached, for the duration of the experiment. A control group had explants that were removed from the gel surface and then discarded.

Statistical analysis

All results from chick explant experiments were reported as average value plus or minus standard error of the mean. For mechanical analysis, the median value of each AFM scan was collected and aggregated into an average median value to represent the sample [189]. Weighted average deformations associated with invaded cells were calculated by weighting the local strain magnitude in a 25x25 pixel volume by the total number of invaded cells present in that volume and dividing that value by total invaded cells. The average values of all groups were compared with ANOVA, while pair-wise multiple comparisons were made using the Holm-Sidak post-hoc testing method.

5.3 Results

EMT on cross-linked Coll-MeHA hydrogels

Combinations of collagen and HA were tested for AVC explant viability and attachment prior to detailed analyses. For these studies, a modified HA containing methacrylate groups (MeHA) was synthesized [130, 203-204]. Most notably, combination crosslinked Coll-MeHA gels that contained only 0.12wt% collagen (the standard collagen concentration) with any amount of MeHA demonstrated poor explant attachment. This may be due to a minimum requirement for collagen presentation in the context of HA gels, as a collagen concentration of at least 0.2wt% was required for explant attachment; likewise, gels with greater than 0.5wt% MeHA demonstrated poor explant attachment. The Coll-MeHA compositions reported in this study gave optimum explant attachment. After 4d in culture, AVCs explanted onto composite Coll-MeHA gels exhibited larger endocardial cell sheets (Fig. 5.1A) and an increased number of transformed cells compared to explants on collagen only gels (Fig. 5.1B). Endocardial sheets on 0.2wt% collagen gels were significantly larger than those on controls and comparable to sheets seen on Coll-MeHA gels; however there was no increase in EMT (Fig. 5.1B). In addition to increased EMT, maximum invasion depth is significantly increased on Coll-MeHA gels after 4d in culture (Fig. 5.1C, Fig. 5.2). MeHA incorporated into 0.12wt% collagen gels uncrosslinked at 0.5 mg/mL (+gel-MeHA) or as a supplement to the media at 0.5 mg/mL (+sol-MeHA) showed no increased cell invasion compared to control groups (Fig. 5.1B,C).

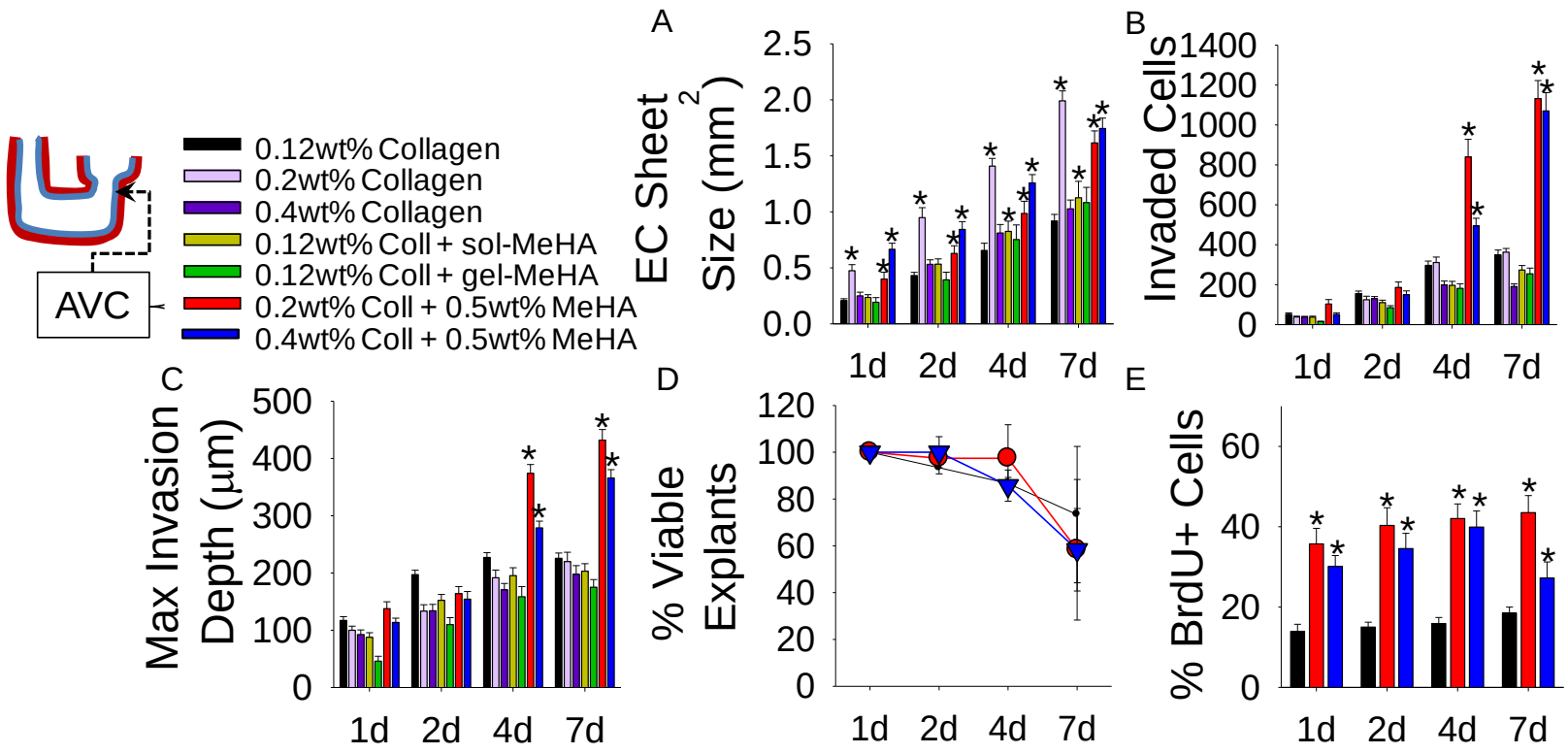

Fig 5.1. EMT behaviors as a function of collagen and MeHA presentation. (A) Explants on Coll-MeHA gels demonstrate significantly larger endocardial (EC) sheet sizes compared to collagen controls at the same time point. (B) Quantification of EMT via counts of invaded cells show higher levels of transformation on Coll-MeHA gels. (C) Maximum invasion depth of invaded cells is higher on Coll-MeHA gels after 4d. (D) Viability of explants seeded on different gel compositions is not significantly different, excluding it as the source of increased EMT on Coll-MeHA gels. (E) Proliferation of cells as measured by BrdU is significantly higher on Coll-MeHA gels but is not sufficient to explain the increase number of transformed cells. All data presented as average ± SEM and represents 3 technical replicates with n ≥ 10 biological replicates. *p < 0.05 vs. 0.12wt% collagen at same time point.

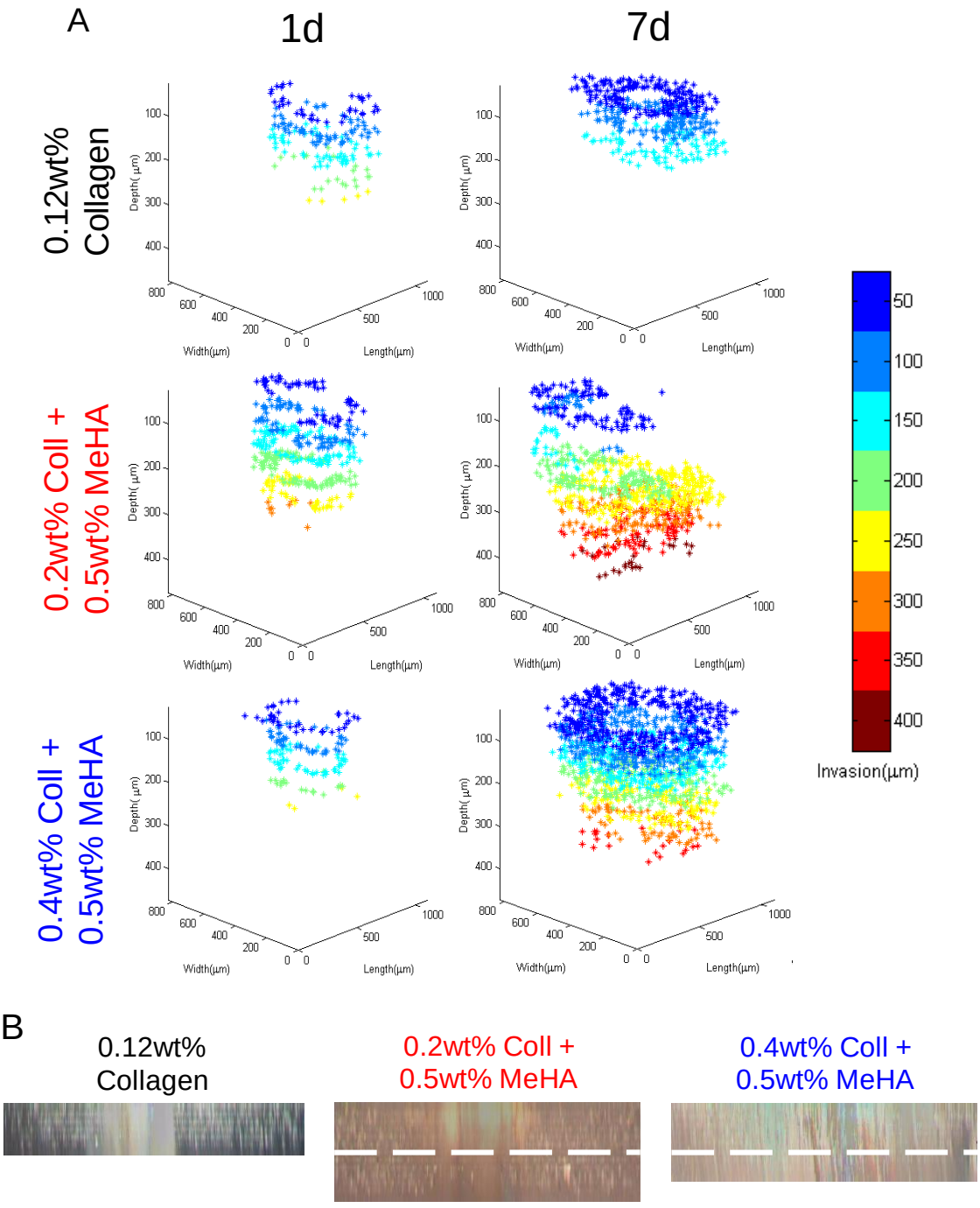

Fig 5.2. 3D invasion into gel substrates. (A) Invasion depths of individual cells were mapped in ImageJ and plotted in MATLAB to visualize differences between gel compositions over time. On average, cells in Coll-MeHA gels (middle and bottom row) migrated further into the substrate than cells in collagen control gels (top row). Average migration depths were calculated by weighting a specific invasion depth by the number of transformed cells at that depth. (B) Side views of a 3D image stack built with ImageJ showing location of invaded cells. White dashed line is at 250 μm below surface of gels.

To determine if Coll-MeHA gels may promote EMT in endocardial cells that do not typically undergo EMT, ventricle explants from stage HH16-17 chick hearts were explanted on Coll-MeHA gels, using collagen only gels as a control. Ventricular explants exhibited no difference in endocardial sheet size or number of invaded cells compared to ventricle explants on collagen only gels (Fig. 5.3). As expected, both endocardial sheet size and number of transformed cells were significantly smaller in ventricle samples compared to AVC explants.

Cell proliferation on Coll-MeHA gels

Differences in EMT did not result from differences in explant viability, as defined by the presence of myocardial contractions (Fig. 5.1D). Proliferation was increased on both compositions of Coll-MeHA gels across all time points when compared to samples on collagen only gels (Fig. 5.1E).

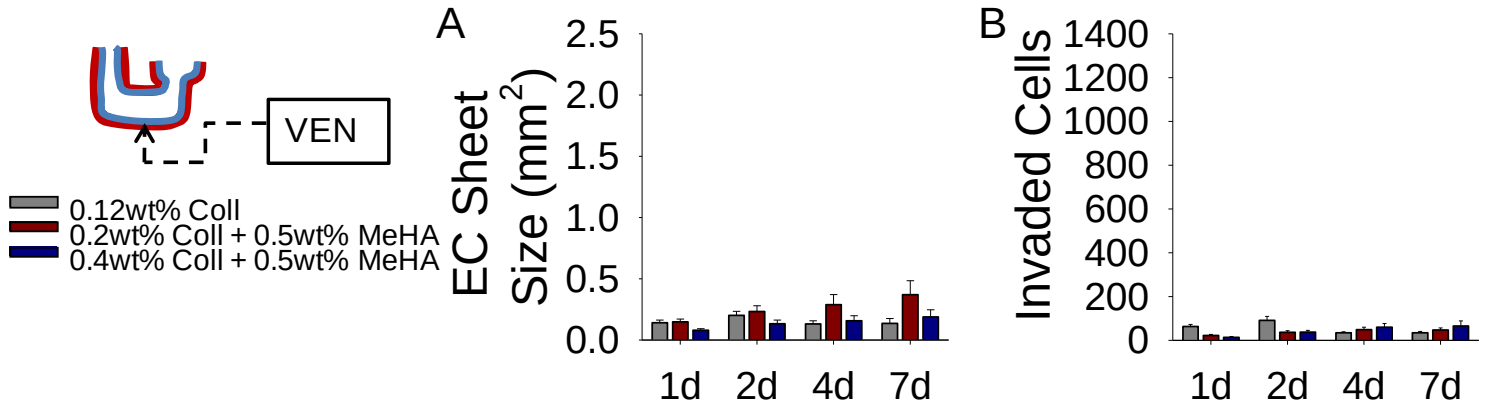

Fig 5.3. EMT behaviors of ventricular explants on Coll-MeHA gels. (A) EC sheet sizes produced by ventricular explants do not differ based on gel composition, and are significantly lower than EC sheets produced by AVC explants. (B) Number of invaded cells are fewer from ventricular explants on all gel types when compared to AVC explants. All data presented as average ± SEM and represents 3 technical replicates with n ≥ 10 biological replicates.

Scaffold characterization

Collagen only gels exhibited a highly fibrous structure, with little organization or alignment of fibers (Fig. 5.4A,B). Combination Coll-MeHA gels also exhibited similar collagen fibrous structures, interspersed with sheets of MeHA (Fig. 5.4C-D, E-F). Mechanical analysis of gels by atomic force microscopy (AFM) showed that the addition of crosslinked MeHA and increasing collagen content increase modulus, as expected (Fig. 5.4G). However, results from AFM of chick AVC explants indicated an average modulus of 7.2 ± 1.9 kPa for endocardial cushions (Fig. 5.4H-K), indicating that all gels used in this study are much stiffer than the AVC stiffness.

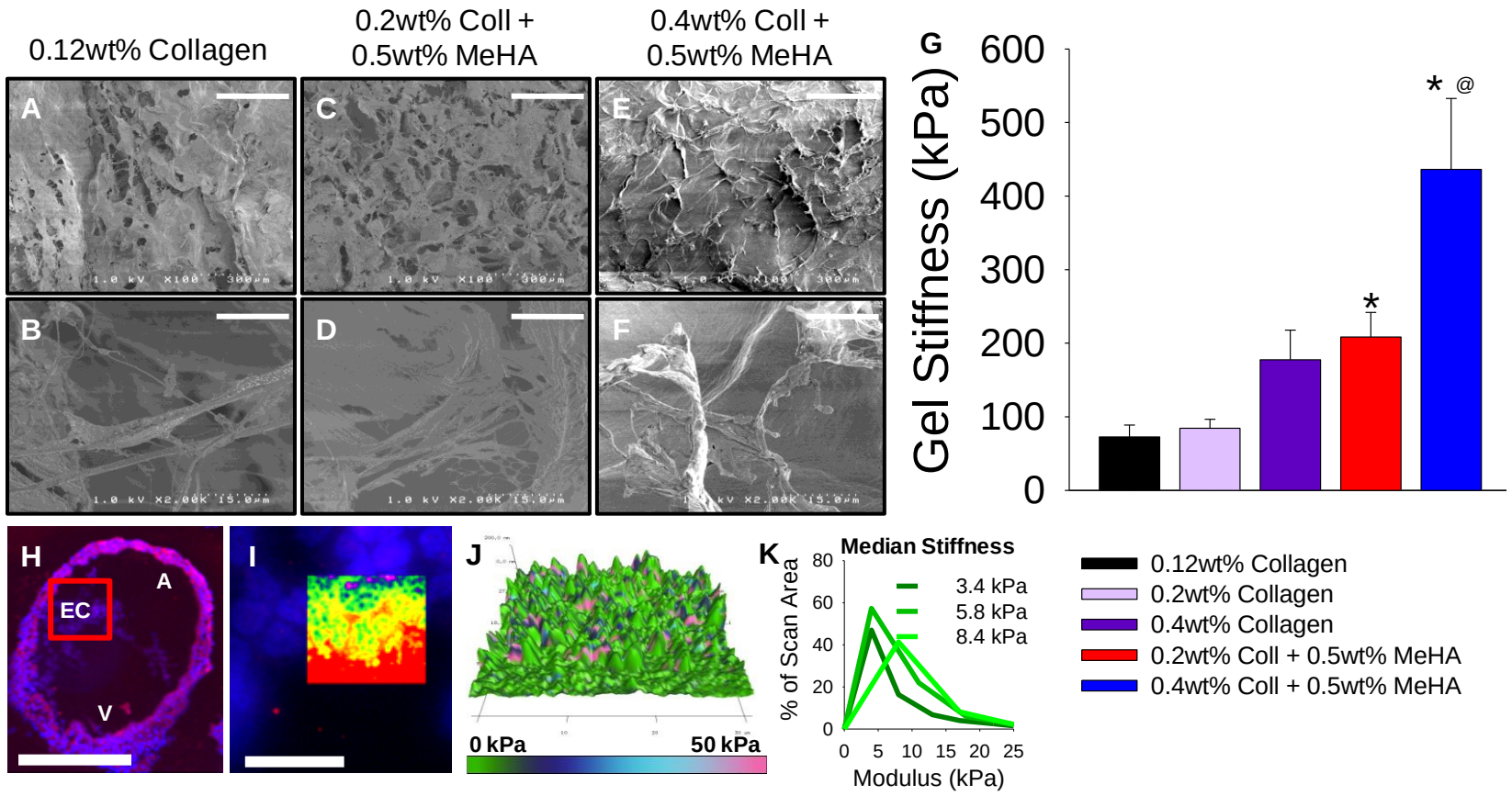

Fig 5.4. Gel characterization. (A-F) SEM images of 0.12wt% collagen (A,B), 0.2wt% Coll + 0.5wt% MeHA (C,D), and 0.4wt% Coll + 0.5wt% MeHA (E,F). Scale bar = 300 μm (A,C,E); Scale Bar = 15 μm (B,D,F). (G) Modulus data of gels obtained via AFM. All data presented as average ± SEM with n ≥ 8 scans per composition on N ≥ 2 different gels. (H-I) Fluorescent images of avian AVC scanned by AFM. A = atrium, V = ventricle, EC = endocardial cushion. Scale bar = 100 μm (H) and 25 μm (I). Inset in (I) highlights scanned area. (J) 3d topographical map with modulus value overlaid. (K) Representative distributions of modulus vs. scan area. Inset numbers represent median values. N = 3 embryos. * $p<0.05$ vs. 0.12wt% collagen; @ $p<0.01$ vs. 0.2wt% Coll + 0.5wt% MeHA.

EMT regulation via active contractile forces

To investigate the role of contractile forces due to the beating myocardium in regulating EMT, we measured the strain transduced into collagen and Coll-MeHA gels. Color maps visualizing regional deformation due to myocardial contraction were generated by digitally subtracting images of a fully relaxed and fully contracted explant (Fig. 5.5). At all time points, explants on Coll-MeHA gels underwent larger deformations compared to explants on control collagen gels (Fig. 5.7A). This was unexpected because gels with HA have comparable or greater stiffness than collagen gels, indicating they would resist deformation. Gel deformations generated during myocardial contractions were not significantly different from control samples in the case of either soluble or uncrosslinked MeHA or increased collagen content, indicating it is biomechanical properties of MeHA and not simply HA signaling increasing cell transformation. By overlaying images of invaded cells with strain field maps generated with MATLAB, we were able to quantify the number of invaded cells at a specific deformation magnitude (Fig. 5.6). These values were aggregated and used to generate histograms depicting the relationship between gel deformation magnitude and EMT (Fig. 5.7B). We additionally calculated weighted average deformation magnitudes associated with invaded cells to compare between sample groups (Fig. 5.7B, inset numbers). Higher average magnitudes on Coll-MeHA gels shows more invaded cells present in higher deformation regions on these gels. Furthermore, for all gels permutations and time points, our results indicated over 98% of all

transformed cells were present in areas where deformation magnitudes are greater than zero.

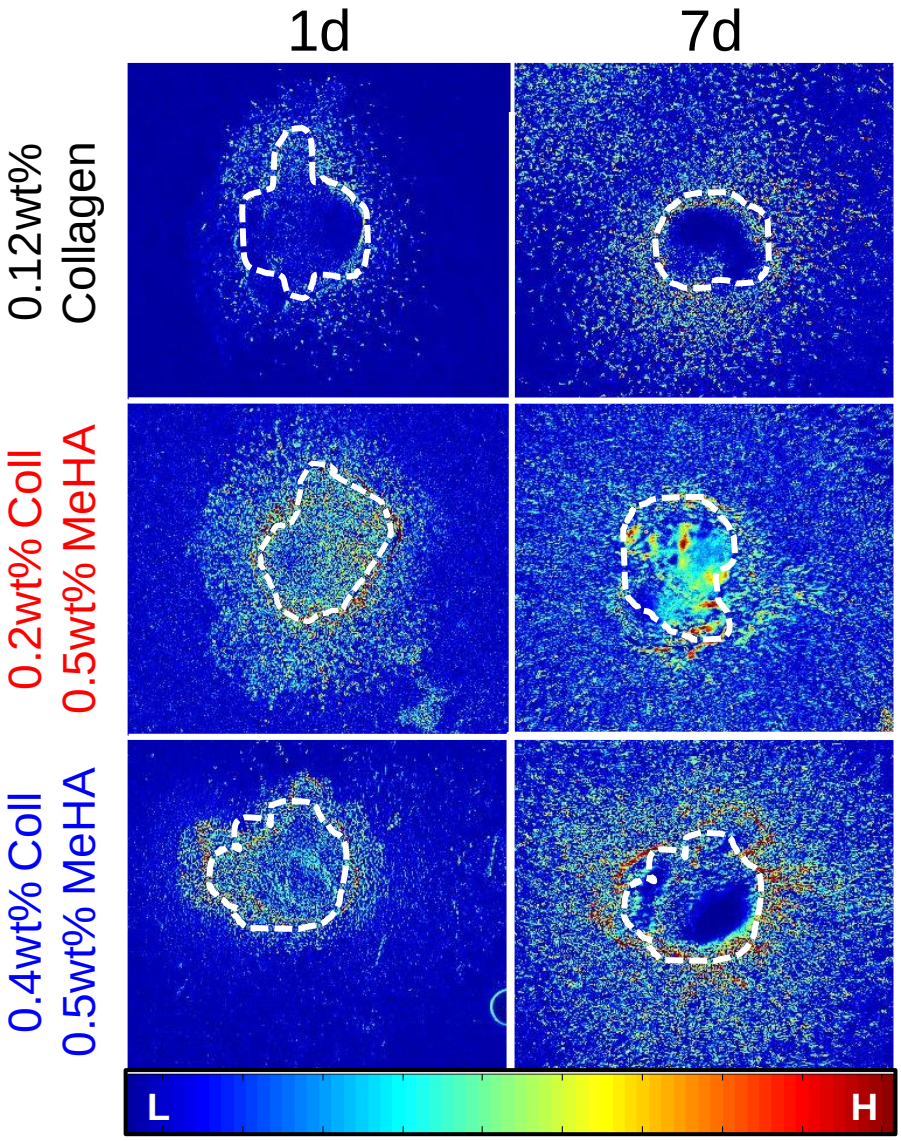

Fig 5.5. Regional gel deformation maps. These representative images show areas of low (L) or high (H) deformation induced during myocardial contraction on the surface of hydrogels. White dashed lines approximate edges of relaxed explant. Overall, explants on Coll-MeHA gels showed larger regions of deformation at all time points compared to explants on collagen only gels. These values were quantified and plotted in Fig. 5.7A.

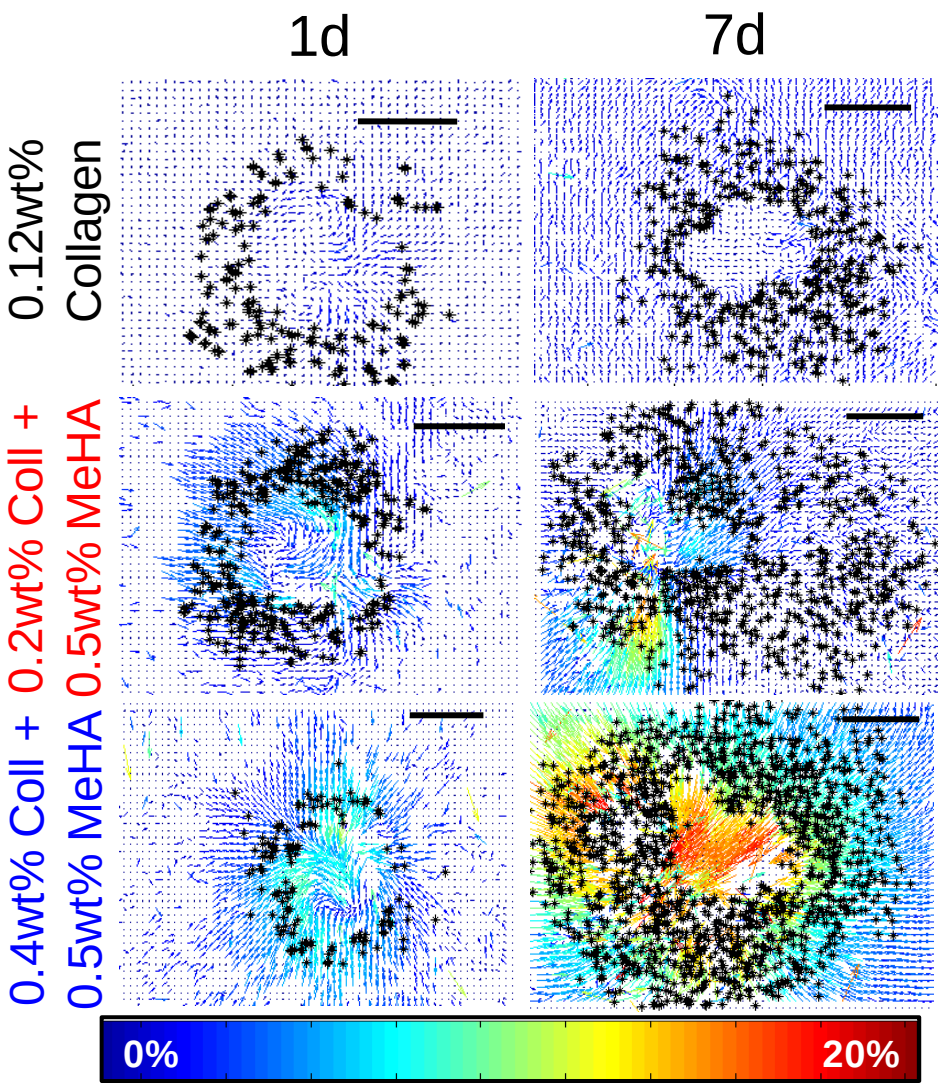

Fig 5.6. Cell transformation mapped with strain magnitude. These representative images show position of invaded cells (*) in relationship to local strain fields induced during myocardial contraction. Scale bars are 200 μm. Higher strains were observed on Coll-MeHA gels, and higher numbers of transformed cells were located at these positions. Weighted average deformation magnitudes were calculated by quantifying number of cells per specific magnitude value based on these images. These values were aggregated and inset in Fig. 5.7B.

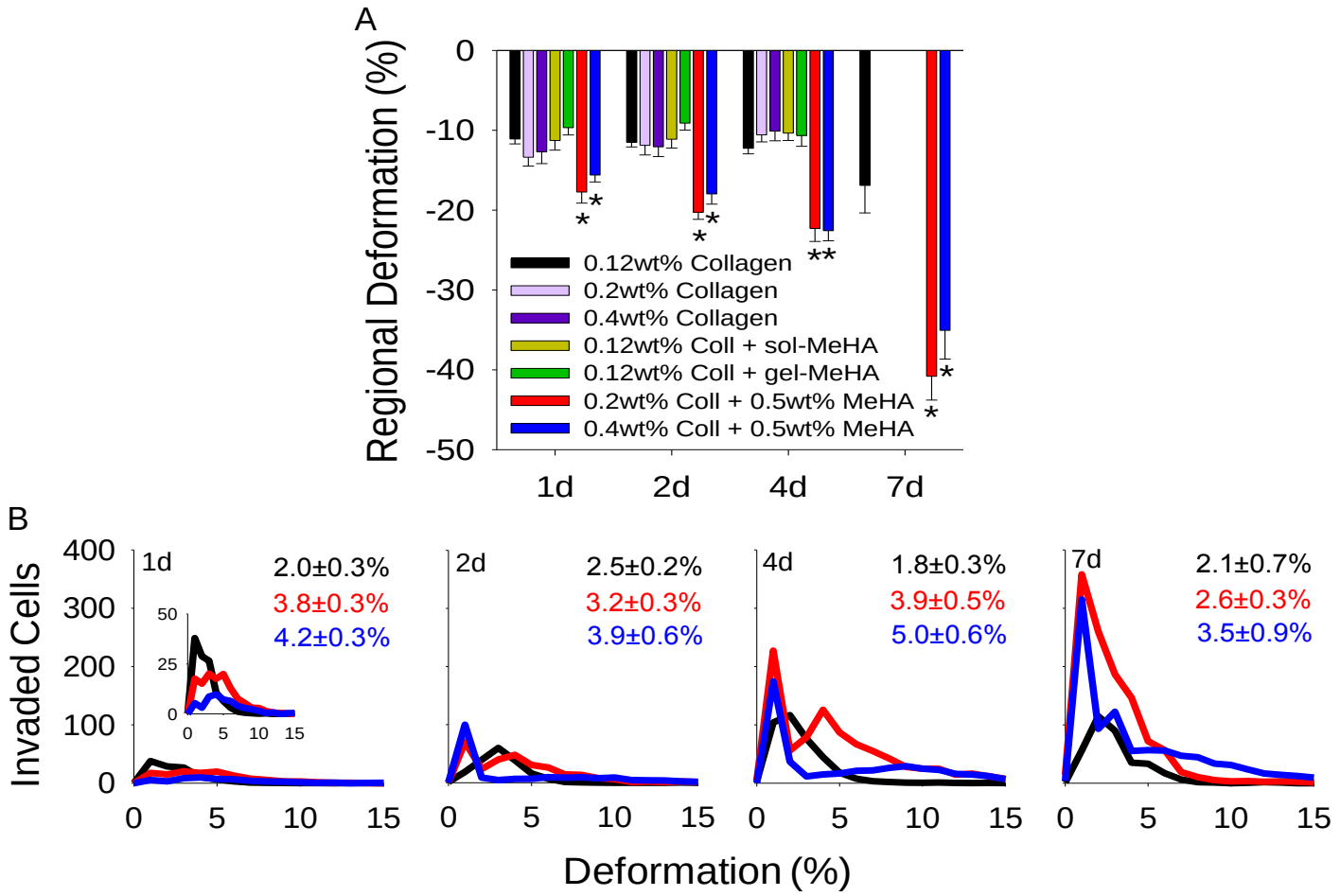

Fig 5.7. Mechanical regulation of EMT. (A) Regional gel deformation for different presentations of collagen and MeHA. 7d data unavailable for some samples due to slow myocardium beating. All data presented as average ± SEM and represents 3 technical replicates with ≥ 4 biological replicates. (B) Histograms showing number of invaded cells as a function of local strain magnitudes. Inset in 1d is re-scaled to show detail. Numbers correspond to weighted average strain ± SEM with n ≥ 3 replicates (see A for color legend). *p < 0.05 vs. 0.12wt% collagen at same time point.

Decreased EMT with pharmacological inhibition of myocardial contraction

Preventing explant beating by administration of the sodium channel inhibitor, tricaine, demonstrated that myocardial contraction significantly contributes to endocardial EMT. Explants incubated with 1.5 mM tricaine demonstrated similar viability staining compared to control groups (Fig. 5.8A,B) but significantly reduced myocardial contraction frequency and force (Fig. 5.8C,D). Endocardial sheet size, number of invaded cells, and maximum invasion depth are all significantly decreased when explants in the presence of tricaine for all gel permutations (Fig. 5.8E-G). Incubation with tricaine did not significantly inhibit cell migration, as verified by a wound assay with mouse embryonic fibroblasts incubated with 1.5 mM tricaine overnight (5.9). This is the first study showing inhibiting myocardial contractions inhibits endocardial EMT.

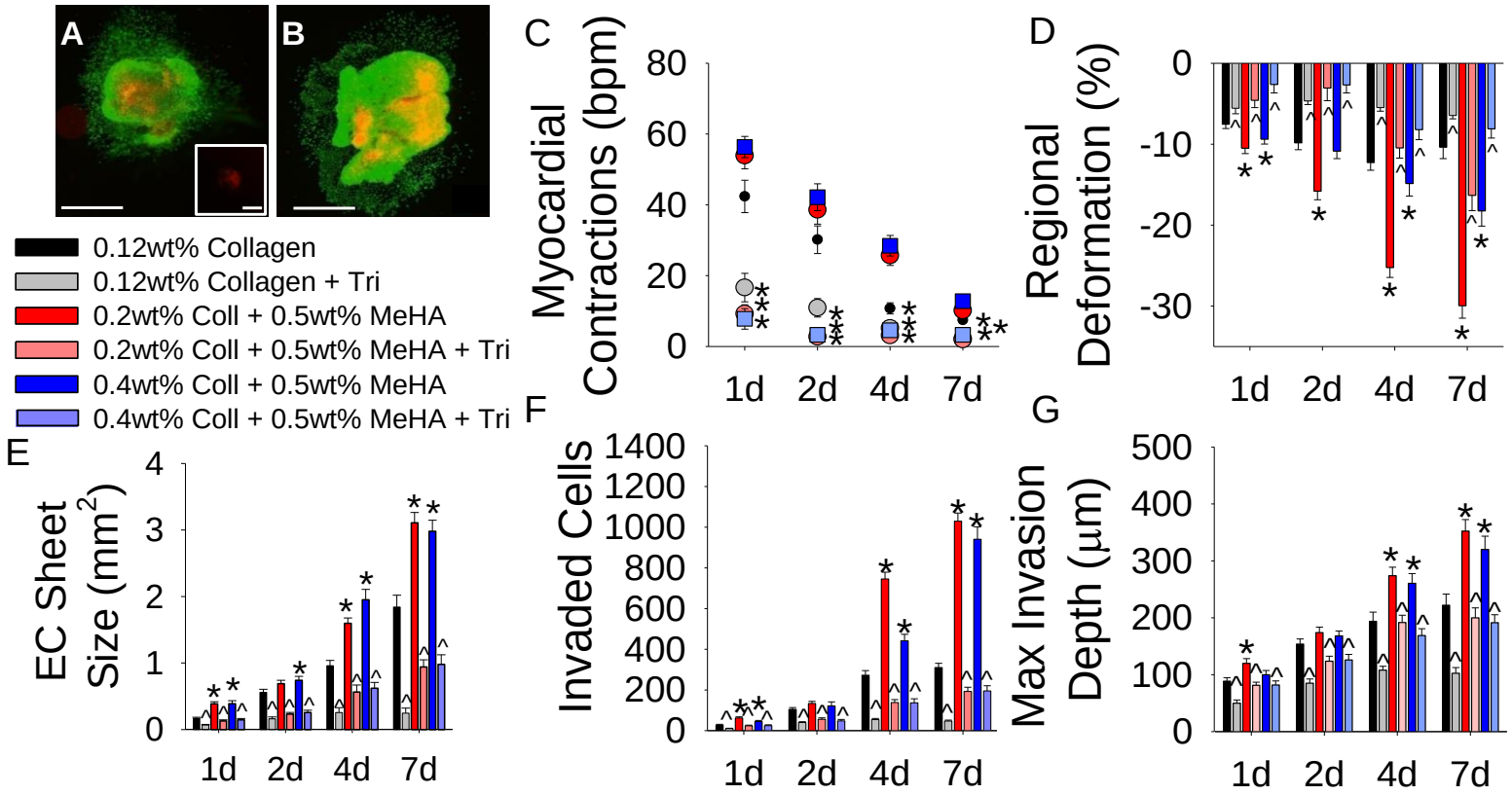

Fig 5.8. Pharmacological inhibition of myocardial contraction. (A-B) Live(green)-Dead(red) staining on explants and cells seeded on 0.12wt% collagen with either no treatment (A) or 1.5 mM tricaine (B). Inset in (A) shows negative control, 4% PFA treatment for 5min. (C) Quantification of myocardial contractions with tricaine treatment. (D) Regional gel deformation induced by explants treated with tricaine. (E) EC sheet areas for tricaine treated explants. (F) EMT quantification via number of invaded cells in the presence of tricaine. (G) Maximum invasion depth of transformed cells. All data presented as average ± SEM and represents 3 technical replicates with $n \geq 6$ biological replicates. *$p < 0.05$ vs. 0.12wt% collagen at same time point. ^$p < 0.05$ vs. same gel type at same time point.

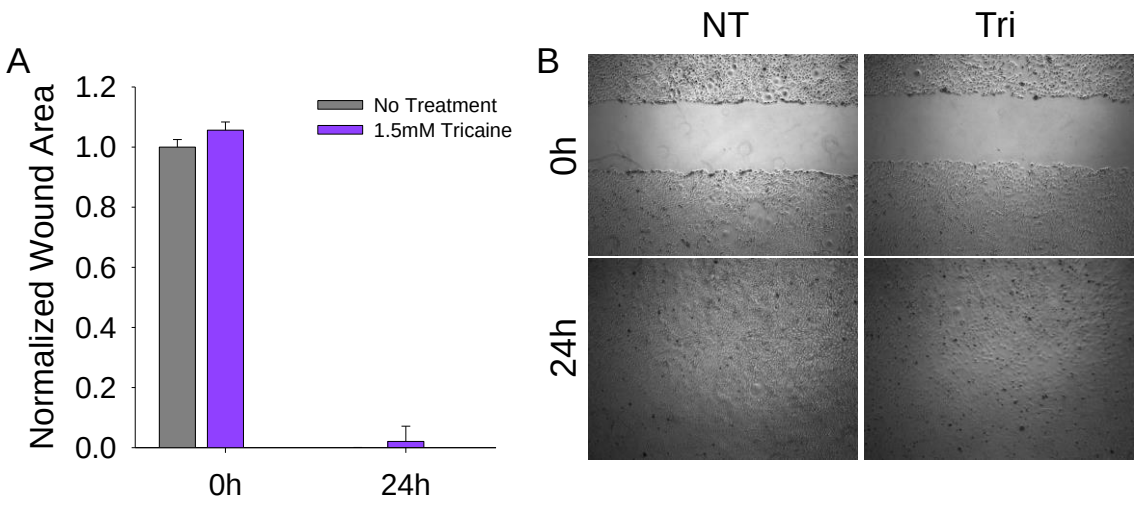

Fig 5.9. Tricaine does inhibit cell migration. (A) Relative wound areas of mouse embryonic fibroblasts incubated with 1.5 mM tricaine compared to controls. Data presented as average ± SEM, n=2. (B) Representative images of controls (left) and cells with tricaine (right) at 0h (top row) and 24h (bottom row).

Partial EMT rescue with myocardial signaling without contraction

To disassociate the roles of soluble signaling and mechanical factors from the myocardium, explants were removed from the surface of the gel after 1d in culture and either discarded (- Myo) or allowed to remain unattached in the media (+ Myo). Significantly smaller endocardial sheets sizes, fewer invaded cells, and decreased invasion depths are observed when the myocardium is physically removed (Fig. 5.10A-C). However, if the explant was allowed to remain free floating in the media for the duration of the experiment, some recovery of EMT occurred. Since the presence of soluble signaling factors from the myocardium is not sufficient to fully rescue EMT, it indicates that myocardial contraction is the source of increased EMT in this study.

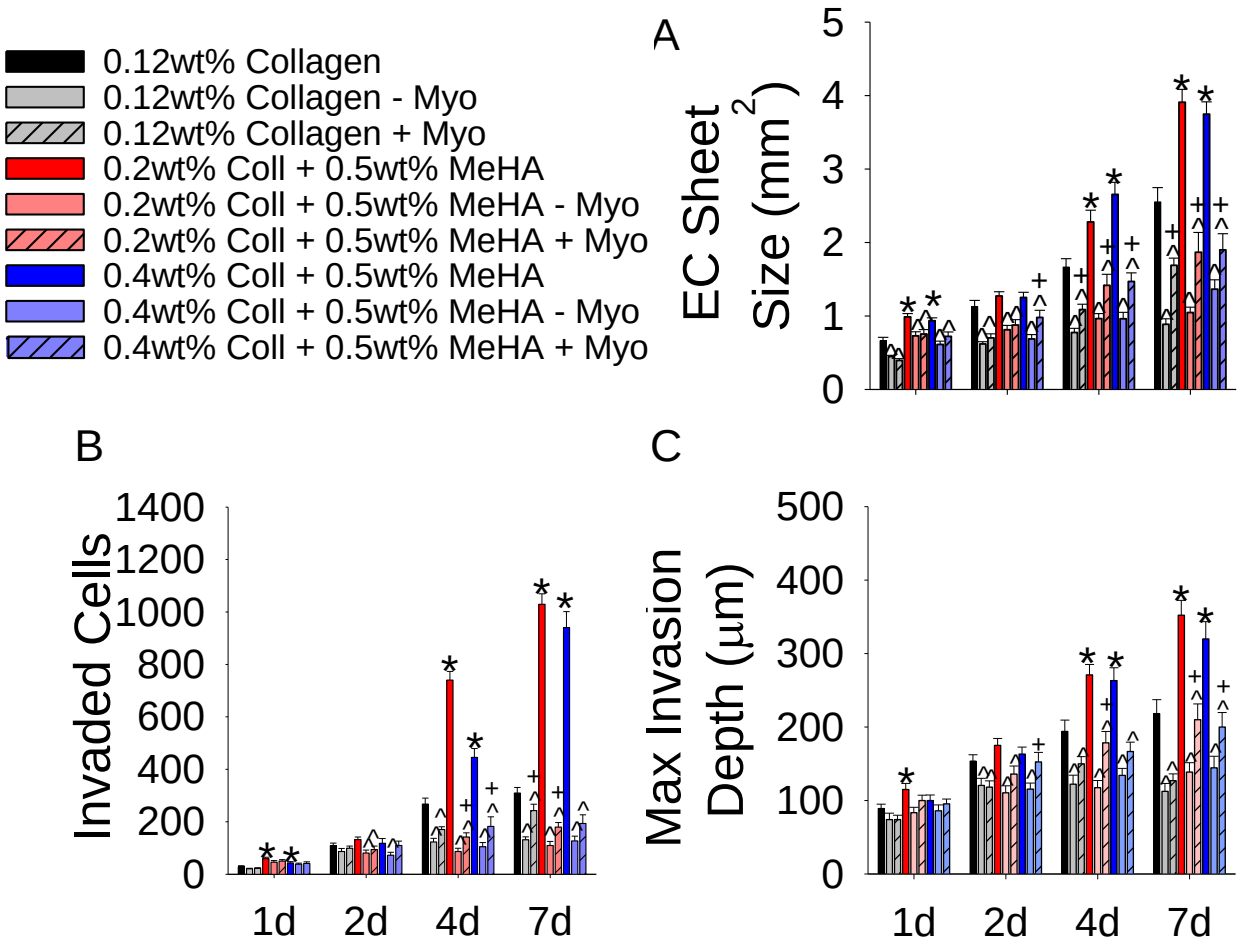

Fig 5.10. Physical inhibition of myocardial contractions. (A) EC sheet sizes as a function of myocardium presence. *Note:* These EC sheet values include area covered by explant. (B) EMT quantification via invaded cell counts with or without myocardium. (C) Maximum invasion depth of transformed cells with or without myocardium. All data presented as average ± SEM and represents 3 technical replicates with $n \geq 10$ biological replicates. *$p < 0.05$ vs. 0.12wt% collagen at same time point. ^$p < 0.05$ vs. same gel type at same time point. +$p < 0.05$ vs. "-Myo" on same gel type at same time point.

5.4 Discussion

The objective of this study was to examine the contribution of HA in endocardial EMT and determine if mechanical factors play a role in EMT regulation. Specifically, the Coll-MeHA system allows for more control of mechanical factors compared to the traditional collagen only system, which provides another tunable variable in the scheme of biomaterials for directing cell fate. We found that combination crosslinked Coll-MeHA gels promote more endocardial cell outgrowth and proliferation, as well as enhance levels of EMT from chick AVC explants compared to the standard collagen gels. Further, we found enhanced mechanical transduction between the AVC cushion and Coll-MeHA gels such that there was greater contractile strain transfer to the gels, which resulted in mechano-influenced EMT.

Biochemical signaling and endocardial EMT

Soluble MeHA in media or uncrosslinked MeHA in 0.12wt% collagen gels did not increase EMT-related behaviors. This seems to contradict studies showing that soluble HA can induce nearly twice the number of invaded cells in a collagen gel assay [201]. However, the molecular weight of the HA used in the previous study was not discussed and has since been shown to be an important factor in HA signaling [119, 206]. Ventricular explants from stage HH16 chick embryos displayed neither increased endocardial sheet size nor number of invaded cells in our study (Fig. 5.3). These results demonstrate that MeHA

signaling alone is insufficient to cause the dramatic increases in endocardial cell outgrowth and transformed cells observed on Coll-MeHA gels.

Additionally, larger endocardial sheet sizes and more transformed cells present on Coll-MeHA gels cannot be explained by differences in explant viability, as explants demonstrate similar viability levels on differing gel compositions at all time points (Fig. 5.1D). Increased proliferation on Coll-MeHA gels (Fig. 5.1E) may produce some of the large number of invaded cells, but the proliferation rate should have little effect on the migration depths, which are also increased in Coll-MeHA gels. In the traditional collagen gel cushion assay, only 1-2% proliferation is seen at 2d post-explantation of AVCs [77]. Collagen control groups in these studies display roughly 15% proliferation at all time points. The increase in proliferation observed on these gels is likely due to effects of media supplementation which was required for longer culture times used in the studies. In a set of control experiments in which explants on 0.12wt% collagen gels did not receive this additional media, average proliferation was ~4% at 2d, similar to previously reported literature values. Moreover, as a large increase in number of transformed cells was not observed in samples with soluble or uncrosslinked MeHA, HA signaling cannot be solely responsible for the increased number of invaded cells in Coll-MeHA gels.

Contractile forces and endocardial EMT

Mechanical factors considered in this study included substrate stiffness and active contractile forces generated during explant beating, which led to gel

deformation. Levels of invasion do not appear to be stiffness-dependent as 0.4wt% collagen and 0.2wt% collagen + 0.5wt% MeHA are approximately the same stiffness but only Coll-MeHA gels promote greater number of invaded cells. Moreover, 0.12wt% and 0.2wt% collagen have similar moduli (Fig. 5.4G) but dramatically different endocardial sheet size (Fig. 5.1A).This suggests that EMT is not directly related to substrate stiffness and prompted further investigation of myocardial induced deformation in this system.

Previous studies have indicated that the myocardium is required to induce EMT in the collagen gel assay [14]. We hypothesized that it was not only soluble signals but also mechanotransduction from the myocardium that affect EMT. To test this, we used a series of experiments to reduce the effective myocardial contraction rate and magnitude without removing myocardial signaling. Through both physical removal of the myocardium and pharmacological impairment via tricaine, we showed that myocardial contraction regulates EMT. Explants incubated with tricaine had slower, weaker contractions which led to significantly smaller endocardial sheets and fewer invaded cells. Experiments in which the myocardium was removed from the gel substrate, but remained unattached in the media, demonstrated the differential contributions of soluble signaling and myocardial contractions in regulating EMT; the presence of the myocardium (unattached in the media) partially rescued EMT which indicates that the role of soluble factors secreted by the myocardium is contributory but not dominant and further highlights the importance of mechanoregulation in endocardial EMT.

Mechanical network of hydrogel in EMT regulation

We observed greater regional gel deformations on Coll-MeHA gels at all time points when compared to collagen only controls (Fig. 5.7A). This was unexpected, but can be explained by the fact that the Coll-MeHA gel is a semi-interpenetrating network (IPN) caused by sequential MeHA crosslinking followed by collagen gelation around the MeHA crosslinks. The semi-IPN nature of the Coll-MeHA gels therefore transduces strains generated by myocardium over a larger area than a collagen only network. We believe this larger area of mechanotransduction promotes enhanced EMT observed in Coll-MeHA systems, as recent work has suggested that HA modulates integrin-mediated mechanotransduction and subsequent cell phenotype [128]. This could provide a potential intracellular mechanism describing the important cross-talk between mechanical forces and soluble signaling factors in Coll-MeHA gels that regulate EMT. This is the first report of mechanical regulation of endocardial EMT which provides insight into the behavior of a widely studied embryonic cell type.

The role of mechanical forces in the regulation of EMT and other developmental pathways will be important in the creation of novel tissue engineering paradigms for TEHVs. This project demonstrated *in vitro* the mechanical regulation of endocardial EMT on Coll-MeHA gels using avian AVC explants. In an *in vivo* study using a much simpler animal model, the zebrafish, similar results were observed regarding the importance of myocardial contraction in heart valve development [205]. In *silent heart* (sih$^{-/-}$) zebrafish, in which *cardiac troponin T* has a mutation that prevents embryos from establishing blood flow or

even heart beats, endocardial cushions fail to form. These animals can survive for ~7 days post fertilization without a heart beat as sufficient oxygen diffusion can occur without circulation and are a much simpler model of cardiac development. In the Ncx1-/- mouse model, where a sodium-calcium ion exchange gene has been knocked out and the heart fails to beat, embryos die around E11.5 with diminished endocardial cushions and a lack of EMT [207]. Notably, the lack of EMT in these animals cannot be attributed exclusively to the lack of myocardial contractions and is also hypothesized to be an affect of somatic growth retardation.

We have shown that Coll-MeHA gels are a more robust platform for *in vitro* studies as they relate to endocardial EMT and subsequent heart valve formation. This system also allows for controlled mechanical properties and substrate composition for varied ECM signaling components, which yields a more physiologically relevant *in vitro* environment. The enhanced EMT observed on Coll-MeHA gels provides a larger population of valve endocardial cells and progenitor VICs, which represent difficult to obtain embryonic cell types. The population of VIC progenitors generated during EMT is of interest to a large body of cardiac research, from developmental etiologies of congenital heart defects to degenerative, age-associated valve disorders, and even TEHVs. Finally, the Coll-MeHA platform has demonstrated a previously unknown connection between active mechanical forces and the regulation of endocardial EMT.

5.5 Conclusions

In summary, we have developed an *in vitro* model for elucidating the role of mechanical factors on EMT and for the first time confirmed mechanoregulation of EMT. As EMT initiates remodeling of endocardial cushions into mature leaflets, we have shown that the active mechanical forces generated during myocardial contraction play a role in controlling valve formation. Our Coll-MeHA platform studies demonstrate a crucial biomechanical link between the cellular process of endocardial EMT and subsequent mechanical remodeling of HV tissues. This kind of feedback loop is just one example of the complex spatiotemporal and mechanical regulation necessary for development and maintenance of HV leaflets. Better understanding these connections between EMT and mechanics will elucidate important biochemical and biomechanical markers necessary for creating viable TEHVs.

Chapter 6

Societal Implications and Future Directions

6.1 Societal Implications

The overall goal of this project was to gain a better understanding of the mechanical context of HV development and formation. To accomplish this, a two-pronged approach was utilized. In aim 1, we developed an AFM technique for the micromechanical analysis of heart valve tissues which allows for concomitant histological analysis. Using this method, we were able to show differences in valve stiffness due to age and genetic alterations. Although murine models of degenerative heart valve disease do not completely mimic the pathologies of human heart valve diseases, the Notch1$^{+/-}$ and ApoE$^{-/-}$ animals represent the most studied and well-understood models for these studies. Our mechanical analysis indicates that both of these genotypes lead to significant increases in aortic valve leaflet stiffness, even as histological analysis revealed that scanned areas contained comparable ECM components. We additionally demonstrated a small but significant increase in valve stiffness due to aging in wild type mice. Finally, using a porcine aortic valve leaflet, we demonstrated that the AFM technique is capable of distinguishing stiffness differences in the separate regions of the trilaminar heart valve structure. This new AFM protocol provides a powerful tool for micromechanical tissue analyses in the field of heart valve

research in both developmental and pathological contexts. Improving our understanding of the mechanical environment that gives rise to native heart valves and the biomechanical changes involved with degenerative valve diseases will permit the development of novel therapeutic strategies for patients suffering from valve disease and aid in the development of viable TEHVs for those who need replacements.

Following the development of our micromechanical analyses technique, we applied this protocol to the examination of HV remodeling in post-natal aortic valve leaflets of mice lacking Tie1 in the valvular endocardial cells of the developing heart valves. As a key regulator in cardiovascular endothelial stability, Tie1 is implicated in both controlling the number of cells that undergo EMT into the cardiac cushions as well as controlling crosstalk between remaining endocardial cells and transformed cells. The loss of Tie1 in the endocardium of the developing valves leads to significant differences in valve structure, content, and mechanical properties. Taken together, these results indicate that aortic valves do not remodel properly in the mutant mice. The onset of noticeable changes in valve size and content indicate that the remodeling defects occur after the onset of EMT during later gestational and post-natal stages, further demonstrating the role of biomechanics and hemodynamics as regulators of valvulogenesis. Using AFM, we showed that the *Tie1*$^{fl/lz}$*;Nfatc1*^{en}*Cre* mutant mice have aortic valve leaflets with moduli significantly lower than littermate control valve leaflets. This study displayed the biomechanical context of ECM remodeling in heart valve development in an application of traditional CHD

research. As we continue to explore the interactions of biochemical and biomechanical regulators in CHD or valvular disease etiologies, we will be able to improve treatment methodologies and prosthetic valve options for these patients.

Continuing to examine the mechanical context of valve development, in aim 2 we developed and refined a novel hydrogel platform for elucidating mechanical cues in the regulation of EMT. As EMT is a critical initial step in valvulogenesis, understanding the biomechanical regulation of this process is necessary for understanding etiologies of CHDs as well as methods to generate TEHV scaffolds. Specifically, we utilized a crosslinkable HA and collagen, both of which are native biomaterials present in developing heart valves. AVC explants on combination Coll-MeHA gels demonstrated significantly more endocardial cell migration, cell transformation as well as increased migration depths compared to the traditional collagen only control. Further examination revealed that these changes were not simply results of enhanced HA-related signaling or differences in explant viability. Using a series of pharmacological and physical inhibition of myocardial contraction, we demonstrated mechanoregulation of EMT on the Coll-MeHA gels. These studies were the first to indicate that forces generated during myocardial contraction are important in inducing and regulating EMT in the developing valves. Thus, at one of the earliest points in valve development, the mechanical environment is extremely important to ensure proper valve formation. The Coll-MeHA hydrogel platform represents a model for EMT that allows researchers to interrogate the interactions between biomechanical and soluble signaling factors important in regulating early events in valvulogenesis.

Ultimately, this system could improve our understanding of important factors in HV formation which would impact our methods of development for novel valve prostheses.

6.2 Future Directions

The results presented in this dissertation provide novel insight to the mechanical context of HV formation and remodeling which have the potential to impact the development of viable TEHV for pediatric patients with CHDs or elderly patients suffering from degenerative valve diseases. Further work is needed to completely characterize the important biomechanical changes involved with valvulogenesis and how this environment interacts with signaling pathways that have already been identified as regulators of this process. This can be accomplished using the AFM technique we developed in conjunction with the Coll-MeHA hydrogel assay as a dual platform for understanding the mechanobiology of embryonic HVs.

First, a thorough examination of biomechanical ‘milestones’ of the developing heart valve is required to better understand what range of mechanical properties are needed in TEHV scaffolds. With this temporal map of mechanical properties, we will be able to synthesize *in vitro* models that mimic the native mechanical valve environment and study how EMT and other signaling pathways are modified by substrate stiffness. This would ultimately provide guidelines for

the design and implementation of scaffold systems for the synthesis of viable THEVs as well.

Future work should also include the examination of the Coll-MeHA hydrogel system as a method to generate and propagate immortalized cell populations important in the field of valvulogenesis. The endocardial cells and transformed cells generated during EMT represent difficult to obtain embryonic populations that are of considerable interest to numerous researchers. Harvesting these cells in large enough quantities to permit efficient analysis of important genetic markers would allow for significant advances in our understanding of CHD etiologies. For example, harvesting *Tie1*$^{fl/lz}$*-Nfatc1*^{en}*Cre* endocardial cushions and explanting them onto the surface of Coll-MeHA gels may elucidate regulators that differentiate between endocardial cells that can and do undergo EMT compared to those that remain in the endocardial lining during valve remodeling.

With an ever increasing need for better HV replacements, due to increases in the aging population suffering from valve disease and infants born with CHDs, researchers are striving to generate a viable TEHV replacement that could appropriately grow and remodel as required by a patient's specific needs. The first step in synthesizing these next generation prosthetics is to understand the native environment that naturally produces the elegant, highly structured architecture that is a mature heart valve. By uniting our understanding of the signaling pathways that regulate valvulogenesis with a novel appreciation for the appreciation of the biomechanical context that controls these processes, we can

explore novel therapeutic methodologies including creation of living heart valve replacements.

Appendix A

Notes on MATLAB Codes Utilized in Analysis of EMT

Below is a step-by-step description of how cell invasion was mapped to areas of strain and how 3D migration maps were generated. It includes a general overview of how the code functions but not the actual codes.

1. Cells are manually counted in ImageJ. The cell positions are saved for each image in an XML file.
    a. This positional data is later loaded into MATLAB.
2. Images are split into a grid by the “Digital Image Correlation and Tracking with Matlab” code, downloaded from the MATLAB file exchange.
    a. This code splits the image into a grid and tracks how much each grid moves between images; grid size is selected by user.
    b. Each grid has specific coordinates, and the magnitude and direction of strain in each grid is matched to those coordinates.
3. The cell positional data and the strain data were loaded into Matlab for each image. For every cell, if the cell’s position fell into the area of a grid, that cell was associated with the magnitude of strain in that area.
    a. For example, if a grid area had a strain magnitude of 4% and within that area there were three cells inside, then those three cells would be grouped under that strain magnitude.
    b. Cells along two grid borders would not be counted (did not occur enough to affect data).
4. Strain graphs were created by loading the strain data into the quiverc function also downloaded from MATLAB file exchange.
    a. Quiverc plots arrows based on position, magnitude, and direction in the Jet color map.
    b. Cell positional data was overlaid on the same plot.
5. 3D graphs were created by loading each image in a stack separately.
    a. Each image corresponded to a certain depth, and the cells found in that image were associated with that depth.

The notes included below were generated as a “Read Me” guide for use with the cell and strain analysis code.

Program Instructions/Descriptions

Steps before beginning:

1. Put all pairs of images for strain analysis in the "Strain" folder.

2. Optionally, put all Cell Counter XML files in the "XML" folder in the "Cell Position" folder, which leads to less navigating later.

Steps after ending to avoid clutter:

1. Delete/move all images from before.

2. Delete/move all .mat files produced during the scripts in the "Cell Position" and "Strain" folder (labeled *_position.mat and *_strain.mat, respectively).

3. Optionally, move all the .mat files from the top folder (labeled *_final.mat).

List of files and scripts needed for these analyses:

1. Corr Def v3.m

   This code calculates correlation between two images from a beating explant. It also calculates regional gel deformation, normalized to endocardial sheet size.

2. MasterScript1.m

   This script produces the strain maps from the pairs of images you put in the Strain folder. Requires little input, only that you select the images you wish to analyze *in order* by pairs.

Tip: To select the multiple images, click the first image and then hold down either shift and click again(to add all items in between clicks) or Control button while clicking (to add individual items per click).

3. MasterScript2.m

This script produces the cell position files from .xml files produced by the Cell Counter tool in ImageJ. Input for each set of images involves navigating to a target folder and then inputting a string that identifies only the target files you are looking for.

To better explain, an example will be placed below.

Example: You have navigated to a folder containing files

* "CellCounter_02C 05H 24h 051212 a0.xml"

* "CellCounter_02C 05H 24h 051212 a01.xml"

* "CellCounter_02C 05H 24h 051212 b03.xml"

* "CellCounter_02C 05H 24h 051212 d07.xml"

You are only interested in the first two .xml files. You would type in the prompt: (without quotes) "051212 a". The string of letters must be in the order they appear in the filename (i.e. "a 051212" will not work), and must be sufficient to clearly identify the file (i.e. "a" will select more files than desired as will "051212" by itself).

Note: The files must be in alphabetical order! If the files are being listed in the "wrong" order, you should go back and rename them so they will list in alphabetical or numerically increasing order. This can be checked by sorting the files by name in Explorer.

4. MasterScript3.m

This final script merges the cell maps and the strain position data and correlates the two. Input involves selecting matching .mat files from

produced for each group from Scripts 1 & 2. A resulting .mat file is created in the top folder.

5. Graphs.m

   This script pulls up a menu with two options to visualize the data.

   These graphs can be saved in different image formats as usual.

6. Stats.m

   This script spits out several variables into the workspace that can be copied and pasted into a spreadsheet. Input involves selecting some or all of the final .mat files produced by MasterScript3.

7. 3DInvasion.m

   This script generates the 3D graph of cell invasion.

8. JRP_correlation.m

   This script aligns cell positions from XML files (ImageJ) to strain maps generated with Digital Image Correlation code.

9. Ncorr.m

   This program feeds a list of images into JRP_correlation.m to help streamline analysis.

10. MegaList.m

    This program generates a list of multiple image pairs for use in correlation and deformation codes.

11. XML2XY.m

    This program takes positional data from XML files generated during cell counting in ImageJ and coverts it to an XY positional matrix for MATLAB analysis.

12. XML_script.m

    This script loops through XML2XY for lists of image pairs generated in Megalist.m to streamline analysis.

Notes:

- These codes assume you have already set up the "Digital Image Correlation and Tracking with Matlab" M files and read through the included guide to make sure it works on your computer. Different versions or incomplete setup can mess up the strain maps, which makes the rest of the analysis inaccurate. Almost all of the files in the folder marked "Strain" (whether they are used or not) are included in this package, and are only slightly modified from the original work of their authors.

- External files were downloaded from the Matlab file exhange available at http://www.mathworks.com/matlabcentral/fileexchange/

  These include: ImSelectROI, quiverc, and Digital Image Correlation file package

Appendix B

Codes for Mechanoregulation of EMT Analysis

This appendix includes m-files necessary for running regional gel deformation analysis, generating strain maps and cell positional overlays, and generating 3D invasion figures. The programs are listed in order they appear in Appendix A and are referenced by those same numbers.

1. Corr Def v3.m

```
% Gel Deformation Analysis--Correlation between Beating Images
   %Also calculates the area of gel deformation

% Written by MKSL
% 09/25/12 v3
% Vanderbilt University


% Load images and form image stack
clear all
close all
clc

directory='C:\Documents and Settings\MK Sewell\My Documents\Whole Heart Def\';
Image_name='Heart Beat ';
numbers={'1';'2'};

for n=1;%length(numbers); % select image/images with endothelial sheet in focus
   number=char(numbers(n));

a=imread([directory, Image_name, number, '.jpg']);
imG_a=rgb2gray(a);
figure(1);
imshow(imG_a);
end
hold on
for n=2;
   number=char(numbers(n));

   b = imread([directory, Image_name, number, '.jpg']);
```

```
   imG_b=rgb2gray(b);
   figure(2);
   imshow(imG_b);
end

% %Calculate correlation between images, use 1-corr to represent (per Dave)
% corr = corr2(imG_a,imG_b);
% XYZ = 1-corr;
% disp(['The correlation is ' num2str(XYZ)])
%%
%Generate colormap of differences gel/cell movements
diff = imabsdiff(imG_a, imG_b);
figure(3)
imshow(diff,colormap(jet))
imsave(3) %Opens a save dialogue box. Must imput gel type, date, timepoint & explant
for calling purposes
Diff_image = 'Heart Beat';
diff_im = imread([directory, Diff_image, '.jpg']);
%%
imG=rgb2gray(diff_im);   % Convert file to B&W image
%figure(4);
%imshow(imG);
[r,c]=size(imG);
%figure(5);
%imhist(diff);

imG_Bin=im2bw(diff_im,0.5);
%figure(6);
%imshow(imG_Bin);

%% Calls function to select rectangular area around explant and returns cell type variable
(ROI) with range of ROI
ROI=imSelectROI(imG_Bin);

%Set up a ellipse to cover explant and convert it all to positive
%% Isolates Elliptical section bounded by Region of interest rectangle
a=round(length(ROI.Xrange)/2);
b=round(length(ROI.Yrange)/2);
y=([1:r]-round(length(ROI.Yrange)/2)-ROI.Ymin);
x=([1:c]-round(length(ROI.Xrange)/2)-ROI.Xmin);

for i=1:r
   for j=1:c
      if (x(j)/a)^2+(y(i)/b)^2>1
      imG_Bin(i,j)=imG_Bin(i,j); % Leave everything outside of small ellipse as is
      elseif (x(j)/a)^2+(y(i)/b)^2<1
      imG_Bin(i,j)=255; % Sets everything inside small ellipse to max
      end
   end
```

```
end
%figure(7);
%imshow(imG_Bin);

Pixel_Count=0;
for i=1:r
   for j = 1:c
      if imG_Bin(i,j) > 0
         Pixel_Count = Pixel_Count + 1;
      end
   end
end

Pixel_Count;
Total_pixels=r*c;
Percent_positive_pixels=(Pixel_Count/Total_pixels)*100;
% Area_Def=Area*Percent_positive_pixels;

disp(['The % deformation in image is ' num2str(Percent_positive_pixels)])
%%
% imGa_Bin=im2bw(imG_a,0.2);
% [ra,ca]=size(imGa_Bin);
% Pixel_Count_a=0;
% for i=1:ra
%    for j = 1:ca
%       if imGa_Bin(i,j) > 0
%          Pixel_Count_a = Pixel_Count_a + 1;
%       end
%    end
% end
% Pixel_Count_a;
% Total_pixels_a=ra*ca;
% Percent_positive_pixels_a=Pixel_Count_a/Total_pixels_a;
% Area_Full=Area*Percent_positive_pixels_a;
% Contractile_Strain = (Area_Def/Area_Full)*100;
%
% disp(['The contractile strain is ' num2str(Contractile_Strain)])
```

2. MasterScript1.m

```
close all
clear all
clc
cd('Folder')
fprintf('\n Welcome to MasterScript Part One! If you havent done so, read the readme
first. Press any key to get started...')
pause
MegaList
clear all
```

```
load filenamelist
fprintf('\n\n Press any key to begin strain analysis. Note that this can take quite some
time...');
pause
cd('Strain')
MegaStrain
cd('../')
cd('../')
fprintf('\n\n\n  Part One complete! Please run MasterScript2.m\n');
close all
clear all
```

3. MasterScript2.m

```
clc
cd('Folder')
load filenamelist
nnn = length(filenamelist(:,1))/2;
cd('Cell Position')
for iii = 1:nnn
   fprintf('\n Press any key to find cell positions for explant %g of %g...',iii,nnn);
   pause
   XML_Script
end
cd('../')
cd('../')
fprintf('\n\n\n  Part Two complete! Please run MasterScript3.m\n');
close all
clear all
```

4. MasterScript3.m

```
clc
cd('Folder')
load filenamelist
nnn = length(filenamelist(:,1))/2;

for iii = 1:nnn
   fprintf('\n Press any key to correlate cell positions with strain for explant %g of
%g...',iii,nnn);
   pause
   NCorr
   cd('Folder')
   clc
end
cd('../')
fprintf('\n\n  Script complete! Run Graphs.m to see your results.\n');
```

5. Graphs.m

```
close all
clear all
clc

[filename,pathname] = uigetfile('*.mat','Choose the final .mat file.');
load(sprintf('%s',pathname,filename))

cd('Folder')
select = 0;
while select ~=6
select = menu(sprintf('%s',filename),'3D Plot of Cells','Cell plots and strain map.','Close');
if select == 1
   figure(1)
   3DInvasion(M);
end
if select == 2
   figure(2)
   quiverc(validx(:,1),validy(:,1),displx(:,2),disply(:,2));
   caxis([0,20]);
   h = colorbar;
   set(gca, 'CLim', [0,20]);, hold on;
   plot(M_coll(:,1),M_coll(:,2),'*k');,
   %title('Cell locations with strain map.'); hold on;
   axis([0 1600 0 1200]);
   axis image
   set(gca,'XTick',(0:200:1000)/.686)
   set(gca,'YTick',(0:200:800)/.686)
   set(gca,'XTickLabel',{'0','200','400','600','800','1000'})
   set(gca,'YTickLabel',{'0','200','400','600','800'})
   xlabel('Length(\mum)');
   ylabel('Width(\mum)');
   xlabel(h, 'Strain(%)');
end
if select == 3
   break
end
end
cd('../')
```

6. Stats.m

```
close all
clear all
clc

[filenames,pathnames] = uigetfile('*.mat','Choose .mat batch.','MultiSelect','on');
cd('Folder')
```

```
for n = 1:length(filenames)
   load(sprintf('%s',pathnames,filenames{n}), 'Magnitude', 'countlist')
   running_average = 0;
   for ii = 1:length(countlist)
      running_average = running_average +
(countlist(ii,1)*countlist(ii,2))/(sum(countlist(:,1)));
   end
   master_median(n,1) = median(countlist(:,2));
   master_weightedaverage(n,1) = running_average;
   output{n} = JRPbar2( countlist,Magnitude );
   master_bardata(n,1:length(output{n})) = output{n};
   master_afilelist(n,1:length(filenames{n})) = filenames{n};
   clear Magnitude countlist
end
clear ii filenames n output pathnames running_average
clc
fprintf('\n\n Complete! Stats are available for manipulation in the workspace.\n')
cd('../')
```

7. 3DInvasion.m

```
function [  ] = 3DInvasion( M )

close all
hold on
n = length(M);
map = colormap(jet(n));
zmax = 50*length(M);
title('3D Plot of Invaded Cells');
axis([0 1100 0 825 25 zmax+25]);
h = colorbar();
set(gca, 'CLim', [.5, n+0.5]);
set(h, 'XTick',1.5:0.5:n);
%set(h,'XTickLabel',{50:25:zmax});
xlabel(h, 'Layer');
%colorbar('YTickLabel',{50:50:zmax,'Depth(microns)'},'YTickMode','manual','YTick',1:n+1
);
xlabel('Length(\mum)');
ylabel('Width(\mum)');
zlabel('Depth(\mum)');
for n = 1:length(M)
   hh = plot3(M{n}(:,1)*.686,M{n}(:,2)*.686,ones(length(M{n}),1)*50*n,'*','color',map(n,:));
end

rotate3d on
hold off

end
```

8. JRP_correlation.m

```
function [ countlist,M_coll,bar_data ] = JRP_correlation( M,validx,validy,Magnitude )

grid_size = 25;

% Collapse M
M_coll = 0; index = 1;
for ii = 1:length(M)
   for jj = 1:length(M{ii}(:,1))
      M_coll(index,1) = M{ii}(jj,1); M_coll(index,2) = M{ii}(jj,2);
      index = index + 1;
   end
end

countlist = zeros(size(validx));
for ii = 1:length(validx(:,1))
   countlist(ii,2) = Magnitude(ii);
   for jj = 1:length(M_coll(:,1))
      if abs(validx(ii,1) - M_coll(jj,1)) < grid_size/2
         if abs(validy(ii,1) - M_coll(jj,2)) < grid_size/2 %<=
            countlist(ii,1) = countlist(ii,1) + 1;
%
%              Bugtesting stuff.
%              validx(ii,1)
%              M_coll(jj,1)
%              abs(validx(ii,1) - M_coll(jj,1))
%              validy(ii,1)
%              M_coll(jj,2)
%              abs(validy(ii,1) - M_coll(jj,2))
%              Magnitude(ii)
%              countlist(ii,1)
%              pause
%
         end
      end
%        if abs(validx(ii,1) - M_coll(jj,1)) == grid_size/2
%           if abs(validy(ii,1) - M_coll(jj,2)) < grid_size/2
%              countlist(ii,1) = countlist(ii,1) + 1;
%           end
%        end
   end
end

n = ceil(max(Magnitude));
bar_data = zeros(1,n);
for ii = 1:n
   for jj = 1:length(countlist(:,1))
      if countlist(jj,2) >= ii-1 && countlist(jj,2) < ii
```

```
            bar_data(1,ii) = bar_data(1,ii) + countlist(jj,1);
        end
    end
end

end
```

9. Ncorr.m

```
check = 0;

while check == 0;

    [filename,pathname] = uigetfile('*.mat','Choose the .mat file containing cell positions.','MultiSelect','on');

    load(sprintf('%s',pathname,filename), 'M')

    filename

    [filename,pathname] = uigetfile('*.mat','Choose the .mat file containing the strain field.','MultiSelect','on');

    load(sprintf('%s',pathname,filename), 'validx', 'validy', 'displx', 'disply', 'Magnitude')

    filename

    [countlist,M_coll] = JRP_correlation(M,validx,validy,Magnitude);

    %[ output ] = JRPbar2( countlist,Magnitude );

    fprintf('\n Do these filenames appear to match? 1 for yes and 0 for no:');

    check = input(' ');

end

savename1 = sprintf(filename(1,:),'%s');

savename2 = sprintf('%s',savename1(1:(length(savename1)-4)),'_final.mat');

cd('../')

save(savename2,'validx', 'validy', 'displx', 'disply', 'Magnitude', 'M', 'countlist', 'M_coll')

fprintf('\nFile saved as %s\n\n',savename2);
```

10. MegaList.m

```
cd('Strain')
```

```
[filenames,pathname] = uigetfile('*.jpg','Choose the pairs of images *in order* that you
wish to produce strain fields for.','MultiSelect','on');
for n = 1:length(filenames)
   for nn = 1:length(filenames{n})
   filenamelist(n,nn) = [filenames{n}(nn)];
   end
end
fprintf('\n');
filenamelist
inp = input('\n Does this list appear correct? 1 for Yes 0 for No: ');
if inp ~= 1
   error('Please try again.')
end
cd('../');
save filenamelist;
```

11. XML2XY.m

```
function [ M,fileout ] = XML2XY( filein )

if isempty(filein) == 1
   filein = 'target images.';
end
string = sprintf('%s','Find dir. of XML files for ',filein);
currentfolder = pwd;
directory = uigetdir('',string);
explant = inputdlg('Please input the letter of the explant you are interested in and the
identifying characters before it. (For example, for  sample2_080613_b03.xml through
sample2_080613_b09.xml, input 080613_b)');
cd(directory);
wildcard = [sprintf('*%s*',explant{1}), '.xml'];
filelist = dir(wildcard);
totalcount = 0;

for ii = 1:length(filelist)
   fid = fopen(filelist(ii).name);
   tline = fgetl(fid);
   n = 1;
   while ischar(tline)
      chop = textscan(tline,'<MarkerX> %s');
      if isempty(chop{1}) == 0
         chop2 = chop{1};
         pohc = chop2{1}(end:-1:1);
         cut = textscan(pohc,'>XrekraM/< %s');
         cut2 = cut{1};
         tuc2 = cut2{1}(end:-1:1);
         M{ii}(n,1) = str2double(tuc2);
      end
      chop = textscan(tline,'<MarkerY> %s');
```

```
        if isempty(chop{1}) == 0
            chop2 = chop{1};
            pohc = chop2{1}(end:-1:1);
            cut = textscan(pohc,'>YrekraM/< %s');
            cut2 = cut{1};
            tuc2 = cut2{1}(end:-1:1);
            M{ii}(n,2) = str2double(tuc2);
            n = n+1;
        end
        tline = fgetl(fid);
    end
    fprintf('\n\n For file %s, the count is %g.',filelist(ii).name,length(M{ii}(:,1)));
    totalcount = length(M{ii}(:,1)) + totalcount;
    fclose(fid);
end

fprintf('\n\n\n Total count is %g.\n',totalcount);
cd(currentfolder);
if isempty(filelist) == 0
    fileout = filelist(1).name;
else
    fileout = 0;
    M = 0;
end

end
```

12. XML_Script.m

```
check = 0;
while check == 0;
    clc
    fprintf('Matching strain image is %s.',filenamelist(iii*2,:));
    filein = filenamelist(iii*2,:);
    [M fileout] = XML2XY(filein);
    fprintf('\n Do these results appear correct? 1 for yes and 0 for no:');
    check = input(' ');
end

savename1 = sprintf(fileout,'%s');
savename2 = sprintf('%s',savename1(1:(length(savename1)-4)),'_position.mat');
save(savename2)
fprintf('\n  File saved as %s\n\n',savename2);
```

REFERENCES

1. Samanek, M., *Congenital heart malformations: prevalence, severity, survival, and quality of life.* Cardiol Young, 2000. **10**(3): p. 179-85.
2. Hoffman, J.I. and S. Kaplan, *The incidence of congenital heart disease.* J Am Coll Cardiol, 2002. **39**(12): p. 1890-900.
3. Loffredo, C.A., *Epidemiology of cardiovascular malformations: prevalence and risk factors.* Am J Med Genet, 2000. **97**(4): p. 319-25.
4. Murray, G., *Homologous aortic-valve-segment transplants as surgical treatment for aortic and mitral insufficiency.* Angiology, 1956. **7**(5): p. 466-71.
5. Hufnagel, C.A., P.D. Villegas, and H. Nahas, *Experiences with new types of aortic valvular prostheses.* Ann Surg, 1958. **147**(5): p. 636-44; discussion 644-5.
6. Braunwald, N.S., T. Cooper, and A.G. Morrow, *Complete replacement of the mitral valve. Successful clinical application of a flexible polyurethane prosthesis.* J Thorac Cardiovasc Surg, 1960. **40**: p. 1-11.
7. Harken, D.E., et al., *Partial and complete prostheses in aortic insufficiency.* J Thorac Cardiovasc Surg, 1960. **40**: p. 744-62.
8. Starr, A. and M.L. Edwards, *Mitral replacement: clinical experience with a ball-valve prosthesis.* Ann Surg, 1961. **154**: p. 726-40.
9. Braunwald, E., *Aortic valve replacement: an update at the turn of the millennium.* Eur Heart J, 2000. **21**(13): p. 1032-3.

10. Cohn, L.H., et al., *Fifteen-year experience with 1678 Hancock porcine bioprosthetic heart valve replacements.* Ann Surg, 1989. **210**(4): p. 435-42; discussion 442-3.
11. Jamieson, W.R., et al., *The Carpentier-Edwards standard porcine bioprosthesis. A first-generation tissue valve with excellent long-term clinical performance.* J Thorac Cardiovasc Surg, 1990. **99**(3): p. 543-61.
12. Mendelson, K. and F.J. Schoen, *Heart valve tissue engineering: concepts, approaches, progress, and challenges.* Ann Biomed Eng, 2006. **34**(12): p. 1799-819.
13. Ingber, D.E., et al., *Tissue engineering and developmental biology: going biomimetic.* Tissue Eng, 2006. **12**(12): p. 3265-83.
14. Runyan, R.B. and R.R. Markwald, *Invasion of mesenchyme into three-dimensional collagen gels: a regional and temporal analysis of interaction in embryonic heart tissue.* Dev Biol, 1983. **95**(1): p. 108-14.
15. Gomez, E.W., et al., *Tissue geometry patterns epithelial-mesenchymal transition via intercellular mechanotransduction.* J Cell Biochem, 2010. **110**(1): p. 44-51.
16. Gjorevski, N., E. Boghaert, and C.M. Nelson, *Regulation of Epithelial-Mesenchymal Transition by Transmission of Mechanical Stress through Epithelial Tissues.* Cancer Microenviron, 2012. **5**(1): p. 29-38.
17. Yacoub, M.H. and J.J. Takkenberg, *Will heart valve tissue engineering change the world?* Nat Clin Pract Cardiovasc Med, 2005. **2**(2): p. 60-1.

18. Merryman, W.D., et al., *Correlation between heart valve interstitial cell stiffness and transvalvular pressure: implications for collagen biosynthesis.* Am J Physiol Heart Circ Physiol, 2006. **290**(1): p. H224-31.

19. Elkins, R., *Is Tissued-engineered Heart Vavle Replacement Clinically Applicable?* Current Cardiology Reports, 2003. **5**: p. 125-128.

20. Filova, E., et al., *Tissue-engineered heart valves.* Physiol Res, 2009. **58 Suppl 2**: p. S141-58.

21. Goldstein, S., et al., *Transpecies heart valve transplant: advanced studies of a bioengineered xeno-autograft.* Ann Thorac Surg, 2000. **70**(6): p. 1962-9.

22. Carpentier, A., et al., *Biological factors affecting long-term results of valvular heterografts.* J Thorac Cardiovasc Surg, 1969. **58**(4): p. 467-83.

23. Schmidt, C.E. and J.M. Baier, *Acellular vascular tissues: natural biomaterials for tissue repair and tissue engineering.* Biomaterials, 2000. **21**(22): p. 2215-31.

24. Dohmen, P.M., et al., *Results of a decellularized porcine heart valve implanted into the juvenile sheep model.* Heart Surg Forum, 2005. **8**(2): p. E100-4; discussion E104.

25. Dohmen, P.M. and W. Konertz, *Tissue-engineered heart valve scaffolds.* Ann Thorac Cardiovasc Surg, 2009. **15**(6): p. 362-7.

26. Dohmen, P.M., et al., *Mid-term clinical results using a tissue-engineered pulmonary valve to reconstruct the right ventricular outflow tract during the Ross procedure.* Ann Thorac Surg, 2007. **84**(3): p. 729-36.

27. Erdbrugger, W., et al., *Decellularized xenogenic heart valves reveal remodeling and growth potential in vivo.* Tissue Eng, 2006. **12**(8): p. 2059-68.

28. Konertz, W., et al., *Hemodynamic characteristics of the Matrix P decellularized xenograft for pulmonary valve replacement during the Ross operation.* J Heart Valve Dis, 2005. **14**(1): p. 78-81.

29. Vesely, I., *Heart valve tissue engineering.* Circ Res, 2005. **97**(8): p. 743-55.

30. Neuenschwander, S. and S.P. Hoerstrup, *Heart valve tissue engineering.* Transpl Immunol, 2004. **12**(3-4): p. 359-65.

31. O'Brien, M.F., et al., *The SynerGraft valve: a new acellular (nonglutaraldehyde-fixed) tissue heart valve for autologous recellularization first experimental studies before clinical implantation.* Semin Thorac Cardiovasc Surg, 1999. **11**(4 Suppl 1): p. 194-200.

32. Bechtel, J.E.M., U. Stierle, and H.H. Sievers, *Fifty-two months' mean follow up of decellularized SynerGraft (TM)-treated pulmonary valve allografts.* Journal of Heart Valve Disease, 2008. **17**(1): p. 98-104.

33. Bechtel, J.F., et al., *Evaluation of the decellularized pulmonary valve homograft (SynerGraft).* J Heart Valve Dis, 2003. **12**(6): p. 734-9; discussion 739-40.

34. Tavakkol, Z., et al., *Superior durability of SynerGraft pulmonary allografts compared with standard cryopreserved allografts.* Ann Thorac Surg, 2005. **80**(5): p. 1610-4.

35. Steinhoff, G., et al., *Tissue engineering of pulmonary heart valves on allogenic acellular matrix conduits: in vivo restoration of valve tissue.* Circulation, 2000. **102**(19 Suppl 3): p. III50-5.

36. Booth, C., et al., *Tissue engineering of cardiac valve prostheses I: development and histological characterization of an acellular porcine scaffold.* J Heart Valve Dis, 2002. **11**(4): p. 457-62.

37. Liao, J., E.M. Joyce, and M.S. Sacks, *Effects of decellularization on the mechanical and structural properties of the porcine aortic valve leaflet.* Biomaterials, 2008. **29**(8): p. 1065-74.

38. Schoen, F.J., *Pathologic findings in explanted clinical bioprosthetic valves fabricated from photooxidized bovine pericardium.* J Heart Valve Dis, 1998. **7**(2): p. 174-9.

39. Schoen, F.J., *Heart valve tissue engineering: quo vadis?* Curr Opin Biotechnol, 2011.

40. Simon, P., et al., *Early failure of the tissue engineered porcine heart valve SYNERGRAFT in pediatric patients.* Eur J Cardiothorac Surg, 2003. **23**(6): p. 1002-6; discussion 1006.

41. Hopkins, R.A., *Tissue engineering of heart valves: decellularized valve scaffolds.* Circulation, 2005. **111**(21): p. 2712-4.

42. Sacks, M.S., W. David Merryman, and D.E. Schmidt, *On the biomechanics of heart valve function.* J Biomech, 2009. **42**(12): p. 1804-24.

43. Merryman, W.D., *Mechano-potential etiologies of aortic valve disease.* Journal of Biomechanics, 2010. **43**(1): p. 87-92.

44. Gottlieb, D., et al., *In vivo monitoring of function of autologous engineered pulmonary valve.* J Thorac Cardiovasc Surg, 2010. **139**(3): p. 723-31.

45. Hildebrand, D.K., et al., *Design and hydrodynamic evaluation of a novel pulsatile bioreactor for biologically active heart valves.* Ann Biomed Eng, 2004. **32**(8): p. 1039-49.

46. Dumont, K., et al., *Design of a new pulsatile bioreactor for tissue engineered aortic heart valve formation.* Artif Organs, 2002. **26**(8): p. 710-4.

47. Engelmayr, G.C., Jr., et al., *A novel bioreactor for the dynamic flexural stimulation of tissue engineered heart valve biomaterials.* Biomaterials, 2003. **24**(14): p. 2523-32.

48. Hoerstrup, S.P., et al., *New pulsatile bioreactor for in vitro formation of tissue engineered heart valves.* Tissue Eng, 2000. **6**(1): p. 75-9.

49. Mol, A., et al., *Tissue engineering of human heart valve leaflets: a novel bioreactor for a strain-based conditioning approach.* Ann Biomed Eng, 2005. **33**(12): p. 1778-88.

50. Ruel, J. and G. Lachance, *A new bioreactor for the development of tissue-engineered heart valves.* Ann Biomed Eng, 2009. **37**(4): p. 674-81.

51. Sierad, L.N., et al., *Design and Testing of a Pulsatile Conditioning System for Dynamic Endothelialization of Polyphenol-Stabilized Tissue*

Engineered Heart Valves. Cardiovasc Eng Technol, 2010. **1**(2): p. 138-153.

52. Merryman, W.D., *Development of a tissue engineered heart valve for pediatrics: a case study in bioengineering ethics.* Sci Eng Ethics, 2008. **14**(1): p. 93-101.

53. Ramaswamy, S., et al., *The role of organ level conditioning on the promotion of engineered heart valve tissue development in-vitro using mesenchymal stem cells.* Biomaterials, 2010. **31**(6): p. 1114-25.

54. Engelmayr, G.C., Jr., et al., *A novel flex-stretch-flow bioreactor for the study of engineered heart valve tissue mechanobiology.* Ann Biomed Eng, 2008. **36**(5): p. 700-12.

55. Butler, D.L., et al., *Functional tissue engineering parameters toward designing repair and replacement strategies.* Clin Orthop Relat Res, 2004(427 Suppl): p. S190-9.

56. Wilson, C.A., et al., *Type C retrovirus released from porcine primary peripheral blood mononuclear cells infects human cells.* J Virol, 1998. **72**(4): p. 3082-7.

57. Knight, R. and S. Collins, *Human prion diseases: cause, clinical and diagnostic aspects.* Contrib Microbiol, 2001. **7**: p. 68-92.

58. Riem Vis, P.W., et al., *Environmental regulation of valvulogenesis: implications for tissue engineering.* Eur J Cardiothorac Surg, 2011. **39**(1): p. 8-17.

59. Lenas, P. and F.P. Luyten, *An Emerging Paradigm in Tissue Engineering: From Chemical Engineering to Developmental Engineering for Bioartificial Tissue Formation through a Series of Unit Operations that Simulate the In Vivo Successive Developmental Stages.* Industrial & Engineering Chemistry Research, 2011. **50**(2): p. 482-522.

60. Ingber, D.E. and M. Levin, *What lies at the interface of regenerative medicine and developmental biology?* Development, 2007. **134**(14): p. 2541-2547.

61. Combs, M.D. and K.E. Yutzey, *Heart valve development: regulatory networks in development and disease.* Circ Res, 2009. **105**(5): p. 408-21.

62. Thiery, J.P. and J.P. Sleeman, *Complex networks orchestrate epithelial-mesenchymal transitions.* Nat Rev Mol Cell Biol, 2006. **7**(2): p. 131-42.

63. Armstrong, E.J. and J. Bischoff, *Heart valve development - Endothelial cell signaling and differentiation.* Circ Res, 2004. **95**(5): p. 459-470.

64. Hinton, R.B. and K.E. Yutzey, *Heart Valve Structure and Function in Development and Disease.* Annu Rev Physiol, 2010.

65. Person, A.D., S.E. Klewer, and R.B. Runyan, *Cell biology of cardiac cushion development.* Int Rev Cytol, 2005. **243**: p. 287-335.

66. Kalluri, R. and R.A. Weinberg, *The basics of epithelial-mesenchymal transition.* J Clin Invest, 2009. **119**(6): p. 1420-8.

67. Thiery, J.P., et al., *Epithelial-mesenchymal transitions in development and disease.* Cell, 2009. **139**(5): p. 871-90.

68. Barnett, J.V. and J.S. Desgrosellier, *Early events in valvulogenesis: a signaling perspective.* Birth Defects Res C Embryo Today, 2003. **69**(1): p. 58-72.

69. Olivey, H.E., et al., *Transforming growth factor-beta stimulates epithelial-mesenchymal transformation in the proepicardium.* Dev Dyn, 2006. **235**(1): p. 50-9.

70. Hay, E.D., *An overview of epithelio-mesenchymal transformation.* Acta Anat (Basel), 1995. **154**(1): p. 8-20.

71. Delaughter, D.M., et al., *What chick and mouse models have taught us about the role of the endocardium in congenital heart disease.* Birth Defects Res A Clin Mol Teratol, 2011.

72. Stevens, M.V., et al., *MEKK3 initiates transforming growth factor beta 2-dependent epithelial-to-mesenchymal transition during endocardial cushion morphogenesis.* Circ Res, 2008. **103**(12): p. 1430-40.

73. Chiu, Y.N., et al., *Transforming growth factor beta, bone morphogenetic protein, and vascular endothelial growth factor mediate phenotype maturation and tissue remodeling by embryonic valve progenitor cells: relevance for heart valve tissue engineering.* Tissue Eng Part A, 2010. **16**(11): p. 3375-83.

74. Hill, C.R., et al., *BMP2 signals loss of epithelial character in epicardial cells but requires the Type III TGFbeta receptor to promote invasion.* Cell Signal, 2012. **24**(5): p. 1012-22.

75. Sanchez, N.S. and J.V. Barnett, *TGFbeta and BMP-2 regulate epicardial cell invasion via TGFbetaR3 activation of the Par6/Smurf1/RhoA pathway.* Cell Signal, 2012. **24**(2): p. 539-48.

76. Sanchez, N.S., et al., *The cytoplasmic domain of TGFbetaR3 through its interaction with the scaffolding protein, GIPC, directs epicardial cell behavior.* Dev Biol, 2011. **358**(2): p. 331-43.

77. Townsend, T.A., et al., *Endocardial cell epithelial-mesenchymal transformation requires Type III TGFbeta receptor interaction with GIPC.* Cell Signal, 2012. **24**(1): p. 247-56.

78. Bernanke, D.H. and R.R. Markwald, *Migratory behavior of cardiac cushion tissue cells in a collagen-lattice culture system.* Dev Biol, 1982. **91**(2): p. 235-45.

79. Camenisch, T.D., et al., *Disruption of hyaluronan synthase-2 abrogates normal cardiac morphogenesis and hyaluronan-mediated transformation of epithelium to mesenchyme.* J Clin Invest, 2000. **106**(3): p. 349-60.

80. Brown, C.B., et al., *Requirement of type III TGF-beta receptor for endocardial cell transformation in the heart.* Science, 1999. **283**(5410): p. 2080-2.

81. Boyden, S., *The chemotactic effect of mixtures of antibody and antigen on polymorphonuclear leucocytes.* J Exp Med, 1962. **115**: p. 453-66.

82. Chen, H.C., *Boyden chamber assay.* Methods Mol Biol, 2005. **294**: p. 15-22.

83. Lencinas, A., et al., *Collagen gel analysis of epithelial-mesenchymal transition in the embryo heart: an in vitro model system for the analysis of tissue interaction, signal transduction, and environmental effects.* Birth Defects Res C Embryo Today, 2011. **93**(4): p. 298-311.

84. Katz, E., et al., *An in vitro model that recapitulates the epithelial to mesenchymal transition (EMT) in human breast cancer.* PLoS One, 2011. **6**(2): p. e17083.

85. Kim, K.K. and H.A. Chapman, *Endothelin-1 as initiator of epithelial-mesenchymal transition: potential new role for endothelin-1 during pulmonary fibrosis.* Am J Respir Cell Mol Biol, 2007. **37**(1): p. 1-2.

86. Azhar, M., et al., *Ligand-specific function of transforming growth factor beta in epithelial-mesenchymal transition in heart development.* Dev Dyn, 2009. **238**(2): p. 431-42.

87. Markwald, R.R., et al., *Developmental basis of adult cardiovascular diseases: valvular heart diseases.* Ann N Y Acad Sci, 2010. **1188**: p. 177-83.

88. Aikawa, E., et al., *Human semilunar cardiac valve remodeling by activated cells from fetus to adult: implications for postnatal adaptation, pathology, and tissue engineering.* Circulation, 2006. **113**(10): p. 1344-52.

89. Hinton, R.B., Jr., et al., *Extracellular matrix remodeling and organization in developing and diseased aortic valves.* Circ Res, 2006. **98**(11): p. 1431-8.

90. Paruchuri, S., et al., *Human pulmonary valve progenitor cells exhibit endothelial/mesenchymal plasticity in response to vascular endothelial*

growth factor-A and transforming growth factor-beta2. Circ Res, 2006. **99**(8): p. 861-9.

91. Fisher, C.I., J. Chen, and W.D. Merryman, *Calcific nodule morphogenesis by heart valve interstitial cells is strain dependent.* Biomech Model Mechanobiol, 2012.
92. Merryman, W.D., *Insights into (the interstitium of) degenerative aortic valve disease.* Journal of the American College of Cardiology, 2008. **51**(14): p. 1415-1415.
93. Sansoucie, D.A. and T.A. Cavaliere, *Transition from fetal to extrauterine circulation.* Neonatal Netw, 1997. **16**(2): p. 5-12.
94. Anderson, P.A., et al., *Developmental changes in cardiac contractility in fetal and postnatal sheep: in vitro and in vivo.* Am J Physiol, 1984. **247**(3 Pt 2): p. H371-9.
95. Friedman, A.H. and J.T. Fahey, *The transition from fetal to neonatal circulation: normal responses and implications for infants with heart disease.* Semin Perinatol, 1993. **17**(2): p. 106-21.
96. McConnell, M. and A. Branigan, *Innocent Heart Murmurs*, in *Pediatric Heart Sounds*. 2008, Springer London. p. 13-25.
97. Stephens, E.H., et al., *Age-related changes in material behavior of porcine mitral and aortic valves and correlation to matrix composition.* Tissue Eng Part A, 2010. **16**(3): p. 867-78.
98. Wirrig, E.E. and K.E. Yutzey, *Developmental Pathways in CAVD*. Calcific Aortic Valve Disease. 2013.

99. Krishnamurthy, V.K., et al., *Regional structure-function relationships in mouse aortic valve tissue.* J Biomech, 2011. **44**(1): p. 77-83.

100. Buskohl, P.R., R.A. Gould, and J.T. Butcher, *Quantification of embryonic atrioventricular valve biomechanics during morphogenesis.* J Biomech, 2011.

101. Butcher, J.T., et al., *Transitions in early embryonic atrioventricular valvular function correspond with changes in cushion biomechanics that are predictable by tissue composition.* Circ Res, 2007. **100**(10): p. 1503-11.

102. Young, J.L. and A.J. Engler, *Hydrogels with time-dependent material properties enhance cardiomyocyte differentiation in vitro.* Biomaterials, 2011. **32**(4): p. 1002-9.

103. Langer, R. and J.P. Vacanti, *Tissue engineering.* Science, 1993. **260**(5110): p. 920-6.

104. Benton, J.A., B.D. Fairbanks, and K.S. Anseth, *Characterization of valvular interstitial cell function in three dimensional matrix metalloproteinase degradable PEG hydrogels.* Biomaterials, 2009. **30**(34): p. 6593-603.

105. Benton, J.A., H.B. Kern, and K.S. Anseth, *Substrate properties influence calcification in valvular interstitial cell culture.* J Heart Valve Dis, 2008. **17**(6): p. 689-99.

106. Kloxin, A.M., et al., *Photodegradable hydrogels for dynamic tuning of physical and chemical properties.* Science, 2009. **324**(5923): p. 59-63.

107. Kloxin, A.M., J.A. Benton, and K.S. Anseth, *In situ elasticity modulation with dynamic substrates to direct cell phenotype.* Biomaterials, 2010. **31**(1): p. 1-8.

108. Kloxin, A.M., M.W. Tibbitt, and K.S. Anseth, *Synthesis of photodegradable hydrogels as dynamically tunable cell culture platforms.* Nat Protoc, 2010. **5**(12): p. 1867-87.

109. Kirschner, C.M., et al., *Clickable, Photodegradable Hydrogels to Dynamically Modulate Valvular Interstitial Cell Phenotype.* Adv Healthc Mater, 2014.

110. Kidane, A.G., et al., *A novel nanocomposite polymer for development of synthetic heart valve leaflets.* Acta Biomater, 2009. **5**(7): p. 2409-17.

111. Shinoka, T., et al., *Tissue engineering heart valves: valve leaflet replacement study in a lamb model.* Ann Thorac Surg, 1995. **60**(6 Suppl): p. S513-6.

112. Zund, G., et al., *The in vitro construction of a tissue engineered bioprosthetic heart valve.* Eur J Cardiothorac Surg, 1997. **11**(3): p. 493-7.

113. Ramamurthi, A. and I. Vesely, *Evaluation of the matrix-synthesis potential of crosslinked hyaluronan gels for tissue engineering of aortic heart valves.* Biomaterials, 2005. **26**(9): p. 999-1010.

114. Sodian, R., et al., *Fabrication of a trileaflet heart valve scaffold from a polyhydroxyalkanoate biopolyester for use in tissue engineering.* Tissue Eng, 2000. **6**(2): p. 183-8.

115. Hoerstrup, S.P., et al., *Functional living trileaflet heart valves grown in vitro.* Circulation, 2000. **102**(19 Suppl 3): p. III44-9.

116. Schmidt, D., et al., *Minimally-invasive implantation of living tissue engineered heart valves: a comprehensive approach from autologous vascular cells to stem cells.* J Am Coll Cardiol, 2010. **56**(6): p. 510-20.

117. Dvorin, E.L., et al., *Quantitative evaluation of endothelial progenitors and cardiac valve endothelial cells: proliferation and differentiation on poly-glycolic acid/poly-4-hydroxybutyrate scaffold in response to vascular endothelial growth factor and transforming growth factor beta1.* Tissue Eng, 2003. **9**(3): p. 487-93.

118. Sales, V.L., et al., *Endothelial progenitor cells as a sole source for ex vivo seeding of tissue-engineered heart valves.* Tissue Eng Part A, 2010. **16**(1): p. 257-67.

119. Masters, K.S., et al., *Crosslinked hyaluronan scaffolds as a biologically active carrier for valvular interstitial cells.* Biomaterials, 2005. **26**(15): p. 2517-25.

120. Flanagan, T.C., et al., *A collagen-glycosaminoglycan co-culture model for heart valve tissue engineering applications.* Biomaterials, 2006. **27**(10): p. 2233-46.

121. Kreger, S.T. and S.L. Voytik-Harbin, *Hyaluronan concentration within a 3D collagen matrix modulates matrix viscoelasticity, but not fibroblast response.* Matrix Biol, 2009. **28**(6): p. 336-46.

122. Suri, S. and C.E. Schmidt, *Photopatterned collagen-hyaluronic acid interpenetrating polymer network hydrogels.* Acta Biomater, 2009. **5**(7): p. 2385-97.

123. Tedder, M.E., et al., *Stabilized collagen scaffolds for heart valve tissue engineering.* Tissue Eng Part A, 2009. **15**(6): p. 1257-68.

124. Masters, K.S., et al., *Designing scaffolds for valvular interstitial cells: cell adhesion and function on naturally derived materials.* J Biomed Mater Res A, 2004. **71**(1): p. 172-80.

125. Merryman, W.D., et al., *Differences in tissue-remodeling potential of aortic and pulmonary heart valve interstitial cells.* Tissue Eng, 2007. **13**(9): p. 2281-9.

126. Rodriguez, K.J., L.M. Piechura, and K.S. Masters, *Regulation of valvular interstitial cell phenotype and function by hyaluronic acid in 2-D and 3-D culture environments.* Matrix Biol, 2011. **30**(1): p. 70-82.

127. Zoltan-Jones, A., et al., *Elevated hyaluronan production induces mesenchymal and transformed properties in epithelial cells.* J Biol Chem, 2003. **278**(46): p. 45801-10.

128. Chopra, A., et al., *Augmentation of integrin-mediated mechanotransduction by hyaluronic acid.* Biomaterials, 2014. **35**(1): p. 71-82.

129. Robinson, P.S., et al., *Functional tissue-engineered valves from cell-remodeled fibrin with commissural alignment of cell-produced collagen.* Tissue Eng Part A, 2008. **14**(1): p. 83-95.

130. Brigham, M.D., et al., *Mechanically robust and bioadhesive collagen and photocrosslinkable hyaluronic acid semi-interpenetrating networks.* Tissue Eng Part A, 2009. **15**(7): p. 1645-53.

131. Burdick, J.A., et al., *Controlled degradation and mechanical behavior of photopolymerized hyaluronic acid networks.* Biomacromolecules, 2005. **6**(1): p. 386-91.

132. Burdick, J.A. and G.D. Prestwich, *Hyaluronic Acid Hydrogels for Biomedical Applications.* Adv Mater, 2011.

133. Ye, Q., et al., *Fibrin gel as a three dimensional matrix in cardiovascular tissue engineering.* Eur J Cardiothorac Surg, 2000. **17**(5): p. 587-91.

134. Jockenhoevel, S., et al., *Fibrin gel -- advantages of a new scaffold in cardiovascular tissue engineering.* Eur J Cardiothorac Surg, 2001. **19**(4): p. 424-30.

135. Flanagan, T.C., et al., *The in vitro development of autologous fibrin-based tissue-engineered heart valves through optimised dynamic conditioning.* Biomaterials, 2007. **28**(23): p. 3388-3397.

136. Flanagan, T.C., et al., *In Vivo Remodeling and Structural Characterization of Fibrin-Based Tissue-Engineered Heart Valves in the Adult Sheep Model.* Tissue Engineering Part A, 2009. **15**(10): p. 2965-2976.

137. Syedain, Z.H., J.S. Weinberg, and R.T. Tranquillo, *Cyclic distension of fibrin-based tissue constructs: evidence of adaptation during growth of engineered connective tissue.* Proc Natl Acad Sci U S A, 2008. **105**(18): p. 6537-42.

138. Syedain, Z., et al., *Implantation of Completely Biological Engineered Grafts Following Decellularization into the Sheep Femoral Artery.* Tissue Eng Part A, 2014.

139. Syedain, Z.H., et al., *Tubular Heart Valves from Decellularized Engineered Tissue.* Annals of Biomedical Engineering, 2013. **41**(12): p. 2645-2654.

140. Sha, J.M., et al., *In-vitro seeding of human umbilical cord vein endothelial cells on hydroxyapatite for mechanical heart valve applications.* J Heart Valve Dis, 2010. **19**(4): p. 506-12.

141. Hong, H., et al., *Fabrication of biomatrix/polymer hybrid scaffold for heart valve tissue engineering in vitro.* ASAIO J, 2008. **54**(6): p. 627-32.

142. Hong, H., et al., *Fabrication of a novel hybrid heart valve leaflet for tissue engineering: an in vitro study.* Artif Organs, 2009. **33**(7): p. 554-8.

143. Del Gaudio, C., et al., *Electrospun bioresorbable heart valve scaffold for tissue engineering.* Int J Artif Organs, 2008. **31**(1): p. 68-75.

144. Del Gaudio, C., A. Bianco, and M. Grigioni, *Electrospun bioresorbable trileaflet heart valve prosthesis for tissue engineering: in vitro functional assessment of a pulmonary cardiac valve design.* Ann Ist Super Sanita, 2008. **44**(2): p. 178-86.

145. van Lieshout, M.I., et al., *Electrospinning versus knitting: two scaffolds for tissue engineering of the aortic valve.* J Biomater Sci Polym Ed, 2006. **17**(1-2): p. 77-89.

146. Courtney, T., et al., *Design and analysis of tissue engineering scaffolds that mimic soft tissue mechanical anisotropy.* Biomaterials, 2006. **27**(19): p. 3631-8.

147. Stankus, J.J., et al., *Microintegrating smooth muscle cells into a biodegradable, elastomeric fiber matrix.* Biomaterials, 2006. **27**(5): p. 735-44.

148. Stella, J.A., et al., *Tissue-to-cellular level deformation coupling in cell micro-integrated elastomeric scaffolds.* Biomaterials, 2008. **29**(22): p. 3228-36.

149. Kalfa, D., et al., *A polydioxanone electrospun valved patch to replace the right ventricular outflow tract in a growing lamb model.* Biomaterials, 2010. **31**(14): p. 4056-63.

150. Stella, J.A., et al., *Tissue-to-cellular level deformation coupling in cell micro-integrated elastomeric scaffolds.* Biomaterials, 2008. **29**(22): p. 3228-36.

151. Hoffman-Kim, D., et al., *Comparison of three myofibroblast cell sources for the tissue engineering of cardiac valves.* Tissue Eng, 2005. **11**(1-2): p. 288-301.

152. Smith, S., et al., *Force generation of different human cardiac valve interstitial cells: relevance to individual valve function and tissue engineering.* J Heart Valve Dis, 2007. **16**(4): p. 440-6.

153. Cebotari, S., et al., *Clinical application of tissue engineered human heart valves using autologous progenitor cells.* Circulation, 2006. **114**(1 Suppl): p. I132-7.

154. Frank, B.S., et al., *Determining Cell Seeding Dosages for Tissue Engineering Human Pulmonary Valves.* J Surg Res, 2010.

155. Appleton, A.J., et al., *Vascular smooth muscle cells as a valvular interstitial cell surrogate in heart valve tissue engineering.* Tissue Eng Part A, 2009. **15**(12): p. 3889-97.

156. DeLaughter, D.M., et al., *Spatial transcriptional profile of the chick and mouse endocardial cushions identify novel regulators of endocardial EMT in vitro.* J Mol Cell Cardiol, 2013. **59**: p. 196-204.

157. Hjortnaes, J., et al., *Translating autologous heart valve tissue engineering from bench to bed.* Tissue Eng Part B Rev, 2009. **15**(3): p. 307-17.

158. Apte, S.S., et al., *Current developments in the tissue engineering of autologous heart valves: moving towards clinical use.* Future Cardiol, 2011. **7**(1): p. 77-97.

159. Sacks, M.S., F.J. Schoen, and J.E. Mayer, *Bioengineering challenges for heart valve tissue engineering.* Annu Rev Biomed Eng, 2009. **11**: p. 289-313.

160. Butcher, J.T., G.J. Mahler, and L.A. Hockaday, *Aortic valve disease and treatment: The need for naturally engineered solutions.* Adv Drug Deliv Rev, 2011.

161. Bouten, C.V., et al., *Substrates for cardiovascular tissue engineering.* Adv Drug Deliv Rev, 2011.

162. Benton, J.A., et al., *Photocrosslinking of gelatin macromers to synthesize porous hydrogels that promote valvular interstitial cell function.* Tissue Eng Part A, 2009. **15**(11): p. 3221-30.

163. Stella, J.A., et al., *On the biomechanical function of scaffolds for engineering load-bearing soft tissues.* Acta Biomater, 2010. **6**(7): p. 2365-81.

164. Garg, V., et al., *Mutations in NOTCH1 cause aortic valve disease.* Nature, 2005. **437**(7056): p. 270-4.

165. Tanaka, K., et al., *Age-associated aortic stenosis in apolipoprotein E-deficient mice.* J Am Coll Cardiol, 2005. **46**(1): p. 134-41.

166. Nigam, V. and D. Srivastava, *Notch1 represses osteogenic pathways in aortic valve cells.* J Mol Cell Cardiol, 2009. **47**(6): p. 828-34.

167. O'Brien, K.D., et al., *Apolipoproteins B, (a), and E accumulate in the morphologically early lesion of 'degenerative' valvular aortic stenosis.* Arterioscler Thromb Vasc Biol, 1996. **16**(4): p. 523-32.

168. Binnig, G., C.F. Quate, and C. Gerber, *Atomic Force Microscope.* Physical Review Letters, 1986. **56**(9): p. 930-933.

169. Rugar, D. and P. Hansma, *Atomic Force Microscopy.* Physics Today, 1990. **43**(10): p. 23-30.

170. Domke, J., et al., *Mapping the mechanical pulse of single cardiomyocytes with the atomic force microscope.* Eur Biophys J, 1999. **28**(3): p. 179-86.

171. Domke, J. and M. Radmacher, *Measuring the elastic properties of thin polymer films with the atomic force microscope.* Langmuir, 1998. **14**: p. 3320-3325.

172. Jalili, N. and K. Laxminarayana, *A review of atomic force microscopy imaging systems: application to molecular metrology and biological sciences.* Mechatronics, 2004. **14**(8): p. 907-945.

173. Duncan, A.C., D. Boughner, and I. Vesely, *Dynamic glutaraldehyde fixation of a porcine aortic valve xenograft. I. Effect of fixation conditions on the final tissue viscoelastic properties.* Biomaterials, 1996. **17**(19): p. 1849-56.

174. Vesely, I. and A. Lozon, *Natural preload of aortic valve leaflet components during glutaraldehyde fixation: effects on tissue mechanics.* J Biomech, 1993. **26**(2): p. 121-31.

175. Merryman, W.D., et al., *The effects of cellular contraction on aortic valve leaflet flexural stiffness.* J Biomech, 2006. **39**(1): p. 88-96.

176. Rousseau, E.P., et al., *Elastic and viscoelastic material behaviour of fresh and glutaraldehyde-treated porcine aortic valve tissue.* J Biomech, 1983. **16**(5): p. 339-48.

177. Hinton, R.B., Jr., et al., *Mouse heart valve structure and function: echocardiographic and morphometric analyses from the fetus through the aged adult.* Am J Physiol Heart Circ Physiol, 2008. **294**(6): p. H2480-8.

178. Schenke-Layland, K., et al., *Impact of cryopreservation on extracellular matrix structures of heart valve leaflets.* Ann Thorac Surg, 2006. **81**(3): p. 918-26.

179. Brockbank, K.G. and Y.C. Song, *Morphological analyses of ice-free and frozen cryopreserved heart valve explants.* J Heart Valve Dis, 2004. **13**(2): p. 297-301.

180. Elder, E., et al., *Enhanced tissue strength in cryopreserved, collagen-based blood vessel constructs.* Transplant Proc, 2005. **37**(10): p. 4625-9.

181. Eckert, C.E., et al., *On the Biomechanical Role of Glycosaminoglycans in the Aortic Heart Valve Leaflet.* Acta Biomater, 2012.

182. Hinton, R.B. and K.E. Yutzey, *Heart Valve Structure and Function in Development and Disease.* Annual Review of Physiology, Vol 73, 2011. **73**: p. 29-46.

183. Rajamannan, N.M., et al., *Calcific aortic valve disease: not simply a degenerative process: A review and agenda for research from the National Heart and Lung and Blood Institute Aortic Stenosis Working Group. Executive summary: Calcific aortic valve disease-2011 update.* Circulation, 2011. **124**(16): p. 1783-91.

184. Hutcheson, J.D., et al., *5-HT(2B) antagonism arrests non-canonical TGF-beta1-induced valvular myofibroblast differentiation.* J Mol Cell Cardiol, 2012. **53**(5): p. 707-14.

185. Merryman, W.D., *Mechano-potential etiologies of aortic valve disease.* J Biomech, 2010. **43**(1): p. 87-92.

186. DeLaughter, D.M., et al., *What chick and mouse models have taught us about the role of the endocardium in congenital heart disease.* Birth Defects Res A Clin Mol Teratol, 2011. **91**(6): p. 511-25.

187. Colvee, E. and J.M. Hurle, *Maturation of the extracellular material of the semilunar heart values in the mouse. A histochemical analysis of collagen and mucopolysaccharides.* Anat Embryol (Berl), 1981. **162**(3): p. 343-52.

188. Krishnamurthy, V.K., et al., *Maladaptive matrix remodeling and regional biomechanical dysfunction in a mouse model of aortic valve disease.* Matrix Biol, 2012. **31**(3): p. 197-205.

189. Sewell-Loftin, M.K., et al., *A novel technique for quantifying mouse heart valve leaflet stiffness with atomic force microscopy.* J Heart Valve Dis, 2012. **21**: p. 513-520.

190. Sato, T.N., et al., *Distinct roles of the receptor tyrosine kinases Tie-1 and Tie-2 in blood vessel formation.* Nature, 1995. **376**(6535): p. 70-4.

191. Puri, M.C., et al., *The receptor tyrosine kinase TIE is required for integrity and survival of vascular endothelial cells.* EMBO J, 1995. **14**(23): p. 5884-91.

192. Qu, X., et al., *Abnormal embryonic lymphatic vessel development in Tie1 hypomorphic mice.* Development, 2010. **137**(8): p. 1285-95.

193. Qu, X., et al., *A novel role for endothelial Tie1 in late gestational and post-natal semilunar valve remodeling.* Circulation, 2014. **In Revision**.

194. Woo, K.V., et al., *Tie1 attenuation reduces murine atherosclerosis in a dose-dependent and shear stress-specific manner.* J Clin Invest, 2011. **121**(4): p. 1624-35.

195. Garcia, J., et al., *Tie1 deficiency induces endothelial-mesenchymal transition.* EMBO Rep, 2012. **13**(5): p. 431-9.

196. Wu, B., et al., *Nfatc1 coordinates valve endocardial cell lineage development required for heart valve formation.* Circ Res, 2011. **109**(2): p. 183-92.

197. Zhou, B., et al., *Characterization of Nfatc1 regulation identifies an enhancer required for gene expression that is specific to pro-valve endocardial cells in the developing heart.* Development, 2005. **132**(5): p. 1137-46.

198. Sewell-Loftin, M.K., et al., *Myocardial contraction and hyaluronic acid mechanotransduction in epithelial-to-mesenchymal transformation of endocardial cells.* Biomaterials, 2014. **35**(9): p. 2809-15.

199. Sewell-Loftin, M.K., et al., *EMT-inducing biomaterials for heart valve engineering: taking cues from developmental biology.* J Cardiovasc Transl Res, 2011. **4**(5): p. 658-71.

200. Craig, E.A., et al., *Involvement of the MEKK1 signaling pathway in the regulation of epicardial cell behavior by hyaluronan.* Cell Signal, 2010. **22**(6): p. 968-76.

201. Bernanke, D.H. and R.R. Markwald, *Effects of two glycosaminoglycans on seeding of cardiac cushion tissue cells into a collagen-lattice culture system.* Anat Rec, 1984. **210**(1): p. 25-31.

202. Baldwin, H.S., T.R. Lloyd, and M. Solursh, *Hyaluronate degradation affects ventricular function of the early postlooped embryonic rat heart in situ.* Circ Res, 1994. **74**(2): p. 244-52.

203. Smeds, K.A., et al., *Synthesis of a novel polysaccharide hydrogel.* J Macromol Sci, Pure Appl Chem, 1999. **A36**(7-8): p. 981-989.

204. Smeds, K.A., et al., *Photocrosslinkable polysaccharides for in situ hydrogel formation.* J Biomed Mater Res, 2001. **54**(1): p. 115-21.

205. Bartman, T., et al., *Early myocardial function affects endocardial cushion development in zebrafish.* PLoS Biol, 2004. **2**(5): p. E129.

206. Rodgers, L.S., et al., *Depolymerized hyaluronan induces vascular endothelial growth factor, a negative regulator of developmental epithelial-to-mesenchymal transformation.* Circ Res, 2006. **99**(6): p. 583-9.

207. Koushik, S.V., et al., *Targeted inactivation of the sodium-calcium exchanger (Ncx1) results in the lack of a heartbeat and abnormal myofibrillar organization.* Faseb Journal, 2001. **15**(7): p. 1209-11.